Tucson Office
3031 West Ina Road
Tucson, AZ 85741
Tel 520.297.7723 Fax 520.297.7724
www.tetratech.com

Technical Memorandum

To:	Kathy Arnold	**From:**	Grady O'Brien, Project Manager
Company:	Rosemont Copper Company	**Date:**	July 26, 2010
Re:	Groundwater Flow Model Construction and Calibration	**Doc #:**	198/10-320874-5.3
CC:	David Krizek, P.E. (Tetra Tech)		

1.0 Introduction

Rosemont Copper Company (Rosemont) is planning the development of an open pit mining and mineral processing operation known as the Rosemont Copper Project (Project) on the east side of the Santa Rita Mountains, approximately 30 miles southeast of Tucson Arizona in Pima, County (Figure 1). As part of the mining operation, dewatering of the Open Pit will continue throughout the 20-25 years of operation and cease at closure. When mining ceases and dewatering is discontinued, the pit will naturally refill with water from groundwater, surface-water, and precipitation contributions and a pit lake will form. It is expected that the pit will remain a perpetual hydraulic sink at a stabilized, equilibrium condition due to the high evaporation rate of the Rosemont area. This implies that groundwater will perpetually flow into the Open Pit, although at a much lower rate than during the active dewatering process.

Tetra Tech has constructed regional groundwater flow models for the Project. These flow models represent pre-mining steady state conditions, active mining conditions, and post-closure mining conditions. In support of the groundwater flow model development, the following supporting tasks were performed such as development of a Davidson Canyon conceptual model, hydrogeologic framework model, recharge distribution, steady-state water levels and potentiometric surface, evaluation of aquifer testing and hydraulic properties, evapotranspiration distribution, and stream-flow conditions.

This Technical Memorandum documents the tasks completed to construct 1) the steady-state groundwater flow model and calibration results, 2) the mining-phase groundwater flow model, and 3) the post-mining phase groundwater flow model. The background information provided in this Technical Memorandum supports the groundwater impact analysis and sensitivity analysis tasks being developed by Tetra Tech. These analyses will be presented in subsequent technical memoranda.

1.1 Task Objectives, Scope, and Approach

Dewatering of the Open Pit during the mining phase, and pit lake formation during the post-mining phase, will result in groundwater drawdown that will propagate through the groundwater flow system. The objective of the groundwater flow modeling is to provide estimates of impacts to area water resources. Potential impacts to Cienega Creek, Davidson Canyon, and regional spring flows are of particular interest.

The regional model scope is limited to the model domain previously developed by Montgomery & Associates (M&A, 2009b). The hydrogeologic framework model, which forms the foundation of the groundwater flow models, was based on the existing horizontal hydrogeologic slices

013230

ROSEMONT COPPER
Resourceful

Memorandum

To: Bev Everson

Cc: Tom Furgason

From: Kathy Arnold Kathy

Doc #: 031/10 – 15.3.2

Subject: **Transmittal of Groundwater Flow Model Construction and Calibration**

Date: July 23, 2010

Rosemont is pleased to transmit the following technical memorandums related to the groundwater modeling work that has been undertaken by Tetra Tech:

- *Groundwater Flow Model Construction and Calibration,* Tetra Tech, July 2010

You will notice that the order of the submittal for the Tetra Tech memoranda is reversed; Rosemont believed transmitting in this revised order would make more sense for the review.

Rosemont is providing three hardcopies and two disk copies for the Forest and two hardcopies and one disk copy for SWCA.

developed for the M&A flow model domain (M&A, 2009a and M&A, 2009b). No additional field investigation or geologic interpretation was completed as part of Tetra Tech's flow modeling or geologic framework modeling tasks. Simulation of a regional area limits the resolution of the finite-difference model grid cells, which limits the resolution and accuracy of the model simulations. Hydrogeologic features smaller than the grid resolution are typically not simulated, and geometries and distributions are approximate. Small magnitude flows, small water-level changes, and steep hydraulic gradients are therefore difficult for a regional model to replicate.

Modeling methods vary depending on the processes being simulated and the available data. The approach used was to construct groundwater flow models for each phase of the Project and to integrate their results to simulate conditions from pre-mining conditions through post-mining steady-state conditions. The pre-mining phase or steady-state conditions were based on historical water level, stream-flow, and hydraulic-property data. The flow model was calibrated to the steady-state water-level data, forming the basis for the subsequent transient flow models. The mining-phase transient model simulates the step-wise deepening of the Open Pit and dewatering during the 20-25 year operational period. Open pit dewatering was simulated with drain cells, which remove water from the model when water levels reach a specified elevation below the bottom of the pit. The post-mining phase uses the LAK2 package (Council, 1999) to simulate the refilling of the pit following the end of dewatering. Other minor differences between the simulation approaches are discussed in detail in the body of this memorandum.

1.2 Previous Work

This groundwater flow modeling task builds upon investigations previously completed by Rosemont, its subcontractors, and other investigators. The hydrogeologic characterization program and groundwater flow modeling completed by M&A (2009a, 2009b, 2009c) provided much of the base data and information used in this modeling effort. Other investigations and data on recharge, precipitation, stream flow, water levels, and evapotranspiration were used to support development of the flow model data sets. These data sources and investigations are referenced throughout this memorandum.

1.3 Memorandum Organization

Organization of this memorandum follows the groundwater flow modeling approach. Details of the pre-mining, steady-state model construction, and calibration are provided, followed by changes required to simulate the mining and post-mining phases. The model domain, grid, external boundary conditions, and geologic framework, which are the same for each model, are discussed. Analyses performed to estimate recharge, evapotranspiration, stream flow, water-level targets, and hydraulic barriers for the steady-state model are presented. Calibration of the pre-mining model, including final recharge, hydraulic conductivity, and water balance are discussed. The calibrated steady-state model's fit to known conditions is then provided to assist in evaluating the model's representation of the regional groundwater flow system.

The transient, predictive models incorporate the Open Pit, but they are based on the steady-state model. The most significant differences between the models are how the pit, storage effects, and recharge in the Project area are simulated. Results of the mining phase and post-mining phase transient models are not presented in this memorandum. These data will be presented in a subsequent memorandum detailing the predicted groundwater flow-system impacts. The sensitivity analysis identifies the most sensitive parameters during calibration and estimates a range of predicted impacts. This analysis will be documented in a companion memorandum.

2.0 Groundwater Flow Model Construction

The components of the groundwater flow models that are consistent in each model are discussed in this section. The model code, domain, grid, and hydrogeologic framework are the same for each model version. Initial recharge, evapotranspiration, stream flow, horizontal flow barriers, and external model boundaries are also simulated in the same manner for each model. Elements specific to the pre-mining steady-state model, mining-phase model, and post-mining phase model are discussed in subsequent sections.

2.1 Model Code Selection

The hydrogeologic conditions to be simulated pose several numerical challenges. Steep hydraulic gradients occur as a result of the natural water-level elevation change of over 2,800 feet and due to dewatering of the approximately 2,000 foot deep Open Pit. The groundwater flow system also takes a relatively long time to equilibrate to pit dewatering and refilling, which requires additional computational time. The dewatering and refilling processes may also create variably-saturated flow conditions. A finite-difference model code, MODFLOW-SURFACT (Version 3, Hydrogeologic, 2010) was selected for use over the traditional MODFLOW model code due to the following capabilities: 1) improved simulation of variably-saturated flow, 2) improved and faster Pre-Conditioned Conjugate Gradient solvers (PCG4 and PCG5); and 3) adaptive time-stepping and output control package (ATO4) that reduces simulation time.

2.2 Model Domain

The model domain encompasses a 457 square-mile area in southern Arizona (Figure 2). The existing hydrogeologic data for the Project necessitated that the lateral extent of the model domain be the same as the M&A groundwater flow model domain (M&A, 2009b). The northern, eastern, and southern model boundaries are far enough away from the Open Pit to minimize potential boundary effects in the mining and post-mining simulations. This model domain allows the ability to evaluate potential impacts to Davidson Canyon and Cienega Creek. The western model boundary was set to the western extent of the Precambrian igneous and metamorphic crystalline formations (pCb) at the western base of the Santa Rita Mountains. These pCb units have low hydraulic conductivity, which limits the propagation of draw-down west of the Open Pit.

2.3 Horizontal and Vertical Model Grid

The finite-difference model grid consists of 205 rows by 169 columns by 20 layers, for a total of 692,900 cells (Figure 3). Of these 692,000 model cells, 433,895 cells are active. Model cells in the southwestern and southeastern portions of the model grid are located outside the Cienega Creek watershed boundary and are designated as no flow cells or inactive cells (Figure 3).

The groundwater flow model grid was designed to 1) maximize accuracy of the regional model in matching water levels, 2) increase accuracy in predicting drawdown and groundwater flow in the Open Pit area, and 3) facilitate analysis of potential impacts to Davidson Canyon and Cienega Creek.

A telescoping horizontal model grid was used to increase the simulation resolution in the pit area, while maintaining a manageable number of model cells. The model grid cell width is 800 feet at the model domain edges, decreasing to a cell width of 200 feet in the vicinity of the pit (Figure 3). The model grid is aligned north-south and east-west.

The vertical groundwater flow model grid was constructed using 20 horizontal model layers with constant thicknesses except for model layer one (1) (Table 1). Model layer one (1) ranges in thickness from 250 to 1,679 feet with the thicker portions underneath the mountain ranges. Uniform thickness model layers were chosen for the other model layers to assist in numerical simulation of the mining phase pit dewatering and post-mining pit-lake development. These conditions create steep hydraulic gradients and thinner, constant thickness model layers reduce numerical instability and improve accuracy. Model layers intersecting the pit were assigned a thickness of approximately 150 feet. Model cells above and below the pit were assigned thicknesses between 200 and 430 feet. Elevations and thicknesses for each model layer are shown in Table 1. The bottom elevation of the Open Pit (3,050 feet above mean sea level [amsl]) was aligned with the bottom of layer 15 to simplify construction of drain cells and lake cells used to simulate dewatering and Open Pit refilling. The horizontal and vertical flow model grid discretization is illustrated in Figure 4.

The base of the model is at an elevation of 1,000 feet amsl. The elevation for the bottom of the model is sufficiently below the anticipated bottom of the pit so that hydraulic stresses should not encounter the bottom model boundary during Open Pit dewatering or refilling.

Table 1. Model Layer Elevations and Thicknesses

Model Layer	Top Elevation (ft amsl)	Layer Thickness (ft)
1	6,929	250 – 1,679
2	5,250	200
3	5,050	150
4	4,900	150
5	4,750	150
6	4,600	150
7	4,450	150
8	4,300	150
9	4,150	150
10	4,000	150
11	3,850	150
12	3,700	150
13	3,550	150
14	3,400	150
15	3,250	200
16	3,050	330
17	2,720	430
18	2,290	430
19	1,860	430
20	1,430	430

2.4 Hydrogeologic Framework

The groundwater flow models developed for this task are based on the regional geology. A three-dimensional representation of the hydrogeologic units was created by Tetra Tech, allowing the geology to be accurately incorporated in the groundwater flow model grid (Tetra Tech, 2010a). Geologic formations were grouped into ten (10) hydrogeologic units (HGU) based on the age and material properties of similar rock types (Table 2; M&A, 2009a). Publically available surface geologic maps and geologic cross sections developed by Rosemont and M&A were used to create 16 horizontal hydrogeologic maps or slices. These slices are at 200 foot intervals from 2,400 feet to 5,400 feet amsl. The three-dimensional hydrogeologic framework model was extended to a depth of 1,000 feet amsl by continuing the hydrogeologic unit trends to depth. The ten (10) HGUs served as the initial hydraulic parameter zones for the groundwater flow modeling. Additional zones were added during the calibration process (discussed in Section 3.2.1, Model Calibration). Details on the hydrogeologic framework model construction are provided in the Technical Memorandum titled *Hydrogeologic Framework Model* dated July 9, 2010 (Tetra Tech, 2010a).

Table 2. Summary of Hydrogeologic Units in the Groundwater Flow Model

HGU Abbreviation	Description
Qal	Quaternary and Recent Alluvium
QTg	Late Tertiary to Early Quaternary basin-fill deposits – highest permeability
QTg1	Late Tertiary to Early Quaternary basin-fill deposits – lower permeability
QTg2	Late Tertiary to Early Quaternary basin-fill deposits – lowest permeability
Tsp	Early to Mid-Tertiary sedimentary and volcanic units
KTi	Upper Cretaceous and Early Tertiary intrusive rocks
Kv	Upper Cretaceous volcanic rocks
Ksd	Lower Cretaceous sedimentary units
Pz	Paleozoic sedimentary and metamorphic formations
pCb	Precambrian igneous and metamorphic crystalline formations

2.5 Recharge Distribution

Recharge is one of the most critical inputs to the groundwater flow model, as it prescribes the volume of water entering the groundwater flow system due to precipitation, including the locations where that water is introduced into the flow system. Development of the initial recharge distribution is presented in this section. Modifications to this recharge distribution were made during the steady-state calibration process and are discussed in the calibration section. Minor changes to the calibrated recharge distribution occur in the different model versions due to simulation of the Open Pit, Project facilities, and pit lake development. These recharge distribution modifications are discussed in the mining-phase and post-mining phase model sections.

2.5.1 Methodology

Estimating recharge is particularly important for groundwater flow models in arid and semi-arid regions. Methods for estimating recharge distributions and rates have therefore been active research topics for many years. Tetra Tech reviewed previous recharge distributions used for the Project and for other investigations in similar terrains.

The regional area being simulated can be generally characterized as having the highest precipitation rates occurring at high elevations on low permeability bedrock, with steep slopes. While recharge occurs in these high elevation bedrock areas, a significant amount of the precipitation runs off and flows down gradient until it reaches areas with flatter slopes and higher permeability deposits where it can more readily infiltrate into the subsurface. The methodology applied to distribute recharge for the groundwater flow models follows this simple and observable process.

Groundwater investigations in the United States desert southwest commonly estimate recharge based on precipitation-elevation relationships (Maxey and Eakin, 1949; Anderson, 1995). The previous groundwater flow model of the Project area (M&A, 2009b) used the precipitation-elevation relationship developed by Anderson (1995) to estimate recharge from precipitation. Higher recharge rates were assigned to mountain-front areas during their model calibration process.

The methodology for this investigation further refines the more common precipitation-elevation approach. The procedure involves a combination of Geographic Information System (GIS) analysis, empirical surface-runoff modeling, and water-balance calculations. The procedure allows for excess precipitation on upland bedrock areas, where precipitation is highest but primary permeability is low, infiltration capacity is limited, and runoff is high, to be conveyed to lower elevations before it infiltrates to recharge the groundwater system. The spatial redistribution of precipitation- and runoff-derived recharge is determined by this process. Recharge rates are scaled or normalized to produce the total amount of recharge determined by independent methods.

A precipitation-distribution data set was obtained from the PRISM Group at Oregon State University [PRISM] (2009). Soil, geologic, and topographic data were used to redistribute the upland area precipitation to the lower-elevation areas. Soil data were obtained from the United States Department of Agriculture Natural Resources Conservation Service (NRCS, 2008; NRCS, 1986). Geologic data were obtained from several published sources (Daffron et. al., 2007; Drewes, 1972; Ferguson et al., 2001; Johnson and Ferguson, 2006; M&A, 2009a). Topographic data were obtained from the U.S. Geological Survey's National Map Seamless Server (USGS, 2010a) (http://seamless.usgs.gov/website/seamless/viewer.htm).

Sub-watersheds or individual drainage basins within the larger Cienega Creek watershed were delineated based on topography. These sub-watersheds were then further subdivided into bedrock, alluvial fan, and valley floor sub-basins (Figure 5). Existing geologic maps were used to delineate bedrock areas and to identify the contact between bedrock and alluvial deposits. The bedrock/alluvium contact was assigned as the upper-elevation limit of the alluvial fan deposits. Slope changes were used to delineate the lower-elevation extent of the alluvial fan deposits. The lower elevation areas with alluvial deposits were designated as the valley floor.

The precipitation within each sub-basin and the hydrologic soil group areas within each sub-basin were determined using GIS methods. Precipitation data from the United States Department of Commerce National Climatic Data Center (NCDC, 2009) for the Santa Rita Experimental Range meteorological station were used to simulate precipitation events and to develop runoff estimates for each of the sub-basins. The Santa Rita station is the nearest station with a long-term daily precipitation record and data are available from 1950 to the present. To simulate precipitation events for each sub-basin, the daily Santa Rita station precipitation data from 1950 to 2009 were scaled by the ratio of the average annual PRISM precipitation for the sub-basin to the average annual precipitation at the Santa Rita station.

Hydrologic soil group classification data were used with the Soil Conservation Service (SCS) Runoff Curve Number (CN) method (USDA, 1986) to calculate the threshold precipitation amount for each sub-basin that would result in surface runoff. Scaled precipitation events that exceeded the threshold precipitation were then identified. The runoff volumes for these events were then subtracted from the precipitation volumes (potential recharge) in the higher-elevation sub-basins. The volume of water difference was added to the precipitation volume in the lower-elevation sub-basin. This procedure routed excess precipitation (runoff) on the bedrock areas to the alluvial fan areas and excess precipitation on the alluvial fan areas to the valley floor areas. In this manner, precipitation is numerically rerouted down gradient to mimic the natural precipitation, runoff, and recharge processes.

Several independent investigations have estimated total recharge over various parts of the region. Based on these existing studies and their own investigation M&A (2009b) simulated total recharge of 10,100 acre-feet per year for the groundwater flow model domain. This recharge estimate is within the range of reasonable estimates and was used by Tetra Tech to maintain consistency between the flow models.

Water-balance calculations were performed to normalize the recharge rates for each sub-basin so that the total recharge for all of the sub-basins equaled 10,100 acre-feet per year (ac-ft/yr). The calculation results and recharge estimates for each sub-watershed and sub-basin are summarized in Attachment 1. The initial recharge estimate of 10,100 ac-ft/yr is approximately 5.4 percent of average annual precipitation. The recharge estimates range from 0.34 to 0.66 inches per year (in/yr) and the spatial distribution is shown on Figure 6. These normalized recharge rates were used as the initial recharge distribution in the steady-state groundwater flow model.

2.6 Evapotranspiration

Groundwater losses due to evapotranspiration (ET) occur primarily in the reaches of Cienega Creek and Davidson Canyon where riparian vegetation is present. The simulated ET was modeled approximately at the same rates and locations as that previously simulated by M&A (2009b). ET rates were estimated based on riparian area, plant types, plant cover density, and riparian plant distributions (M&A, 2009b, pp. 28-29). ET measurements were based on riparian plants in the San Pedro River basin and other areas in the desert southwestern United States. Previous investigators estimate that ET ranges from 3,300 to 5,097 ac-ft/yr in Cienega Creek Basin (M&A, 1985; Chong-Diaz, 1995; Knight, 1996; Bota, 1997) and M&A simulated a constant ET withdrawal of 4,244 ac-ft/yr (M&A, 2009b).

ET was being simulated with MODFLOW’s evapotranspiration (EVT) package. Maximum ET rates were assigned to each model cell and simulated ET varies with the groundwater level rather than occurring at a constant rate, regardless of the depth to groundwater. ET varies linearly between a location-specific maximum value that occurs when the simulated head in a model cell is at the land surface and zero when the simulated head is below an assigned extinction depth. The ET rates assigned in the model are shown on Figure 7. Extinction depth varies with the types of soil and vegetative cover, ranging from about 1.5 feet under bare conditions in sandy soil to about 27 feet under forest cover conditions in clayey soil (Shah et al., 2007). In the flow models, the extinction depth was set to 16.4 feet (5 meters) below the land surface. The result of the linear relationship between water level and ET (when head is above the extinction depth) is that the assigned ET values represent the maximum potential ET. As the water level decreases to the extinction depth, the simulated ET rate also decreases, reaching zero when the depth-to-water is equal to the extinction depth.

2.7 Stream Flow

Cienega Creek has several reaches of perennial flow that are separated by dry or intermittent flow reaches (Figure 1). Mean monthly stream discharge has historically varied between zero and 9.3 cubic feet per second (cfs) at U.S. Geological Survey (USGS) stream gauges (Table 3). Davidson Canyon has one reach with historical stream flow measurements (1968-1981), but the USGS gage has been discontinued. A conceptual model of groundwater and surface-water flow conditions in Davidson Canyon has been documented in Tetra Tech (2010b).

Stream-flow data available from the USGS for two (2) stations on Cienega Creek and one station on Davidson Canyon Wash were evaluated for use as qualitative targets for model calibration. The gaging station locations and identifications are shown on Figure 8, and monthly mean flow data are summarized in Table 3. The data show relatively consistent and small flows during October through June and a strong influence from high discharges during the July to September monsoon season. Because of the large scale and long time-frame of the model, the median flows at each station are the most appropriate values for comparison to model results.

The intermittent interaction of surface water and groundwater along Cienega Creek and Davidson Canyon was simulated using MODFLOW's Stream Flow Routing (SFR) package (Prudic et al., 2004). The SFR package allows the groundwater system to lose water to a stream when the head in the cell containing the stream boundary is higher than the streambed or stream stage elevation and to gain water from the stream when the head in the cell is lower than the streambed or stream stage elevation. The SFR package is an appropriate method for simulating the exchange of water between the streams and the groundwater system for this regional model scale and long time-frames.

Stream channel locations were identified from the National Hydrography Dataset (USGS, 2010b), and elevations were obtained from the 10 meter National Elevation Dataset (NED). The minimum elevation within each model cell was used as an approximation for the streambed elevation in each model cell. The resulting stream profile was then checked for any uphill stream segments (i.e., segments that gained elevation moving downstream). Streams were associated with model grid cells and their length in each cell calculated and combined with the width estimated from aerial photography and streambed hydraulic conductivity to produce streambed conductance values. A stream boundary was assigned to the model layers corresponding to the stream elevation at each cell that intersected the stream channel. Model layers 7 through 14 contain stream cells (Figure 8).

Stream flows were used as calibration targets only in a qualitative manner, due to the regional model scale that limits the accuracy of incorporating alluvial stream-channel aquifers as discrete model components. The qualitative calibration consisted of obtaining surface-water flow at the gage locations, but the model was not expected to quantitatively reproduce the observed flows.

Table 3. Summary of Monthly Mean Stream Flows

Month	USGS 09484550 Cienega Creek near Sonoita, AZ (cfs)	USGS 09484560 Cienega Creek near Pantano, AZ (cfs)	USGS 09484590 Davidson Canyon Wash near Vail, AZ (cfs)
Jan	0.94	0	0.11
Feb	1	1.1	0.18
Mar	1.1	0.17	0.2
Apr	0.83	0	0.15
May	0.47	0	0.11
Jun	0.31	0.32	0.07
Jul	9.3	11	2.5
Aug	5	9.2	3.4
Sep	2.6	5.5	2.1
Oct	0.53	0.31	0.1
Nov	0.66	0	0.14
Dec	0.81	0	0.23
Median	**0.885**	**0.24**	**0.165**

Source: USGS

2.8 Groundwater Flow Barriers

Geologic mapping from the Arizona Geologic Survey (AZGS) has delineated several geologic structures including faults and dikes in the pit area and throughout upper Davidson Canyon (Ferguson, 2009; Ferguson et al., 2001, Spencer et al., 2001). One of the objectives of the aquifer testing was to determine if these geologic structures were conduits or barriers to groundwater flow. Drawdown and recovery observed during aquifer testing suggested that faults were acting as flow barriers that compartmentalize the groundwater flow system (M&A, 2009a). Due to aquifer test limitations, the role of specific faults and fractures on controlling groundwater flow was not conclusively determined. Faults and fractures were therefore not explicitly simulated due to the regional model scale and lack of data defining their characteristics.

Geologic mapping and observations, however, indicate that faults and fractures play an important role in controlling groundwater flow. Evidence of faults and fractures influence on groundwater flow is observed in upper Davidson Canyon, in the western pit area, and along a large mapped quartz-porphyry dike. Faults mapped by the Arizona Geological Survey in upper Davidson Canyon impede horizontal groundwater flow, as evidenced by the presence of several springs where the faults daylight at the land surface.

The north-south trending “Backbone Fault” is present along the ridge of the Santa Rita Mountains and through the western pit area. This faulting appears to have created a higher conductivity rubble zone parallel to the fault, which may enhance north-south groundwater flow. However, the Precambrian geologic units to the west of the fault have low conductivity, which may have been further enhanced by thermal and mineral alteration over time. These alterations typically reduce rock permeability by sealing fractures or faults. Simulation of this area is discussed further in Section 3.2.1, Model Calibration.

A northwest-striking quartz-porphyry dike has been mapped on the Mount Fagan and Empire Ranch 7.5' quadrangles (Ferguson, 2009; Ferguson et al., 2001). This dike crosses Davidson Canyon approximately 3,000 feet northeast of monitoring well RP-7 (Figure 9). This Tertiary age geologic feature is described in (Ferguson, 2009) as "*felsic porphyry containing 10-30% quartz and feldspar phenocrysts (1-3 mm) and sparse biotite in a fine-grained light-colored matrix, locally flow-foliated. Forms dikes and sills, and a plug-like stock in the northwest corner of the map area*." The quartz-porphyry dike was not mapped in the 16 horizontal hydrogeologic slices used to create the hydrogeologic framework model. The quartz-porphyry dike strikes sub-perpendicular to groundwater flow in the Davidson Canyon area, it is over four (4) miles long, and based on a field investigation, it has low fracture density and a thickness generally greater than 100 feet. The steep hydraulic gradient from the Open Pit area to Davidson Spring in Davidson Canyon is likely due, at least in part, to the quartz-porphyry dike. The dike was incorporated as a base feature in each of the groundwater flow models as a Horizontal Flow Barrier (HFB).

The quartz-porphyry dike is a nearly continuous feature, but there is an approximately 3,000 foot gap between the two (2) major mapped sections. The dike was simulated in two (2) segments due to the length of this gap (Figure 10). Further field investigation is needed to determine if the dike is a continuous feature under this large surface gap. Smaller gaps of less than 800 feet, which is the grid-cell size, occur in the southeastern segment of the dike. These small gaps were assumed to be areas where Quaternary alluvium was covering the surface expression of the dike. The dike was simulated as a continuous HFB in this segment (Figure 10). The entire extent of the quartz-porphyry dike was simulated to extend to the bottom of the model.

2.9 External Model Boundaries

Similar to the definition of the model domain, the external model boundary locations are the same as those used by M&A (2009b). No-flow boundaries represent groundwater divides on the southeastern and southwestern Cienega Basin watershed boundary. The areas southeast and southwest of these groundwater divides are inactivate, no-flow cells. Constant-head cells are located around the remainder of the active model area. The horizontal model layers create situations where the upper layers are above the land surface, so no-flow boundaries were assigned to cells above the land surface.

The hydraulic head assigned to the constant-head boundaries was based on contoured water levels (potentiometric surface elevation) from wells within and surrounding the model domain. Within the model domain, steady-state target water levels from M&A were used. These water levels are a revised version of target water levels used in the original M&A flow model (M&A, 2009b). A significant difference is that most of the original 67 springs were removed as target observations in the revised data set because their seasonal flow does not represent the regional groundwater flow system. Only water-level elevations from 2 perennial springs, Rosemont and Questa Springs, were retained. An initial Tetra Tech review of these water-level data indicated that it represented the best available data set. An additional data review removed potentiometric heads that might be affected by vertical hydraulic gradients and data from wells with marked upward or downward water-level trends. Data from wells with deep screened intervals were assumed to be influenced by vertical gradients, so they were also omitted. The resulting data set was used to develop a potentiometric surface map that represents the water-table elevation within the model domain.

Outside of the model domain, water-level data were obtained from the Arizona Department of Water Resources Well Registry Web (ADWR, 2010) and United States Geological Survey

(USGS, 2010c) databases. Water-level data were obtained for the surrounding Cienega Creek, Tucson, and Upper San Pedro Basins. These data were not rigorously reviewed; however, anomalous data were removed from the data set. These additional water-level data allowed contouring outside of the model domain, which reduced edge effects and minimized errors in the constant-head elevations.

Water-level contours for the larger regional area were created by kriging the data inside and outside of the model domain (Figure 11) using Surfer version 9, (Golden Software, 2009). The head values assigned to the constant-head boundary cells at the model perimeter were the average head within each cell, as determined from the potentiometric surface map.

3.0 Steady-State Model Calibration

The pre-mining, steady-state groundwater flow model provides hydraulic properties and initial hydraulic heads for the mining-phase flow. The steady-state model is calibrated to obtain a satisfactory match to existing water-level and stream-flow data. The calibration process and fitting the model to observed data provides confidence that the model parameters are appropriate for simulating mining and post-mining conditions. The steady-state groundwater flow model calibration and model fit are discussed in this section and the mining and post-mining model constructions are discussed in subsequent sections.

The objective of the model calibration was to 1) obtain appropriate model parameters that are representative of the hydrogeologic conditions and 2) simulate observed groundwater flow system water levels and stream flows. A measure of flow model accuracy and representativeness is the magnitude of the difference between observed and measured water levels, which are termed residuals. A good model fit minimizes the water-level residuals.

Stream flows were not quantitatively matched during calibration due to their low base flow rates (< 1 cfs). Stream flows in the model domain are largely controlled by the interaction of complex geology, incised stream channels, small groundwater level fluctuations, and stormwater runoff. Bedrock outcrops commonly force shallow groundwater to the surface where it flows until it is consumed by ET or infiltrates back into alluvial deposits or fractured bedrock. The regional model scale necessitates 800 foot x 800 foot model cells over most of the stream channel reaches. It is not possible to accurately represent the geologic complexity, stream-channel geometry, and precise water levels at this regional scale. Adjusting regional model parameters to match low stream flows resulting from unique and isolated hydrogeologic conditions would require complexity far greater than could be justified based on the available data and model resolution. Based on these conditions, a qualitative approach to matching stream flows in Davidson Canyon and Cienega Creek was employed. Large discrepancies between observed and simulated stream flows would be an indication of inaccurate model parameters and poor representation of the groundwater flow system that needed to be corrected.

The calibration approach consisted of iteratively using automated parameter estimation methods (Doherty, 2010) and manual calibration to achieve the calibration objectives and the best possible model fit.

3.1 Water-Level Targets and Weights

Water-level elevation data from 377 wells, 12 piezometers, and 67 springs within the model domain were evaluated for use as water-level (head) targets for calibration of the steady-state model. The initial water-level and well data set was provided by M&A (2009a) after they had re-evaluated the target data set used in their M&A (2009b) groundwater flow model. This data set had been repeatedly evaluated by M&A over the course of their investigations and was considered to be the best-available data.

Target water levels were weighted to reflect their relative value in the flow model calibration process. Water levels representative of steady-state, regional flow system conditions at specific depths were the most valuable and they were assigned the highest weighting. Water-level data of lesser quality and ambiguous regarding the conditions being monitored were assigned lower weights. These weights were used by the parameter estimation process when calculating the parameter values that result in the best model fit. Higher weighted targets were preferentially matched over the lower weighted targets.

Water-level targets were assigned calibration weights based on the following criteria:

- Availability and completeness of well construction information;
- Well completion interval depth and screen length;
- Water level trends; and
- Period of water-level data.

All targets were assigned to model layers based on the well completion and water-level data. Using the elevations of the screened interval, water level, and total depth, each well was assigned to the model layer containing:

1. the midpoint of the screened interval, for wells where both the top and bottom of the screen were known;
2. the midpoint between the water level and the well's total depth, for wells where the screened interval was unknown, but the water level and total depth were known; or
3. the water level, where the screened interval and total depth were unknown.

Data from wells screened across a single model layer, and with recent water level data, were assigned the highest weights. Data from wells screened over multiple layers, lacking construction information, exhibiting strong trends or large water-level fluctuations, or with water levels measured before 1980 were assigned lower weights. Data from wells in constant-head cells of the model were assigned a weight of zero, because the heads in those cells were not changed by the model calculations, and using the target heads in those cells would have skewed the model-calibration statistics. Rosemont and Questa Springs are considered perennial (Tetra Tech, 2010b) springs and they were assigned a weight of 0.5. This lower weight represents the uncertainty associated with the model layer it should be simulated. Ephemeral (seasonal or intermittent) springs were not retained in the target set or were assigned weights of zero. The water-level target weighting criteria is summarized in Table 4. Data for the wells and springs used as steady-state calibration targets are provided in Appendix B. Steady-state calibration head target locations and weights are shown on Figure 12.

Table 4. Weighting Criteria for Steady-State Calibration Water-Level Targets

Group	Weight	Criteria
1	1.0	Screened interval known and in one (1) model layer only
1	1.0	Screened interval is unknown but Total Depth and water level are both within one (1) model layer only
2	0.9	Screened interval known and across two (2) model layers
2	0.9	Screened interval unknown and TD and WL span two (2) model layers
3	0.8	Screened interval known and across three (3) model layers
4	0.5	Perennial springs
5	0.4	Screened interval known and across four (4) or more model layers
5	0.4	Screened interval unknown and total depth and water level span three (3) or more model layers
6	0.2	Water level only; total depth and screen depth unknown; model layer assigned based on water-level elevation
7	0	Water-level time series shows range >25 feet
8	0	Water-level time series shows range >50 feet
9	0	Water level time series shows strong trend upward or downward
10	0.5 X group weight	Water-level date before 1980 but otherwise acceptable
11	0	Rejected – water level time series shows large range and strong trend up or down or unexplained large recent change
12	0	Well located in constant-head cell; weight set to zero
13	0.5 X group weight	Flowing well (reported water level at or above ground surface (unless pressure transducer is known to be in well - i.e., PC-2 and PC-5)
14	0	Intermittent springs

3.2 Model Parameter Values

Hydrogeologic parameter values for many of the HGUs were obtained from analyzing the short-term and long-term aquifer tests conducted by M&A (M&A 2009a, 2009c). Analytical methods and numerical radial flow modeling (Tetra Tech, 2010c) were also used to estimate horizontal and vertical hydraulic conductivity. A literature review and professional judgment was used to assign initial values for HGUs that did not have parameter estimates from an aquifer test. The initial and final calibrated steady-state model parameter values are presented in Table 5.

Parameters not HGU specific, such as recharge, were modified during calibration and are discussed in detail later in this section. Constant heads and evapotranspiration values were not modified during calibration.

Table 5. Steady-State Model Initial and Calibrated Parameter Values

Zone	HGU	Initial Horizontal Hydraulic Conductivity (feet/day)	Initial Vertical Hydraulic Conductivity (feet/day)	Final Horizontal Hydraulic Conductivity (feet/day)	Final Vertical Hydraulic Conductivity (feet/day)
1	Qal	2.39E+02	2.39E+01	8.53E+01	3.87E+01
2	QTg	8.86E-01	8.86E-02	7.87E-01	5.58E-01
3	QTg1	2.00E-02	2.00E-03	1.64E-01	1.18E-02
4	QTg2	2.00E-03	2.00E-04	1.31E-02	6.56E-04
5	Tsp	1.71E-02	1.71E-03	1.64E-02	1.64E-04
6	Kti	3.28E-03	3.28E-03	1.31E-02	1.31E-03
7	Kv	2.39E-02	2.39E-03	8.53E-02	2.00E-02
8	Ksd	1.28E-01	1.31E-01	6.56E-02	4.92E-03
9	Pz	2.89E-02	6.89E-02	2.23E-02	1.08E-02
10	PCb	2.82E-03	2.82E-03	2.38E-03	2.38E-03
11	Pz_Pit	N/A	N/A	X - 3.28E-04 Y- 3.28E-03	3.28E-03
15	QTg_TB	N/A	N/A	3.61E-01	1.31E-01
Streambed	--	3.28E+00	--	6.56E+00	--
Zone	**HGU**	**Initial Conductance (day^{-1})**	**Initial Vertical Hydraulic Conductivity (feet/day)**	**Final Conductance (day^{-1})**	**Final Vertical Hydraulic Conductivity (feet/day)**
HFB	OPD*	3.28E-05 day^{-1}	--	3.28E-04 day^{-1}	--
Zone	**HGU**	**Initial Recharge (in/yr)**	**Initial Vertical Hydraulic Conductivity (feet/day)**	**Final Recharge (in.yr)**	**Final Vertical Hydraulic Conductivity (feet/day)**
Rch_2	--	0.35	--	0.33	--
Rch_3	--	0.39	--	0.37	--
Rch_4	--	0.43	--	0.42	--
Rch_5	--	0.50	--	0.53	--
Rch_6	--	0.63	--	0.68	--
Rch_7	--	0.68	--	1.31	--

*Quartz-porphyry dike

3.2.1 Horizontal Hydraulic Conductivity

Model calibrated horizontal hydraulic conductivity (K_h) values are reasonable based on estimates obtained from aquifer testing. The median, lower quartile, upper quartile, maximum and minimum horizontal hydraulic conductivity values from aquifer tests are illustrated on Figure 13. Calibrated model values are generally within the range of measured values (Figure 13). The exceptions are for Quaternary units that had limited aquifer test data, but can exhibit a wide range of hydraulic properties due to heterogeneous depositional environments. The calibrated hydraulic conductivity values for the Quaternary units are within the range of typical values. The Qal K_h-value was lowered during calibration to reduce the hydraulic gradient through this unit to better match water-level elevation data and stream flows. The QTg1 and QTg2 K_h-values were increased to better match water levels in Upper Cienega Basin. The initial values for these three (3) HGUs were based on short-term aquifer tests that only stressed a small portion of the aquifer near the pumping well. The changes during calibration are reasonable due to scale differences between the tests and the regional model. For K_h-values not derived from an aquifer test (i.e., Tsp, KTi, and pCb), professional judgment was used to adjust these values during calibration.

Two (2) additional material property zones were added during the model calibration. Based on hydraulic testing in HC-1B the north-south trending "Backbone Fault" along the ridge of the Santa Rita Mountains is a discrete zone of higher hydraulic conductivity within relatively low permeability bedrock. This area also has steeply dipping beds with nearly vertical bedding planes that create intervals of higher vertical hydraulic conductivity and lower horizontal hydraulic conductivity perpendicular to the orientation of the bedding planes. Hydraulic testing has indicated that the aquifer drawdown is greater than expected for an infinite-acting aquifer and does not fully recover due to pumping in the expected time. These observations indicate that the aquifer in this area is compartmentalized. The backbone fault, steeply dipping beds, and compartmentalization were simulated by creating a zone for Paleozoic units in the western side of the pit area (Zone 11 – Pz_Pit). The lower x-direction hydraulic conductivity zone assisted in increasing water levels in the pit area. This zone also included horizontal anisotropy with higher K_h in the y-direction, which is parallel to the fault's north-south strike. The relatively higher vertical hydraulic conductivity due to the steeply dipping beds was simulated by setting Kz equivalent to Ky, which are an order of magnitude higher than Kx.

Quaternary-Tertiary gravels in the Tucson Basin (Zone 15 – QTg_TB) were assigned a zone parameter to divide the QTg by hydrographic basin. Based on the type and size of sands and gravels observed from core and hydrogeologic data, the Tucson Basin has different lithology, hydraulic gradients, and water-level elevations than Cienega Basin. The K_h-distributions by model layer are illustrated on Figures 14 through 33.

3.2.2 Vertical Hydraulic Conductivity

Two (2) HGUs (Ksd and Pz) were analyzed using radial flow modeling to obtain vertical hydraulic conductivity (K_v) values (Tetra Tech, 2010c). Steady-state model calibrated K_v-values for Pz (0.01 and 0.003) fall within the range of values obtained from radial flow modeling (0.0013 to 0.35). The steady-state Ksd K_v-value (0.005), however, is slightly lower than values obtained from the radial flow modeling (0.006 to 2.8). The higher K_v-values were required in the radial flow modeling to simulate drawdown at depth or to match drawdown at observation wells completed within the steeply dipping beds present in these HGUs near the pit. In the steady-state model, the objective was to match water-level elevation data at a regional scale, not just at the pit. Lower K_v-values were needed to elevate water levels near the pit and to better match water levels across the model.

Differences between horizontal and vertical hydraulic conductivity values at a local scale (i.e., aquifer test) versus a regional scale (i.e., steady-state model) are common due to the small stress imposed on the groundwater system by pumping during a short-term aquifer test or the relatively low pumping rates (≤ 40 gallons per minute (gpm)) during the multi-well long-term test. The aquifer tests results are more representative of small areas of heterogeneous fractured rock, but the three-dimensional groundwater flow model is simulating a regional-scale equivalent porous medium.

Other K_v-values in the steady-state model were adjusted during calibration based on professional judgment. The initial range of K_v-values was one (1) to ten (10) times lower than the initial K_h-values. In the calibrated model, K_v-values were 1 to 100 times lower than the K_h-values. A larger anisotropy between horizontal and vertical hydraulic conductivity is required in the regional model to accurately match water levels and hydraulic gradients throughout the model domain. The need for lower K_v-values to maintain higher water levels than would be expected based on the steeply dipping HGUs could be due to the lack of faults simulated in the pit area. Aquifer-testing results indicated that the groundwater flow system was likely compartmentalized by low permeability faults. These faults may be limiting horizontal groundwater flow, which would tend to raise water levels. The distribution of K_v-values, by model layer, is also shown on Figures 14 through 33.

3.2.3 Recharge

Recharge estimates from previous investigations of areas within the model domain vary substantially. M&A (2009b) cited previous studies (M&A, 1985; ADWR, 2004; Freethey and Anderson, 1986) that presented recharge estimates ranging from 6,900 to 25,500 ac-ft/yr for the Cienega Creek basin, which is only part of the modeled area. This large range of estimated recharge values reflects uncertainty in the estimates. Modification of the initial recharge rates was used as a calibration tool to maintain a reasonable balance with simulated hydraulic conductivity values. However, calibration of the steady-state model required only relatively small changes to the initial recharge distribution. The total recharge calculated by the calibrated steady-state model was 9,909 ac-ft/yr, which is slightly lower than the initial total recharge of 10,100 ac-ft/yr.

The initial recharge distribution had 58 recharge zones due to the finely-divided recharge increments and numerous sub-basins. Preliminary model simulations indicated that this initial recharge distribution could be simplified by consolidating recharge into six (6) zones. This facilitated recharge adjustments on a zoned basis within the model. Zones were combined that had similar values based on natural breaks in the range of initial recharge values (0.33 to 0.68 in/yr). The most significant recharge adjustment was made in bedrock areas west and southwest of the Open Pit. Recharge was increased from the initial estimates of about 0.51 to 0.63 in/yr to final values of about 0.68 to 1.31 in/yr. The higher vertical permeability due to fractures and faults of the steeply-dipping bedrock in that area can accommodate higher rates of recharge. The simulated water levels in these areas were significantly below the observed (target) water levels when the initial recharge values were used. The increased recharge resulted in a much closer fit of modeled heads to the target heads. The distribution of recharge values in the calibrated steady-state model is shown on Figure 34.

3.2.4 Evapotranspiration

The EVT package was used to simulate ET in the Cienega Creek and Davidson Canyon areas. The ET rates and distribution presented by M&A (2009b) were incorporated into the flow model. No changes were made to evapotranspiration rates or extinction depths during model calibration. The total ET calculated by the calibrated steady-state model was 5,638 ac-ft/yr, which is consistent with the range of ET values reported by M&A (2009b).

3.2.5 Stream Flow

During model calibration, the streambed hydraulic conductivity was the only parameter modified as part of the SFR package. Streambed conductance, which is the streambed hydraulic conductivity multiplied by the area of the streambed divided by the streambed thickness, is a sensitive parameter in determining the amount of stream-aquifer interaction. There are considerable differences between the scale at which streambed conductance is typically measured and the scale at which it is applied in a flow model. Streambed conductance in groundwater flow models is often similar to hydraulic aquifer properties obtained from pumping tests. Streambed conductance data are not available within the regional model domain, so professional judgment was used to adjust this parameter during model calibration.

The initial streambed hydraulic conductivity was 3.28 feet per day (ft/d) and during calibration and was increased by a factor of two (2) to 6.56 ft/d (Table 5). The increase in streambed hydraulic conductivity allowed a better match to data from stream flow gages and water levels in wells completed in the Qal within the stream channels.

3.2.6 Quartz-Porphyry Dike

The HFB package in MODFLOW was used to simulate the quartz-porphyry dike. The hydraulic characteristic of the dike is defined as the hydraulic conductivity divided by the width and is a required input to the HFB package. The width of the dike was assumed to be 100 feet based upon the minimum width measured from geologic maps and observed in the field. The HFB is present in the model from land surface to the bottom of the model. The two (2) major mapped sections of the dike were simulated in the model. Hydraulic conductivity of the HFB was initially set to 3.28e-3 ft/d, which was the initial hydraulic conductivity for the intrusive HGU (KTi), this is equivalent to a hydraulic characteristic value of 3.28e-5 day^{-1}.

The HFB hydraulic characteristic (i.e., hydraulic conductivity divided by the width) was adjusted during model calibration to better match water-level elevation data on the up and down gradient sides of the quartz-porphyry dike. The final calibrated HFB hydraulic characteristic was 3.28e-4 day^{-1}, which is a significant barrier to groundwater flow. Including the HFB in the flow model allowed reasonable and consistent bedrock K-values to be simulated in the Davidson Canyon area. Before addition of the HFB, the model was under predicting water levels upgradient of the HFB and over predicting water levels down gradient of the HFB. The HFB improved the match to water levels on the up- and down gradient sides of the dike and improves the match to the observed hydraulic gradient in Davidson Canyon.

3.3 Steady-State Calibration Statistics

Several statistical measures were calculated to assess the quality of the steady-state model calibration. These calibration statistics are summarized in Table 6. Unweighted and weighted statistics are reported to provide a comparison between the model fit to all water-level targets (unweighted) and those targets that are most representative of the regional groundwater flow system (weighted). The goal of the calibration is to minimize the statistical values, since lower values represent a better fit to the observed conditions. The residual mean for this model calibration is slightly negative, indicating a slight model bias toward under predicting water levels. The difference between observed and simulated water levels is expected to be larger in a regional-scale model than a site-scale model. The calibration statistics for this regional model indicate an acceptable model fit at this scale. For example, the residual standard deviation divided by the range of observations is considered acceptable if it is below ten (10) percent (Anderson and Woessner, 1992). For the steady-state model, this value is below five (5) percent for both unweighted and weighted residuals. The residual sum of squares is meaningless by itself, but is useful in comparing the sensitivity of parameters in the model calibration. A complete parameter sensitivity analysis will be documented in a companion technical memorandum.

The spatial distributions of weighted and unweighted residuals are illustrated on Figures 35 and 36. The minimum and maximum residuals occur at wells where the hydraulic gradient is very steep or in flowing wells. These steep hydraulic gradients and flowing wells occur in the Santa Rita Mountains, particularly near the Open Pit. Several wells near the Open Pit have water-level elevations near land surface or flowing, which is several hundred feet above nearby measured water levels considered to be representative of regional groundwater flow system.

The comparison between observed and simulated water-level elevations for the steady-state model is shown on Figure 37. A perfect model fit would have all of the data plotting on the 1:1 line. A good model fit is indicated by the data points being well distributed above and below the 1:1 line with slightly more points below the line. This indicates a small negative model bias due to simulated water levels being below the observed water levels. This bias is evident near the pit area where the model tends to under predict water levels due to the measured water levels near or above land surface. A random pattern on the observed water levels versus unweighted residuals is shown on Figure 38, which indicates a good calibration. An accurate steady-state model tends to have unweighted residuals that are randomly distributed and do not display consistent spatial trends.

Table 6. Steady-State Model Calibration Statistics

Statistic	Unweighted (ft)	Weighted (ft)
Residual Mean	-1.18	-4.47
Residual Standard Deviation	133.12	90.17
Absolute Residual Mean	97.61	55.05
Residual Sum of Squares	6.60E+06	996E+05
RMS Error	133.12	90.28
Minimum Residual	-333.88	-333.88
Maximum Residual	465.77	465.77
Range of Observations	2,886.19	2,886.19
SD/Range as a percentage	4.6%	3.1%

3.4 Model Results

A summary of the steady-state model mass balance is presented in Table 7. Due to the steep hydraulic gradients and low permeability rocks that exist in the model domain, the PCG4/5 solver was critical in obtaining a stable solution that converged with approximately zero percent discrepancy between inflows and outflows. Over 60 percent of the water budget is from groundwater flow in and out of the model through the external model boundaries simulated as constant heads.

The contoured simulated water levels are compared to the observed water levels on Figure 39. The observed water level contours include all measurements (i.e., low and high weights). The simulated contours follow the general trends displayed with the observed water-level contours. Discrepancies exist typically along drainage channels and the pit area where the model had difficultly matching the steep hydraulic gradients.

The simulated stream flows versus the observed base flows for USGS gages within the model domain are shown on Figure 40. Simulated stream flow values are presented as the cumulative net stream flow at each stream segment. The model over predicts flow at the gages, but this is a reasonable match to the low observed discharge.

Table 7. Summary of Mass Balance for Steady-State Model

Cumulative	Rate [ft^3/d]	Rate [ac-ft/yr]
IN	5,096,910	42,738
Evapotranspiration	0	0
Recharge	1,181,704	9,909
Streams	995,072	8,344
Constant Head	2,920,134	24,485
OUT	5,096,912	42,738
Evapotranspiration	672,391	5,638
Recharge	0	0
Streams	1,307,318	10,962
Constant Head	3,117,202	26,138
IN - OUT	-.2.0	0
PERCENT DISCREPANCY	0.00	0.00

4.0 Development of the Transient Models

The predictive models utilize two (2) transient models to evaluate the interaction between the groundwater flow system and the Open Pit. The first predictive model simulates the period of mine operations when there will be active dewatering of the Open Pit. The second predictive model begins simulating the combined groundwater – pit lake system beginning at the end of mining operations when active dewatering has ceased and the pit begins filling with water. The models are based on the calibrated steady-state model, but incorporate different MODFLOW packages to simulate the hydraulic stresses created by the presence of the pit. The MODFLOW drain (DRN) package was used to simulate pit dewatering. The LAK2 package (Council 1999) was used to simulate the interaction between the pit lake and aquifer in the post-mining predictive model. These models utilize the adaptive time-stepping and output control package (ATO4) and the PCG5 solver for MODFLOW-SURFACT (Hydrogeologic, 2010). For each transient model, a base-case model without the hydraulic stresses associated with the Open Pit was simulated for the same time period with the same solver parameters. This permits a direct comparison of the simulated effects due to the Open Pit versus a simulated scenario with no Open Pit.

4.1 Hydraulic Parameters for Transient Simulation

The absence of observed long-term, regional stresses in the groundwater flow system prevented a traditional transient regional model calibration. Hydraulic conductivity values obtained during the steady-state flow model calibration were therefore directly used in the predictive models (Figures 14-33).

4.1.1 Storage Parameters

Predictive transient models are time dependant and require that aquifer storage parameters be defined. Three (3) parameters are required for these transient simulations: Storativity, Specific Storage, and Specific Yield. Specific Yield is the volume of water that an unconfined aquifer releases from storage per unit surface area of the aquifer per unit decline in the water table. Specific Storage applies to confined aquifers and is the volume of water released from storage under a unit decline in hydraulic head. These input parameters are used to determine the Storativity for each model cell.

Site-specific information for specific storage in the bedrock aquifer comes primarily from analysis of the 30-day pumping test (Tetra Tech, 2010c). The specific storage estimates obtained from the radial flow modeling ranged from $7x10^{-7}$ to 0.004 per foot, with a geometric mean of $9.84\ x10^{-6}$ per foot. The geometric mean from the multiple Willow Canyon specific storage values was obtained first to prevent over-representing that unit. The Willow Canyon's geometric mean was used in the subsequent bulk geometric mean calculation. The specific storage ($9.84x10^{-6}$ per foot) estimate was used for all bedrock units in the transient three-dimensional groundwater flow modeling. The specific storage estimates indicated there was high variability and that a bulk estimate for all bedrock units would be the most appropriate approach. Variability in the specific storage estimates will be accounted for in the sensitivity analysis. The specific yield of the bedrock was estimated to be one (1) percent based on the relatively low fracture density throughout most of the bedrock. Similar to specific storage, a range of specific yield values will be simulated for the bedrock in the sensitivity analysis.

The specific storage of the alluvial materials is largely untested and likely highly spatially variable due to the observed variation in lithologic facies. Estimates from studies in similar geologic settings were used to guide the initial specific storage estimate. The groundwater flow model for the Upper San Pedro Basin utilizes a specific storage of $6.56\ x\ 10^{-5}$ per foot for interbedded Upper Basin fill (Pool and Dickinson, 2007). The specific yield of the near surface basin fill varies spatially with higher hydraulic conductivity zones having higher specific yields that range from five (5) percent to 15 percent. The storage parameter zones for the alluvial and bedrock units are presented in Table 8.

The effect of storage parameter variability will be assessed in the sensitivity analysis. The sensitivity simulations will bracket a range of potential storage values, which will produce a corresponding range of aquifer diffusivity that will govern the rate of drawdown propagation. The long-term, post-mining simulation results will represent steady-state conditions that are not dependant on storage parameters, so the long-term drawdown will be insensitive to the storage parameter values.

Table 8. Storage Parameters Simulated in the Mining-Phase and Post-Mining Phase Predictive Flow Models

Zone	HGU	Specific Storage (ft^1)	Specific Yield
1	Qal	6.56e-5	0.15
2	QTg	6.56e-5	0.1
3	QTg1	6.56e-5	0.05
4	QTg2	6.56e-5	0.05
5	Tsp	9.84e-6	0.01
6	Kti	9.84e-6	0.01
7	Kv	9.84e-6	0.01
8	Ksd	9.84e-6	0.01
9	Pz	9.84e-6	0.01
10	PCb	9.84e-6	0.01
11	Pz_Pit	9.84e-6	0.01
15	QTg_TB	6.56e-5	0.1

4.1.2 Recharge

The simulations of mining and post-closure conditions included the effects that the Open Pit, waste rock pile, tailings pile, and flow-through drains would have on recharge. Changes from the recharge used in the steady-state calibration were made only in the vicinity of those features (Figure 41).

Dewatering of the pit during the mining phase will effectively negate recharge in the Open Pit area. The Open Pit was simulated as a series of drain cells with heads approximately 50 feet below the bottom of the pit. These drain cells remove all recharge entering the pit area. Similarly in the post-mining phase when recovery of groundwater levels in the pit area results in formation of a pit lake, the pit will serve as a groundwater sink. Although precipitation falling directly on the lake surface would recharge the lake, and by implication the groundwater system, evaporation from the lake surface will greatly exceed precipitation and will result in a net loss of water. Post-mining recharge below the final pit lake level was set to zero. The detailed water balance in the pit area was simulated with MODFLOW's LAK2 package and it is discussed in subsequent sections.

Post-closure recharge in the Rosemont Ridge landform area, which includes a waste rock storage area and a dry-stack tailings facility, will be affected by those features. Previous modeling of both features (AMEC, 2009; Tetra Tech, 2010d; Tetra Tech, 2010e) indicated that post-mining precipitation-related recharge beneath the footprint of the dry-stack tailings and the waste rock will be zero. Consequently, the pre-mining precipitation-related recharge in those areas was removed and was replaced by recharge as described below.

The dry-stack tailings will contain excess water when initially placed, which will result in recharge to the groundwater system from the tailings drain-down (AMEC, 2009). The recharge resulting from tailings drain-down was distributed uniformly throughout the tailings footprint and temporally at rates based on information presented by AMEC (2009, Figure 6.8). The temporal allocation of recharge from drain-down during the post-mining period was divided into six (6) periods: five (5) periods of 100 years each, during which the recharge from drain-down was decreased step-wise from the initial 8.4 gpm (13.6 ac-ft/yr) to zero at 500 years, and a final period after 500 years, during which there was no recharge from drain-down. The recharge rate shown on Figure 41 for the dry-stack tailings is the initial recharge rate due to tailings drain-down. Figure 42 shows the drain-down curve developed by AMEC (2009) and the step-wise recharge simulated in the model.

A network of flow-through drains is planned beneath the waste rock and tailings areas to direct stormwater flows down gradient and past the piles. The main segments of the drain system, which are primarily beneath the tailings, will result in recharge to the groundwater system from infiltration of stormwater runoff in the drains (Tetra Tech, 2010d; Tetra Tech, 2010e). Recharge rates in the flow-through drains were based on the results of Tetra Tech (2010e) modeling, which assigned infiltration values to each of the major segments of the drain system (N1, N2, N3, S1, S1C, and S2; Figure 42). Recharge from infiltration through the drain system totals 273.5 ac-ft/yr, as compared to the total pre-mining recharge of about 40 ac-ft/yr within the dry-stack tailings footprint and about 208 ac-ft/yr within the waste rock storage area footprint. This results in a net increase in recharge of about 25 ac-ft/yr under the tailings area.

Recharge values for the model were calculated by distributing the infiltration over the entire lengths of the drains, including the North Main and South Main. Recharge was allocated in proportion to the lengths of the individual segments (Table 9). For input to the model, the post-mining recharge in the model cells containing flow-through drains in the dry-stack tailings area was the sum of the time-varying recharge from tailings drain-down and the recharge from infiltration through the drain system.

A stormwater runoff diversion channel around the pit will have a containment pond (Pond PCA-2) near the southwest edge of the waste rock storage area (Figure 41). Stormwater runoff infiltration in Pond PCA-2 will also be a source of recharge. An average of 56.21 ac-ft/yr of infiltration was estimated for the pond (Tetra Tech, 2010e). This recharge was distributed over the model cells containing the pond, resulting in a recharge rate of 61.1 in/yr within those model cells (Figure 41).

Overall, the recharge the mine facilities area will increase about 81 to 95 ac-ft/yr after mining, due to recharge via the flow-through drain system, containment pond PCA-2, and drain-down of the tailings. The total estimated recharge is about 249 ac-ft/yr pre-mining versus 343 to 330 ac-ft/yr post-mining.

Recharge resulting from infiltration due to the heap leach and other facilities was not simulated. The low infiltration rates and short-time periods that these facilities would be active would not alter the long-term simulation results. Any recharge due to these facilities would offset groundwater that would otherwise be captured from other sources. Not including these small potential recharge sources theoretically results in more drawdown, but in reality the differences would be indiscernible.

Table 9. Distribution of Recharge Within Rosemont Ridge Landform Flow-Through Drain System

Flow-Through Drain Segment	Segment length (ft)	Infiltration (ac-ft/yr)	Allocated Infiltration (ac-ft/yr)	Area in model (ft^2)	Recharge Rate from Infiltration in Flow-Through Drain (in/yr)
N1	2,200	137.05	41.42	1,132,519	1.59
N2 + N3	3,880	45.33	19.63	2,126,122	0.40
North Main	5,080		121.33	2,047,633	2.58
S1 (inlet to S. Main)	2,880	41.80	14.54	1,190,847	0.53
S1C (to confluence with S1)	2,920	8.67	3.04	1,022,019	0.13
S2 (waste rock area only)	1,680	11.16	2.65	406,931	0.28
S2 (tailings area only)	4,440	29.49	13.31	2,089,666	0.28
South Main	5,400		57.58	2,723,504	0.92
TOTALS	28,480	273.50	273.50	12,739,241	

5.0 Mining Phase Groundwater Flow Model

A mining-phase model was developed to simulate the flow system's response to stresses from pit dewatering. The mining phase model was developed to coincide with the Mine Plan of Operations (MPO) (Westland, 2007). The deepening and expansion of the Open Pit and the preliminary pit dewatering plan (Call & Nicholas Inc., 2010) were incorporated.

5.1 Model Construction

A combination of wells, horizontal drains, and sumps are planned for use in the dewatering of the pit (Call & Nicholas Inc., 2010). This dewatering was simulated in the mining-phase model using the drain boundary condition. The drains are useful for simulating the effects of dewatering a pit because they only remove water from the groundwater system when heads in the adjoining cells are greater than an elevation just below the pit. Drain cells can also be easily modified to account for deepening of the pit. Model nodes simulated as drain cells are illustrated in the final pit shell (Figure 43).

Based on the MPO (Westland Resources, 2007), the mining phase is expected to last for a period of 22 years. This mining period was subdivided into 12 phases or stress periods in the mining-phase flow model (Table 10). The progressive deepening of the Open Pit and its simulation in the mining-phase flow model is illustrated on Figure 44.

Table 10. Mining Model Stress Period Set-Up

Stress Period	Time Length [days]	Maximum Pit Depth [ft amsl]	Stress Period	Time Length [days]	Maximum Pit Depth [ft amsl]
1	365	5200	7	730	3650
2	731	4600	8	731	3650
3	730	4300	9	730	3550
4	731	4250	10	731	3400
5	730	4100	11	730	3250
6	731	3800	12	366	3050
			Total	**8036**	

The Drain Package was developed by intersecting the model grid with the three-dimensional pit shells developed from the mine plan for each stress period. The pit shell at the end of each stress period is used for the entire length of the stress period (start to finish). Drains were assigned to each layer based on the elevation determined by intersecting the grid with the pit shell. An additional 33 to 65 feet was subtracted from this elevation to create a more realistic cone of depression and to ensure that the pit was dewatered below the pit bottom. The drain configuration changes with increasing pit depth by lowering the drain elevations over time.

Achieving full pit dewatering required additional drains to “fill in” the entire pit volume. These “infill” drains have a drain elevation equal to an average pit low point. A total of 4,560 drain cells are used to simulate the dewatering of the pit. The low hydraulic conductivity of the bedrock within the pit still created instances where the water was not draining from some model cells. These rocks within the pit will be physically removed by mining, so the hydraulic conductivity of these cells was increased to 6.6 ft/day to facilitate dewatering. The results indicate that pit dewaters in an appropriate manner and that the final pit shell is dewatered below the final footprint of the pit.

6.0 Post-Mining Groundwater Flow Model

Predictive simulations of post-mining conditions were completed by modifying the numerical models previously discussed. These modifications were made to simulate post-closure conditions related to recharge and pit-lake development. Recharge was modified to incorporate the post-mining waste rock pile, tailings pike, and flow-through drains. The pit lake water balance is simulated with the LAK 2 Package (Council, 1999).

6.1 Pit Lake Water Balance

Upon cessation of mining activities and active pit dewatering, the pit will begin to fill with water. The rate at which the pit fills and the ultimate depth and stage of the pit lake are dependant on the pit lake water balance. The water balance of a pit lake describes how water flows into and out of the lake. Depending on the relative magnitudes of these flows, a pit lake will form or the pit could remain dry. Conceptually, the post-closure water balance for the Rosemont Pit can be expressed as:

$$\Delta_{\text{pit lake volume}} = I_{precip} + I_{runoff} + I_{\text{pit runoff}} + GW_{inflow} - E_{pit} - GW_{outflow} \qquad \text{(Eqn. 1)}$$

where:

I_{precip} is the inflow from direct precipitation falling on the lake surface;

I_{runoff} is the inflow from runoff from upgradient drainages (no runoff from drainages beyond the pit catchment are planned for the reclaimed post-mining pit);

$I_{\text{pit runoff}}$ is the inflow from pit wall runoff (the fraction of precipitation falling on the pit walls that ultimately reaches the pit lake);

GW_{inflow} is the groundwater inflow to the pit lake;

E_{pit} is the open water evaporation from the pit lake surface based on a modified pan evaporation rate; and

$GW_{outflow}$ is the outflow of groundwater from the pit lake.

The interaction between these parameters for a terminal pit, which has no groundwater outflow ($GW_{outflow} = 0$), is presented schematically on Figure 45.

There are two (2) types of pit lakes: terminal sink and flow through. A terminal-sink pit lake has no groundwater leaving the pit (Eqn 1: $GW_{outflow} = 0$). A flow-through pit has a component of groundwater leaving the pit (Eqn 1: $GW_{outflow} > 0$). Evaporation must be greater than the sum of precipitation, runoff, and groundwater inflow for a terminal pit lake to form. This water balance is solved in the groundwater flow model using the LAK2 package (Council, 1999). The stabilized lake stage dictates the steady-state groundwater inflow and the long-term drawdown associated with the perpetual pit lake.

Due to the steep, roughly cone shaped walls of the proposed Open Pit, the surface area of the pit lake is initially small, but as the lake stage rises, the surface area increases. The evaporation losses increase as the surface area increases. The lake level will stabilize when the evaporation rate equals the sum of the inflow components.

6.2 Pit Lake Simulation

The LAK2 package was selected to simulate the pit lake because it can calculate the transient stage of a pit lake as it fills, determine groundwater inflow or outflows across multiple model layers, and was found to be more numerically stable then the LAK3 package. Application of the LAK2 package allows for coupling between the lake water balance and the groundwater flow model, which allows for the lake stage to vary according the hydraulic stresses applied to the aquifer and the lake water budget. The inputs and outputs for the LAK 2 package are:

- Direct precipitation onto the lake (L/T);
- Lake Evaporation (L/T);
- Runoff into the pit (L^3);
- Pit Wall Runoff (L/T); and
- Conductance values for LAK cells (L/T).

A three-dimensional representation of the final pit was developed (Westland, 2007) and model cells adjacent to the exterior of the pit were designated as “lake cells”. The lake cell conductance was set equal to or greater than the conductance of the adjacent aquifer material. The bottom of the lake was set to the base of the pit at 3,050 feet amsl, so the lake cells span 15 model layers (Figure 46). The top elevations of the bottom cells of the lake were set to the elevation of the grid node when intersected with the pit shell. In this way, the lake cells, stage-area, and stage-volume relationships are refined beyond the vertical discretization of the model grid. The stage-volume relationship generated by the LAK2 package is a function of the simulated lake cell areas for each layer and the layer thickness. The stage-volume relationship simulated by the LAK2 package was checked against the elevation-volume relationship of the final pit shells and was found to accurately represent the Open Pit. Similarly, accurate simulation of the stage-area relationships is essential to accurately predicting evaporation, precipitation and pit wall run-off. The simulated and stage-area relationship compared to the MPO is provided on Figure 47**.**

The groundwater inflow into the pit varies depending on heads in the surrounding aquifer cells, lake stage, and cell conductance. The conductance of the lake cells was based on the aquifer materials properties and the grid block geometry.

Precipitation is estimated to be 17.37 inches per year for the Rosemont Site (Tetra Tech, 2009). Annual pan evaporation is estimated to be 71.52 inches per year (Tetra Tech, 2009). The conversion of pan evaporation to free surface lake evaporation is complex due to the heat-storage capacities between the lake and the pan. Water depth, heat-storage capacity of surrounding materials, exposure of the pan to the sun and air influence the estimated evaporation. These factors significantly affect the energy balance, elevating warm-season average temperature and vapor pressure of the water surface of a pan relative to a lake (Dingman, 1994). The conversion from pan evaporation to lake evaporation was estimated using a pan coefficient of 0.7.

Precipitation falling on the catchment of the pit that does not infiltrate, pond, or evaporate will runoff the pit walls and flow towards the lake at the base of the pit. This parameter is known as the pit wall runoff coefficient, and is estimated to be 30%. In practice, this parameter will vary over time as the pit fills, but 30 percent is a reasonable estimate for this climate.

The input values for the LAK2 package do not explicitly match the values presented above. The input for precipitation in the LAK2 package results in the precipitation rate being assigned to the entire footprint of the lake catchment. However, only 30 percent of the water falling on the pit walls is estimated to reach the lake. Furthermore, 100 percent of the precipitation on the lake surface must be accounted for in the water balance. This is accomplished by using the precipitation input parameter for defining the 30 percent of precipitation for the LAK2 area catchment (value of 5.21 inches/year). The second step is to account for the precipitation and evaporation over the lake, as dictated by the lake surface area for a given time step. The evaporation parameter is defined as a rate and only affects the surface area of the lake. Therefore, a net average annual evaporation rate is defined as the input. This parameter is defined as the lake evaporation rate minus 70 percent of the precipitation rate, since 30 percent of the precipitation was already applied as part of the precipitation input parameter).

$$\text{NET LAKE EVAPORATION} = \text{LAKE EVAPORATION} - 0.70(\text{PRECIPITATION}) \qquad \text{(Eqn 2)}$$
$$= 50.06 \text{ in/yr} - 12.16 \text{ in/yr} = 37.9 \text{ in/yr}$$

The final step is assigning any runoff to the lake not already included. No stormwater diversions are expected to flow into the pit from beyond the pit catchment area. The total pit catchment area based on the pit shells is 702.7 acres, but the catchment simulated in the model is 501.1 acres. The area difference is due to dry model layers not being included in the LAK2 package area calculation. The lake footprint in layer 3 is used for layers 1 and 2, even though the pit area is increasing in these layers. Some of the precipitation falling on this area will flow towards the pit, so the pit wall runoff coefficient of 30 percent was assumed. The total runoff is 54.3 gpm.

6.3 Stress Period Set-up

The pit lake is expected to reach steady state within 1,000 years of mine closure based on simulations conducted with M&A's post-mining model. Thus, a 1,000 year simulation period was selected for the post mining model. This simulation period was divided into six (6) stress periods (Table 11). The stress periods coincide with the transient recharge conditions associated with the dry stack tailings facility drain-down.

Table 11. Post Mining Simulation Stress Period Set-Up

Stress Period	Time Length [years]	Maximum Time Step [days]
1	100	30
2	100	90
3	100	90
4	100	90
5	100	90
6	500	365

7.0 Summary

Tetra Tech has constructed regional groundwater flow models of the Rosemont Project area. These groundwater flow models will be used to assess the potential impacts to the water resources resulting from the Rosemont Copper Project. A steady-state groundwater flow model has been constructed and calibrated to the best-available water-level data. Stream-flow data were used qualitatively in the calibration process to ensure that the flows and controlling geology were adequately simulated. Calibration statistics and the simulated potentiometric surface indicate that the flow model adequately represents the regional groundwater system.

A mining-phase groundwater flow model, based on the steady-state model, was constructed using drain cells to simulate the Open Pit dewatering process. The post-mining phase conditions were also simulated. Refilling of the Open Pit after the end of active dewatering was simulated using the LAK2 package. Recharge was modified in the post-mining phase flow model to simulate changes caused by the waste-rock pile, tailings drain down, tailings flow-through drains, and the pit diversion catchment pond. These facilities resulted in a net increase of approximately 81 ac-ft/yr of recharge.

Companion Technical Memoranda documenting the predicted impacts and results of the model sensitivity analyses will be submitted separately.

8.0 References

AMEC Earth & Environmental, Inc. (2009). *Dry Stack Tailings Storage Facility, Final Design Report*. Prepared for Rosemont Copper Company. Report dated April 15, 2009.

Anderson, T.W., 1995. Summary of the Southwest Alluvial Basins, Regional Aquifer System Analysis, South-Central Arizona and Parts of Adjacent States: U.S. Geological Survey Professional Paper 1406-A, pp. A1-A33.

Anderson, M. P. & Woessner W. W. 1992, Applied groundwater modeling simulation of flow and advective transport. Academic Press.

Arizona Department of Water Resources, 2004, Rural Water Resources 2003. Questionnaire Report: Rural water resources study, ADWR Office of Regional Strategic Planning.

Arizona Department of Water Resources (ADWR), 2010. Well Registry Web. Online link: https://gisweb.azwater.gov/waterresourcedata/WellRegistry.aspx

Bota, L. (1997). *Modeling of groundwater flow and surface/groundwater interaction for upper Cienega Creek basin*: Master of Science Thesis, Department of Hydrology and Water Resources, University of Arizona, July 25, 1997.

Chong-Diaz, D. (1995). *Modeling of stream aquifer interaction in lower Cienega Creek basin using a finite element technique*: Master of Science Thesis, Department of Hydrology and Water Resources, University of Arizona, May 1995.

Daffron, W.J., Metz, R.A., Parks, S.W., and Sandwell-Weiss, K.L., 2007. Geologic report, relogging program at the Rosemont porphyry skarn copper deposit, Augusta Resource Corporation: Augusta Resource Corporation, March 2007.

Drewes, Harald (1972). Structural Geology of the Santa Rita Mountains, Southeast of Tucson, Arizona. U.S. Geological Survey Professional Paper 748. 35 p.

Ferguson, C.A. (2009). *Bedrock Geologic Map of the Northern Part of the Empire Ranch 7 ½' Quadrangle, Pima County, Arizona*: Arizona Geological Survey Open-File Report OFR-09-05, scale 1:24,000.

Ferguson, C.A., Youberg, A., Gilbert, W.G., Orr, T.R., Richard, S.M. and Spencer, J. (2001). *Geologic Map of the Mount Fagan 7.5' Quadrangle, Eastern Pima County, Arizona*. Arizona Geological Survey Digital Geologic Map 11. November 2001.

Freethey, G.W., and Anderson, T.W., 1986, Predevelopment hydrologic conditions in the alluvial basins of Arizona and adjacent parts of California and New Mexico: U.S. Geological Survey Hydrologic Investigations Atlas HA-664, 3 pl.

Johnson, B.J., and Ferguson, C.A., 2006. Geologic map of the Rosemont area, northern Santa Rita Mountains, Pima County, Arizona: Arizona Geological Survey Digital Geologic Map 59, version 1.0 (preliminary). December 2006.

Knight, E.L. (1996). *A water budget and land management recommendations for upper Cienega Creek basin*: Master of Science Thesis, Department of Hydrology and Water Resources, University of Arizona.

Maxey, G.B. and Eakin, T.E., 1949, Groundwater in White River Valley, White Pine, Nye and Lincoln Counties, Nevada: Water Resources Bulletin No. 8, State of Nevada.

Montgomery & Associates (1985). *Water adequacy report, Stage One Development, Empirita Ranch area, Pima County, Arizona*: prepared for submittal to Arizona Department of Water Resources by Errol L. Montgomery & Associates, Inc. Report dated January 24, 1985.

Montgomery & Associates, Inc. (M&A) (2009a). *Results of Phase 2 Hydrogeologic Investigations and Monitoring Program, Rosemont Project, Pima County, Arizona*. Prepared for Rosemont Copper Company. Report dated February 26, 2009.

Montgomery & Associates (2009b). *Groundwater Flow Modeling Conducted for Simulation of Proposed Rosemont Pit Dewatering and Post-Closure*. Prepared for Rosemont Copper Company. Report dated October 28, 2009.

Montgomery & Associates (2009c). *Analysis of Long-Term, Multi-Well Aquifer Test – November 2008 through January 2009, Rosemont Project, Pima County, Arizona*. Prepared for Rosemont Copper Company. Report dated October 28, 2009.

Pool, D.R., and Dickinson, J.E., 2007, Ground-water flow model of the Sierra Vista Subwatershed and Sonoran portions of the Upper San Pedro Basin, southeastern Arizona, United States, and northern Sonora, Mexico: U.S. Geological Survey Scientific Investigations Report 2006-5228 48 p.

PRISM Group at Oregon State University (PRISM), 2009. Average Annual Precipitation (30-Year Average, 1971 - 2000). Online link: http://www.prism.oregonstate.edu/products/viewer.phtml?file=/pub/prism/us_30s/grids/ppt/Normals/us_ppt_1971_2000.14.gz&year=1971_2000&vartype=ppt&month=14&status=final.

Prudic, D.E., L.F. Konikow, and E.R. Banta (2004). *A New Streamflow-Routing (SFR1) Package to Simulate Stream-Aquifer Interaction with MODFLOW-2000*. U.S. Geological Survey Open-File Report 2004-1042.

Shah, N., M. Nachabe and M. Ross (2007). *Extinction Depth and Evapotranspiration from Ground Water under Sselected Land Covers*. Ground Water, vol. 45, no. 3, pp. 329 – 338.

Spencer, J.E., Ferguson, C.A., Richard, S.M., Orr, T.R., Pearthree, P.A., Gilbert, W.G., and R.W. Krantz, Arizona Geological Survey, Digital Geologic Map 10, September, 2001.

Tetra Tech (2009), *Rosemont Copper Project Design Storm and Precipitation Data/Design Criteria*. Internal Technical Memorandum. Technical Memorandum dated July 3, 2010.

Tetra Tech (2010a), *Hydrogeologic Framework Model*. Internal Technical Memorandum. Technical Memorandum dated July 3, 2010.

Tetra Tech (2010b). *Davidson Canyon Hydrogeologic Conceptual Model and Assessment of Spring Impacts*. Prepared for Rosemont Copper Company. Report dated April 2010.

Tetra Tech (2010c). *Hydraulic –Property Estimates*. Prepared for Rosemont Copper Company. Technical Memorandum dated July 9, 2010.

Tetra Tech (2010d). *Infiltration, Seepage, Fate, and Transport Modeling Report*. Prepared for Rosemont Copper Company. Report dated February 2010.

Tetra Tech (2010e). *Rosemont Infiltration Analysis*. Technical Memorandum to Kathy Arnold (Rosemont Copper Company). Technical Memorandum dated April 5, 2010.

United States Department of Agriculture Natural Resources Conservation Service (NRCS), 2008. Soil Survey Geographic (SSURGO) database for Pima County, Arizona, Eastern Part (AZ669). Online link: http://SoilDataMart.nrcs.usda.gov/.

United States Department of Agriculture Natural Resources Conservation Service (NRCS), 1986. Urban Hydrology for Small Watersheds. Technical Release 55 (TR-55). June 1986.

United States Department of Commerce National Climatic Data Center (NCDC), 2009. NCDC Climate Data Online, Santa Rita Exp Range, AZ, COOP ID 027596, May 1950 to February 2010 Daily Precipitation Data. Online link: http://cdo.ncdc.noaa.gov/pls/plclimprod/poemain.cdobystn.

U.S. Geological Survey (USGS) (2010a) National Map Seamless Server, 2010. 1/3” National Elevation Dataset (NED). Online link: http://seamless.usgs.gov/website/seamless/viewer.htm.

United States Geological Survey (2010c). Well Data. Online link: https://gisweb.azwater.gov/waterresourcedata/GWSI.aspx

United States Geological Survey (2010b). National Hydrographic Dataset. Online link: http://nhd.usgs.gov/data.html

WestLand Resources, Inc. (2007) Rosemont Project Mine Plan of Operations. Prepared for Augusta Resource Corporation. Report Dated July 11, 2007.

FIGURES

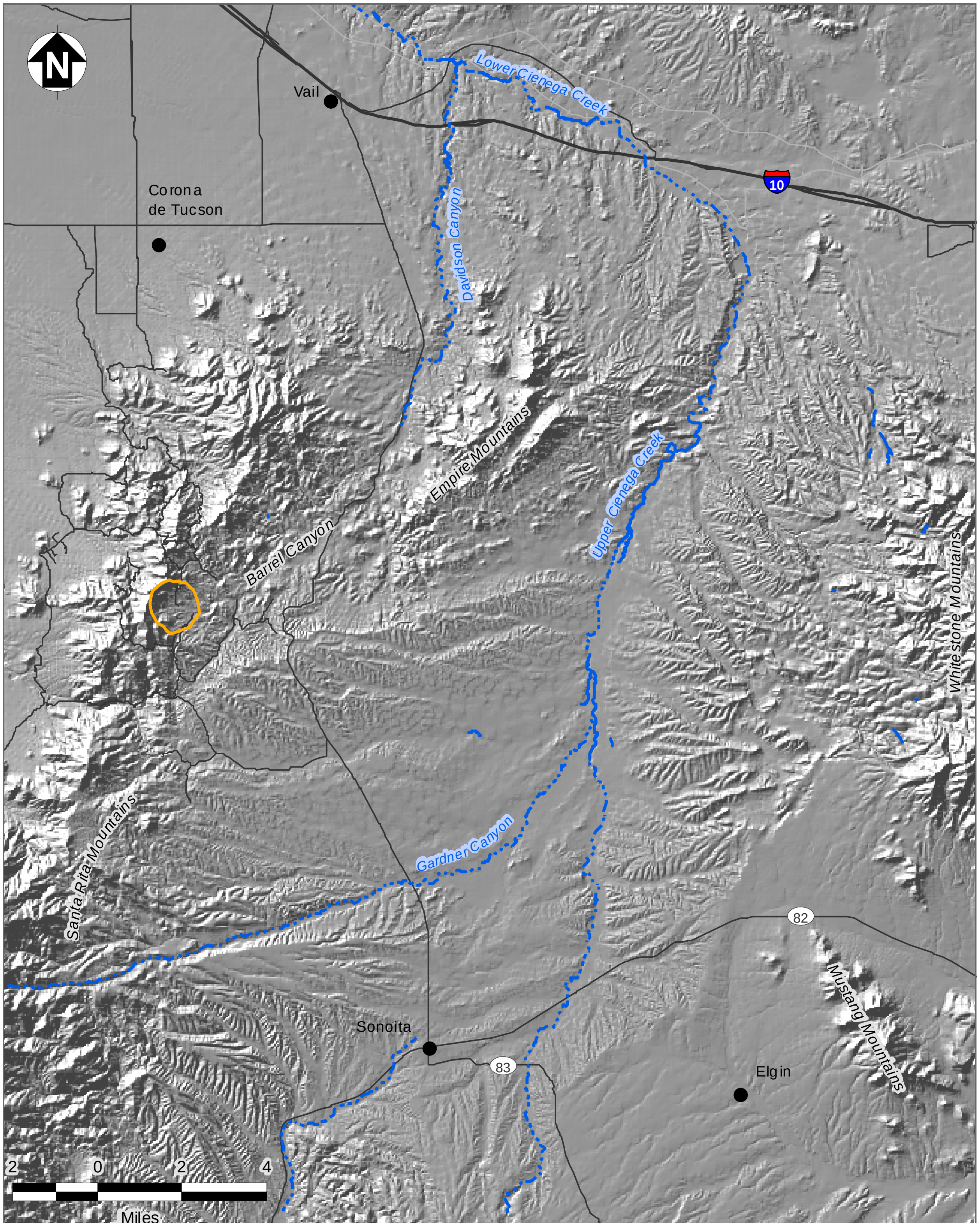

Legend

Perennial Stream

Ephemeral Drainage

Railroad

Proposed Rosemont Open Pit

Roads

Towns

TETRA TECH

ROSEMONT COPPER

FIGURE 1. SITE LOCATION MAP

2010-07-16

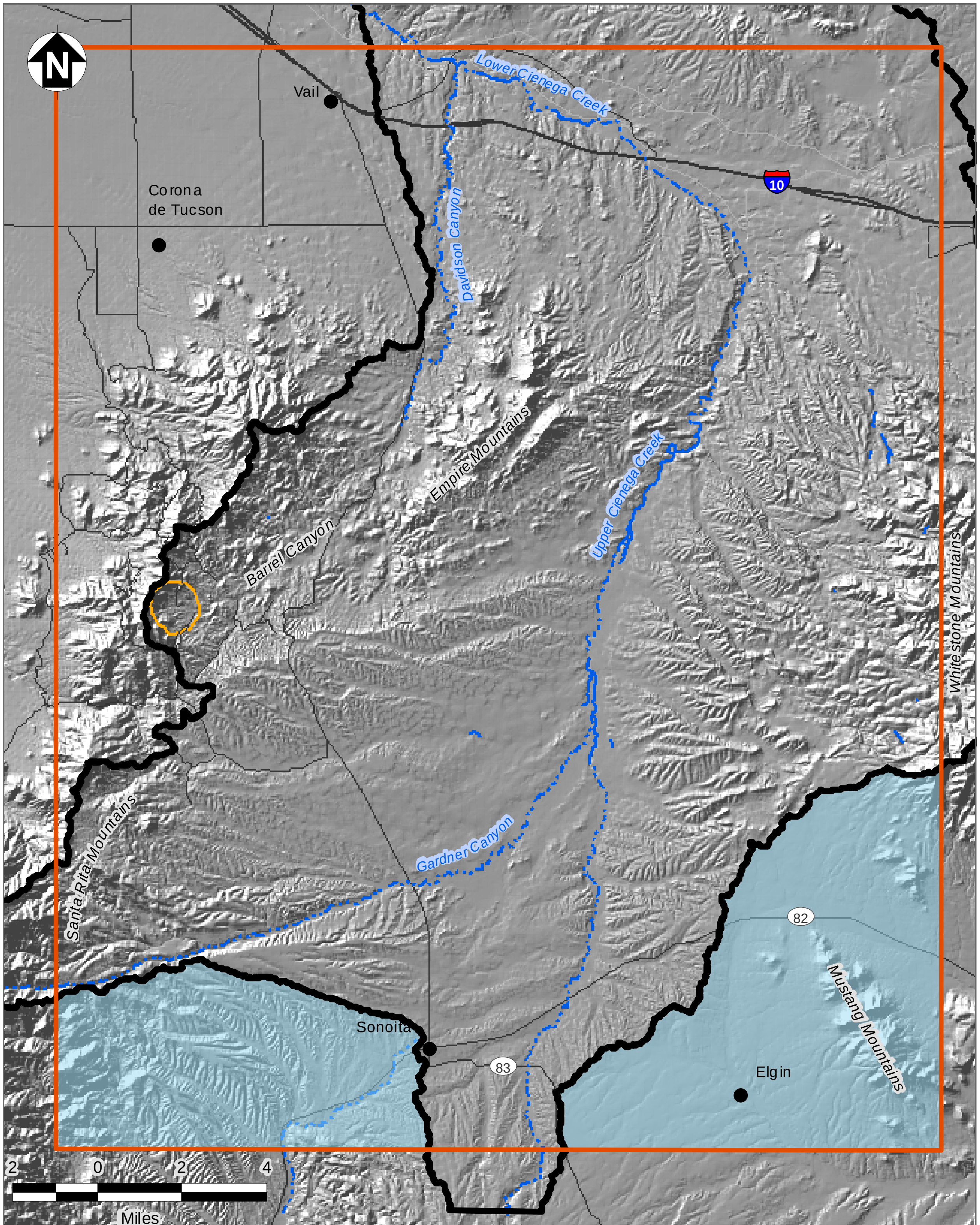

Legend

- Perennial Stream
- Ephemeral Drainage
- Extent of Model Domain
- No Flow Cells
- Cienega Creek Watershed
- Proposed Rosemont Open Pit
- Railroad
- Roads
- Towns

TETRA TECH

ROSEMONT COPPER

FIGURE 2. GROUNDWATER FLOW MODEL DOMAIN

2010-07-16

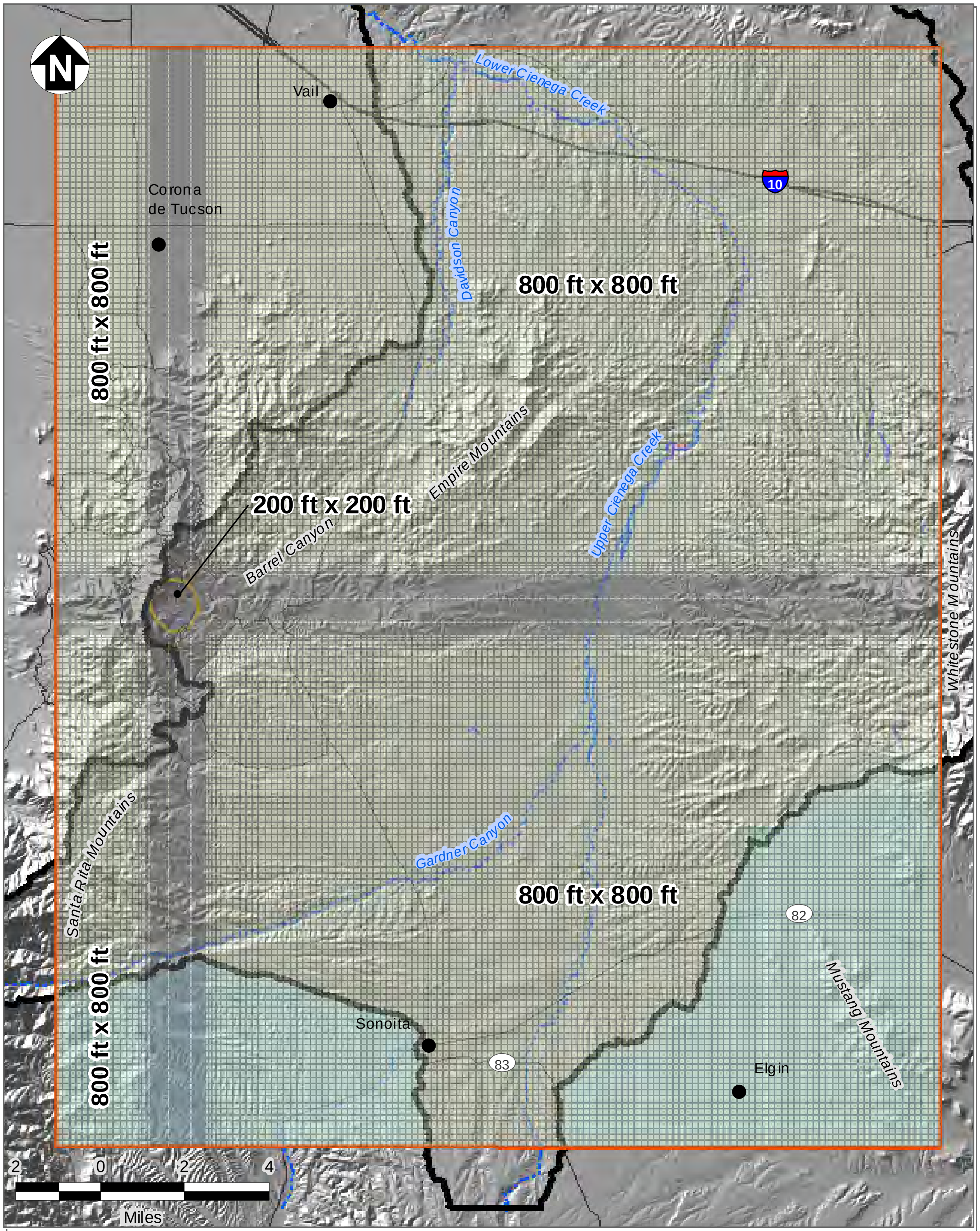

Legend

Perennial Stream
Ephemeral Drainage
Extent of Model Domain
No Flow Cells
Model Grid
Cienega Creek Watershed
Proposed Rosemont Open Pit
Railroad
Roads
Towns

TETRA TECH

ROSEMONT COPPER

FIGURE 3. GROUNDWATER FLOW MODEL GRID

2010-07-16

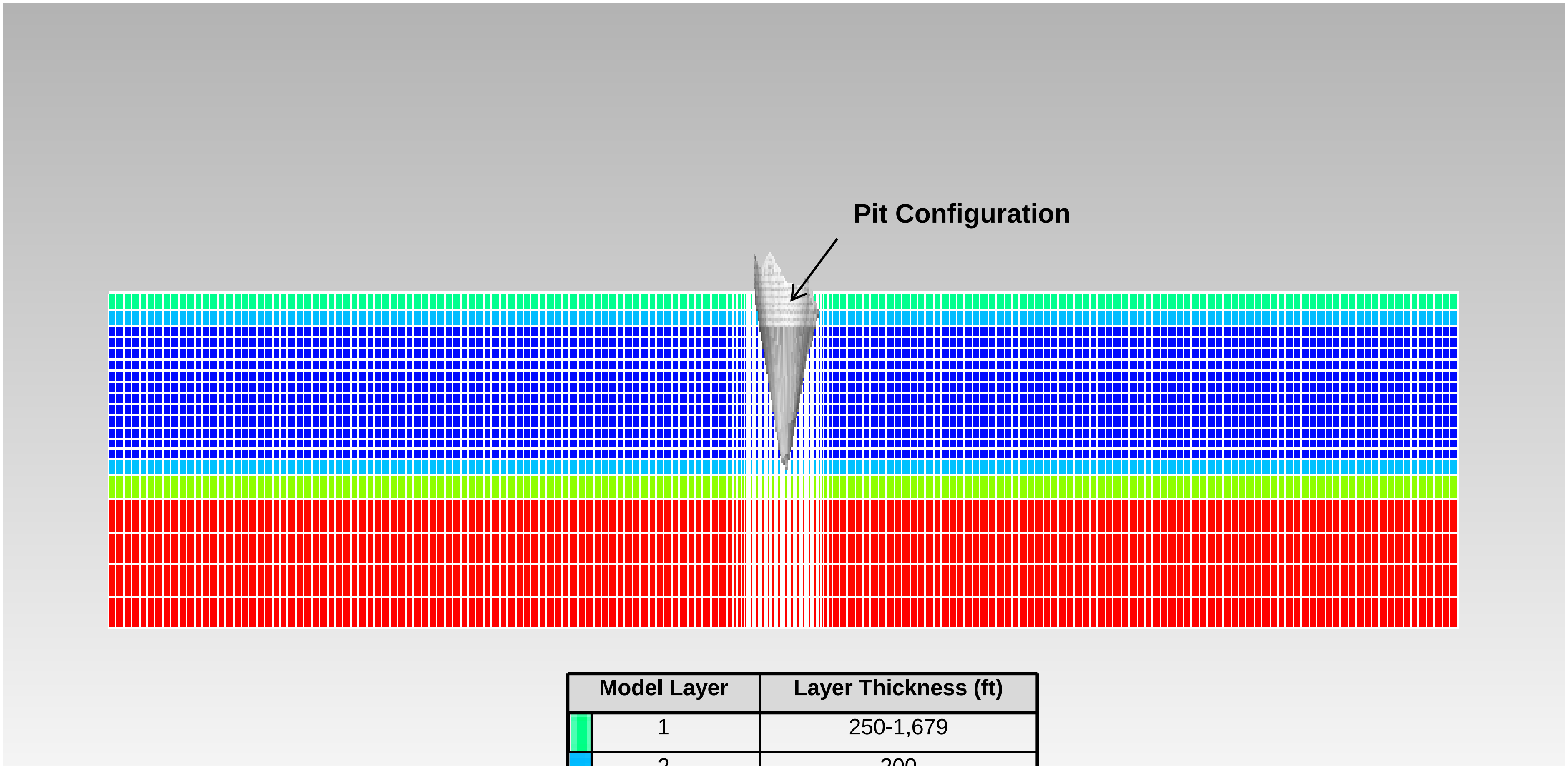

Model Layer	Layer Thickness (ft)
1	250-1,679
2	200
3-14	150
15	200
16	330
17-20	430

Notes: Vertical Exaggeration (10x)
Land Surface is not shown

Figure 4
Groundwater Flow Model Layers
Vertical Discretization

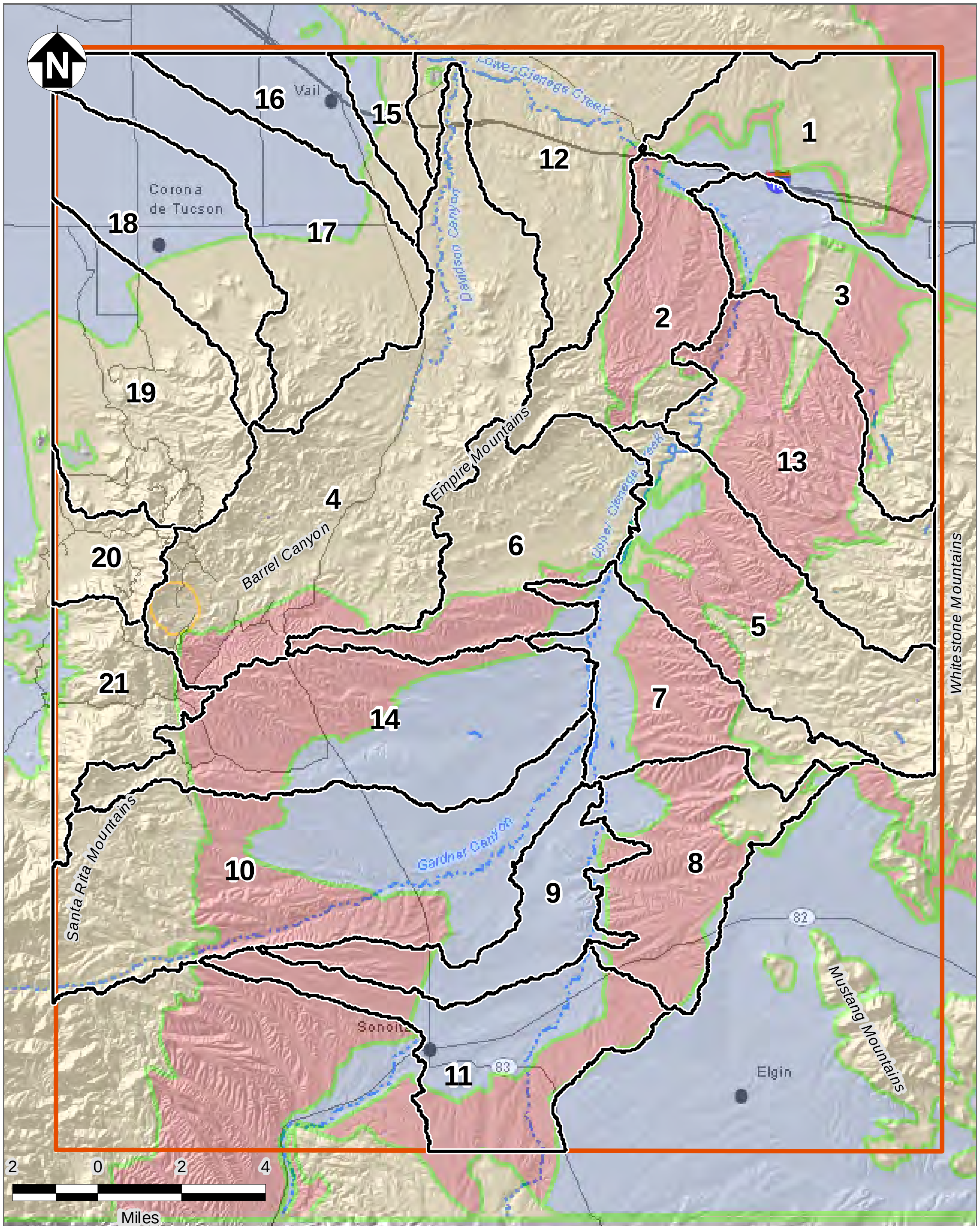

TETRA TECH

ROSEMONT COPPER

FIGURE 5. SURFACE-WATER SUB-BASINS WITH BEDROCK, ALLUVIAL FAN, AND VALLEY-FLOOR AREAS

2010-07-16

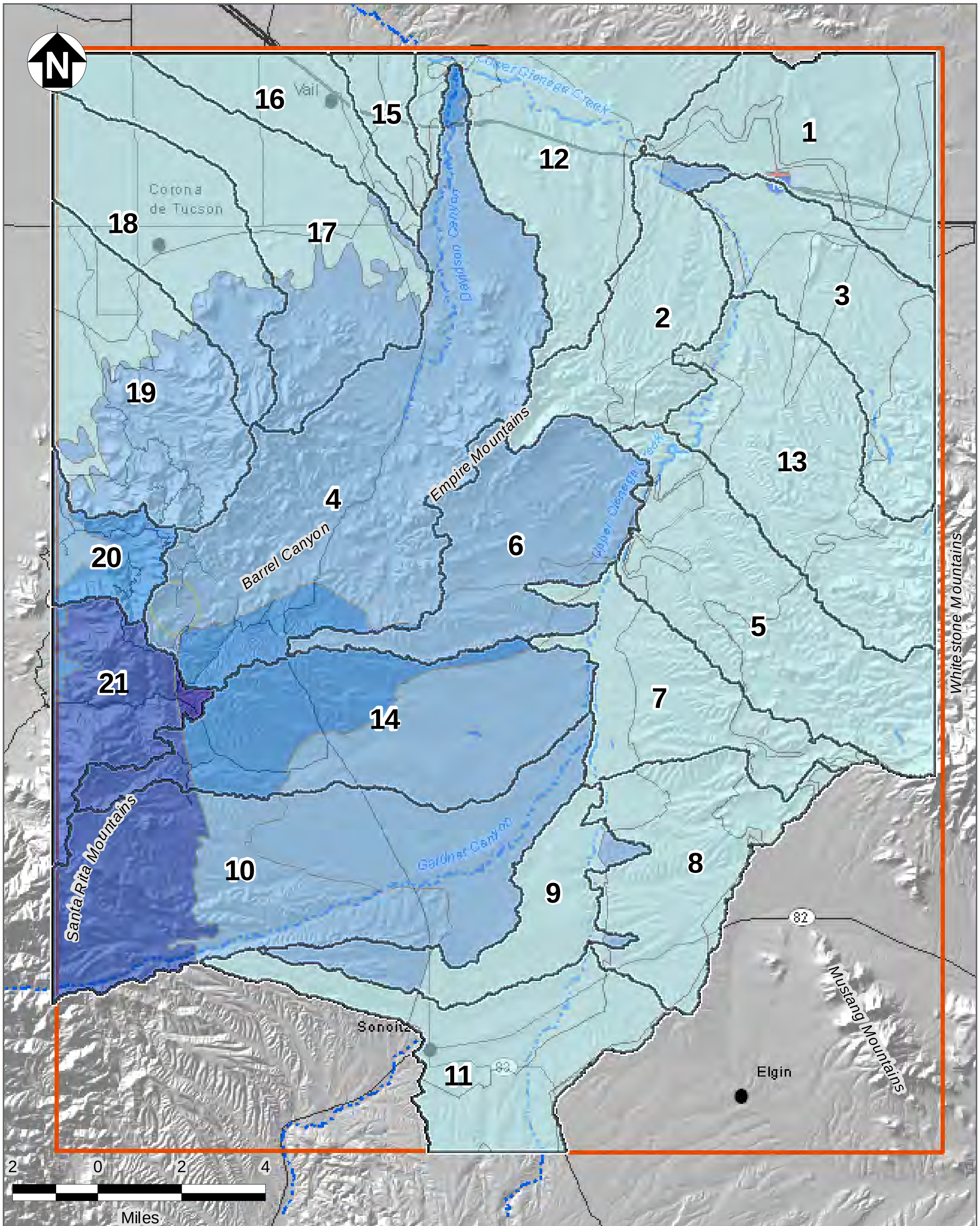

Legend

Perennial Stream

Ephemeral Drainage

Railroad

Proposed Rosemont Open Pit

Roads

Towns

21 Sub-Basins

Recharge (in/yr)

Normalized

- 0.34 - 0.39
- 0.40 - 0.45
- 0.46 - 0.51
- 0.52 - 0.57
- 0.58 - 0.63

TETRA TECH

ROSEMONT COPPER

FIGURE 6. ESTIMATED RECHARGE DISTRIBUTION

2010-07-16

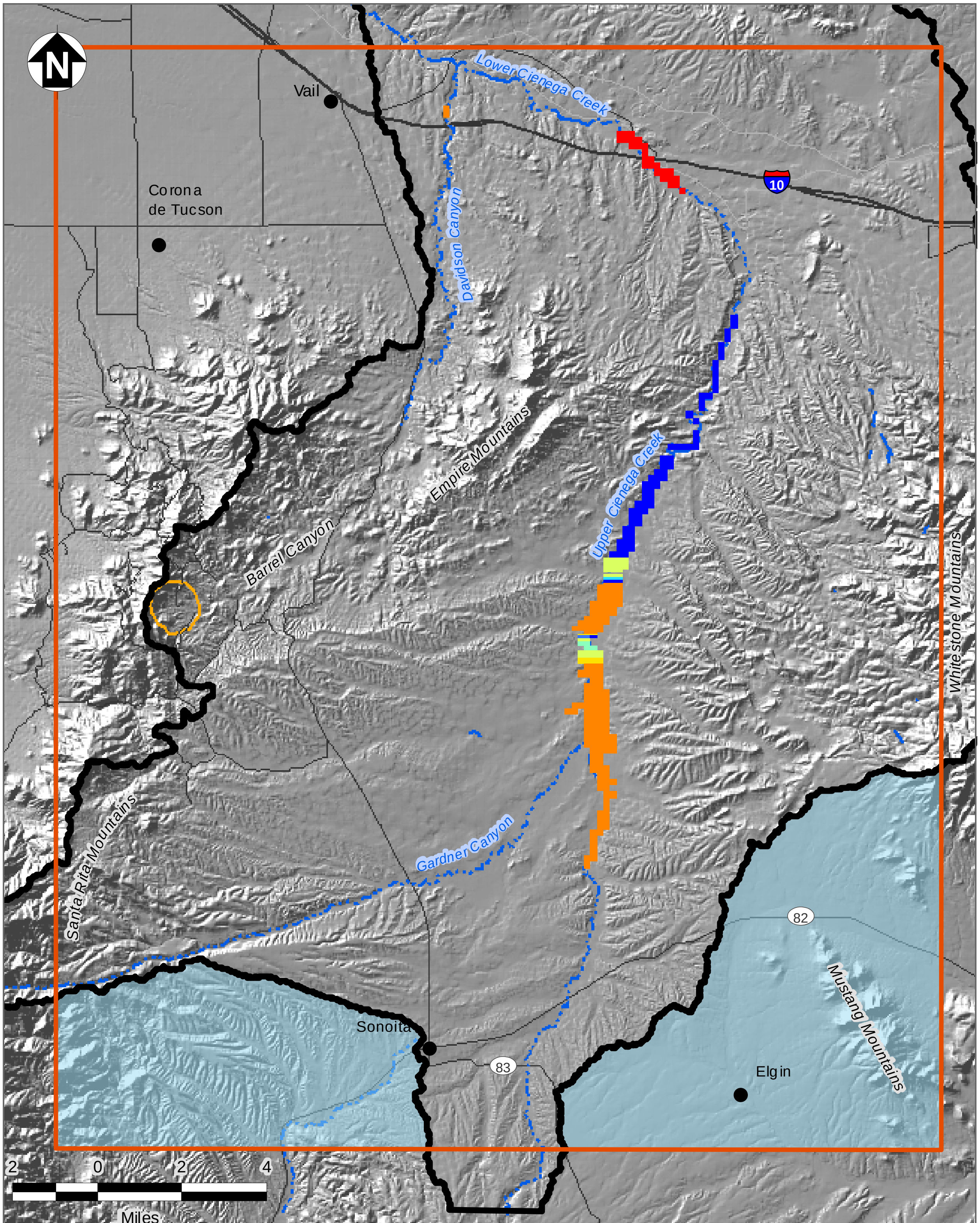

Legend

- Perennial Stream
- Ephemeral Drainage
- Extent of Model Domain
- No Flow Cells
- Cienega Creek Watershed
- Railroad
- Proposed Rosemont Open Pit
- Roads
- Towns

Evapotranspiration Rates (in/yr)

ET

- 10.91 - 14.16
- 14.17 - 26.33
- 26.34 - 29.67
- 29.68 - 31.79
- 31.80 - 32.92
- 32.93 - 35.12
- 35.13 - 36.65
- 36.66 - 39.40

TETRA TECH

ROSEMONT COPPER

FIGURE 7. MAXIMUM SIMULATED EVAPOTRANSPIRATION RATES

2010-07-16

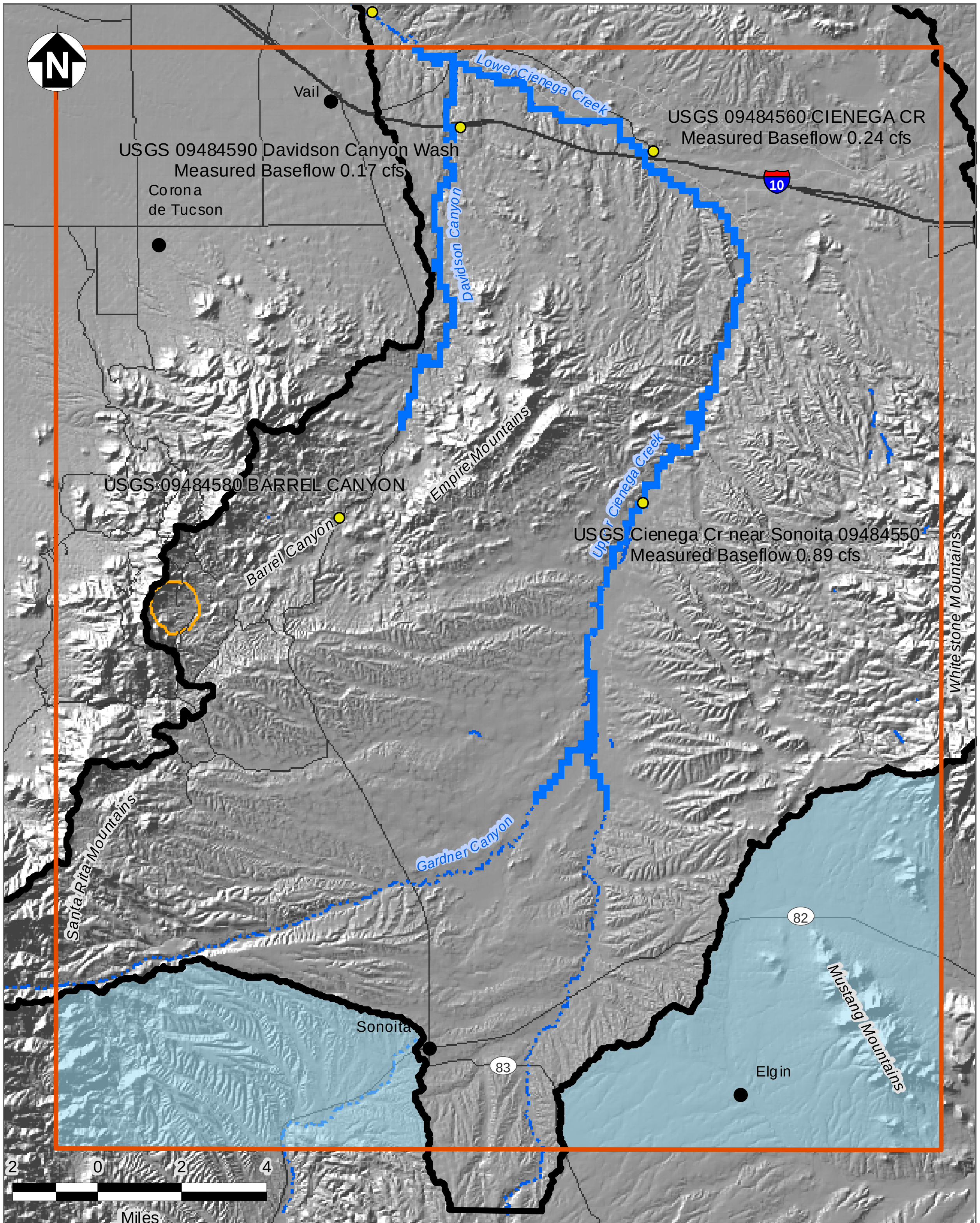

Legend

- Perennial Stream
- Ephemeral Drainage
- Railroad
- Roads
- Towns
- Proposed Rosemont Open Pit
- Stream Gage
- Stream Cells
- Extent of Model Domain
- No Flow Cells
- Cienega Creek Watershed

TETRA TECH

ROSEMONT COPPER

FIGURE 8. STREAM GAGE LOCATIONS AND SIMULATED STREAM FLOW ROUTING (SFR) PACKAGE CELLS

2010-07-16

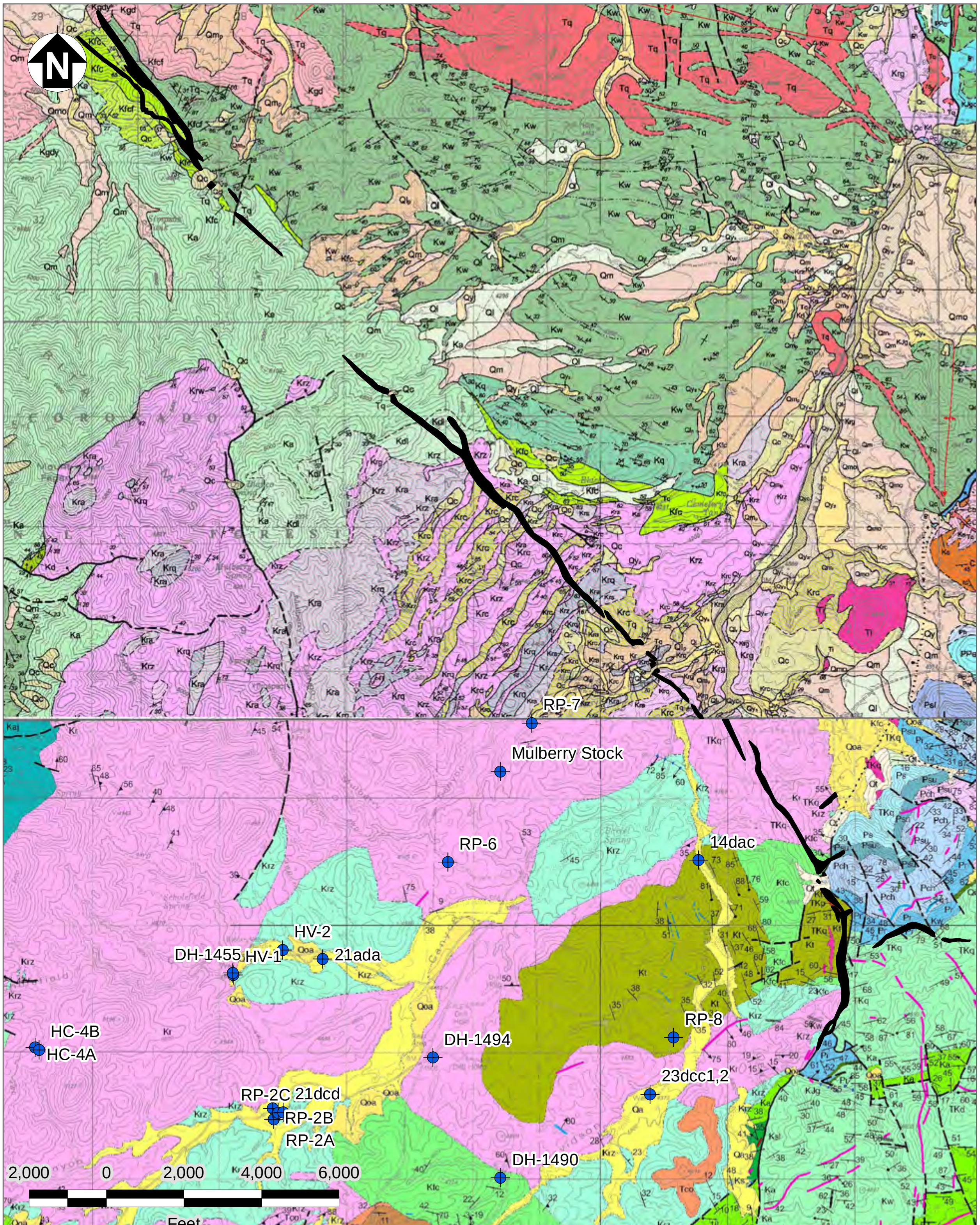

Legend

Wells

Quartz Porphry Dike

Note: Please refer to Ferguson (2009) and Ferguson et al., (2001) for a description of map symbols and units

TETRA TECH

ROSEMONT COPPER

FIGURE 9. GEOLOGIC MAP WITH QUARTZ-PORPHRY DIKE

2010-07-16

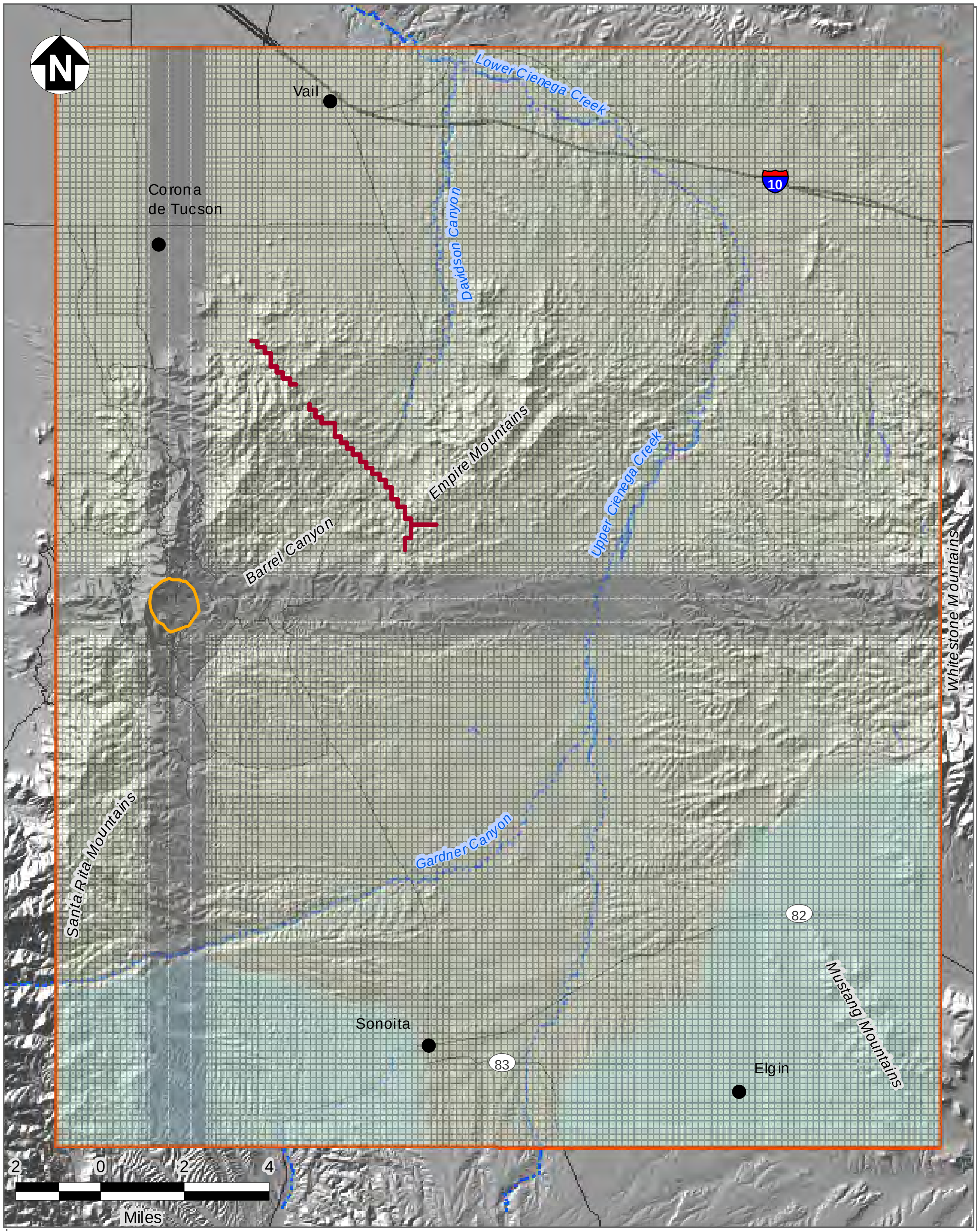

Legend

- Perennial Stream
- Ephemeral Drainage
- Extent of Model Domain
- No Flow Cells
- Model Grid
- Proposed Rosemont Open Pit
- Railroad
- Roads
- Towns
- HFB

TETRA TECH

ROSEMONT COPPER

FIGURE 10. QUARTZ-PORPHYRY DIKE SIMULATED AS A HORIZONTAL FLOW BARRIER

2010-07-16

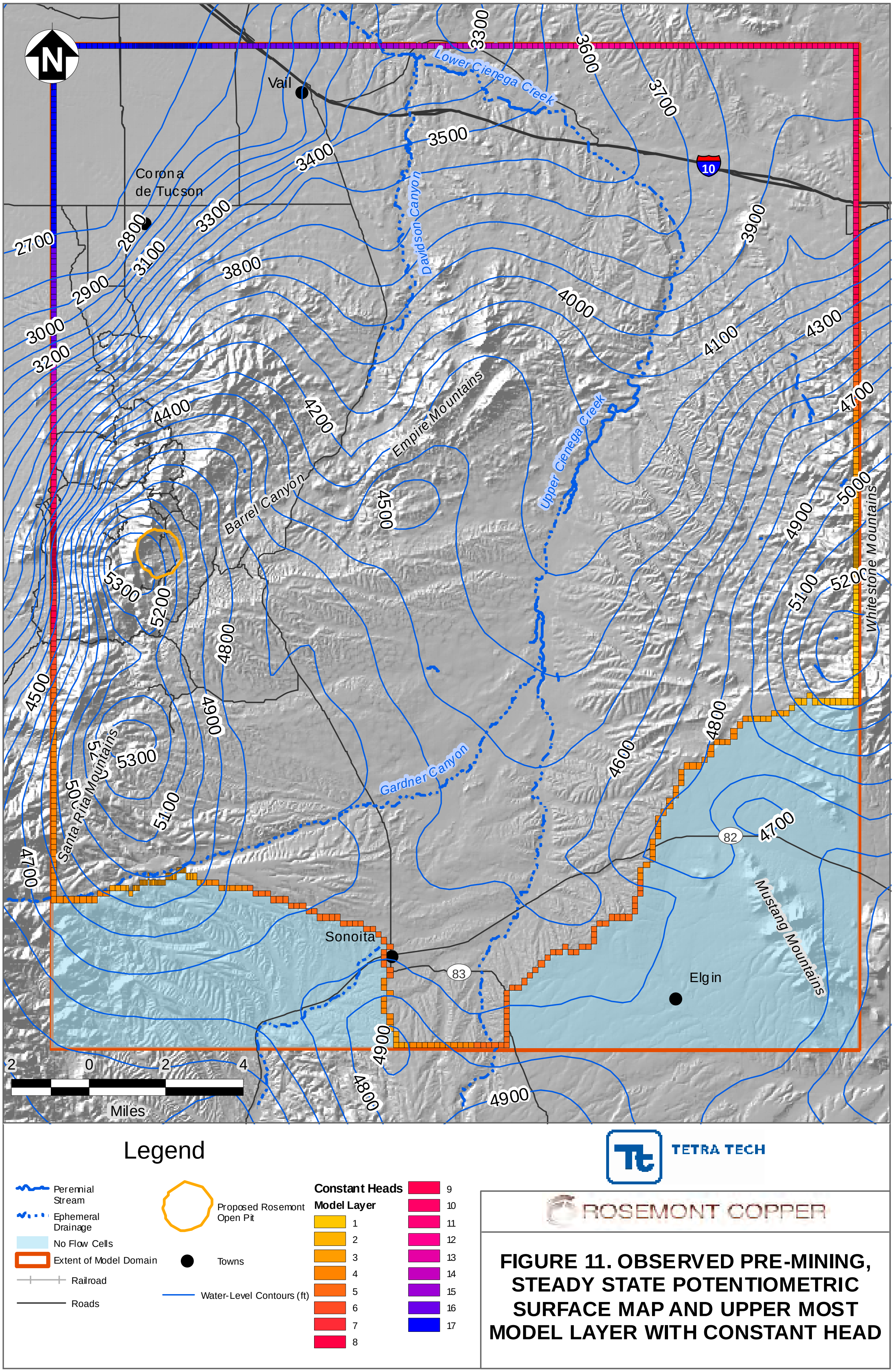

FIGURE 11. OBSERVED PRE-MINING, STEADY STATE POTENTIOMETRIC SURFACE MAP AND UPPER MOST MODEL LAYER WITH CONSTANT HEAD

2010-07-16

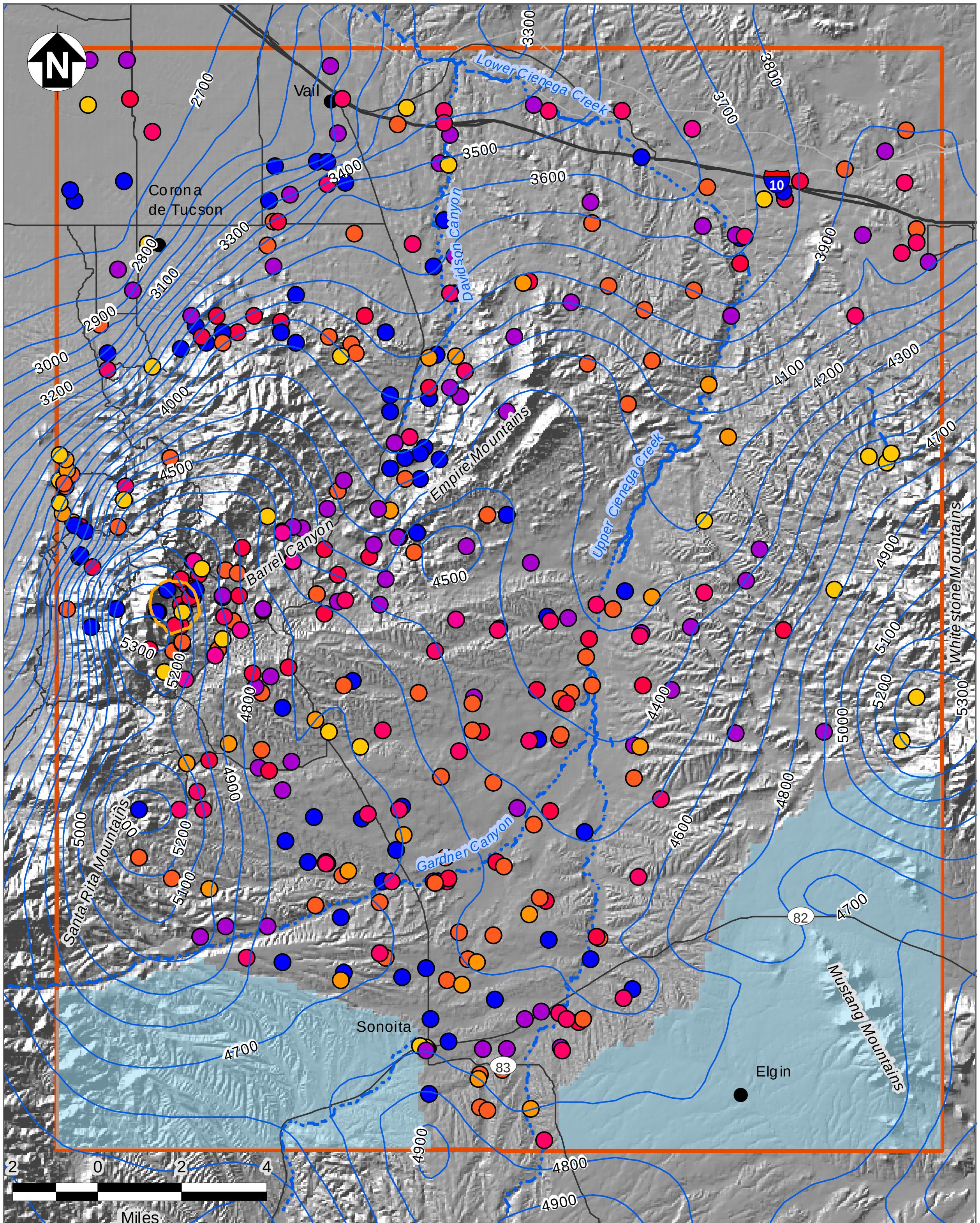

Legend

Perennial Stream
Ephemeral Drainage
No Flow Cells
Extent of Model Domain
Water-Level Contours (ft)
Proposed Rosemont Open Pit
Railroad
Roads
Towns

Weight

0	0.5
0.1	0.8
0.2	0.9
0.4	1

TETRA TECH

ROSEMONT COPPER

FIGURE 12. CALIBRATION WEIGHTS FOR TARGET WATER LEVELS

2010-07-16

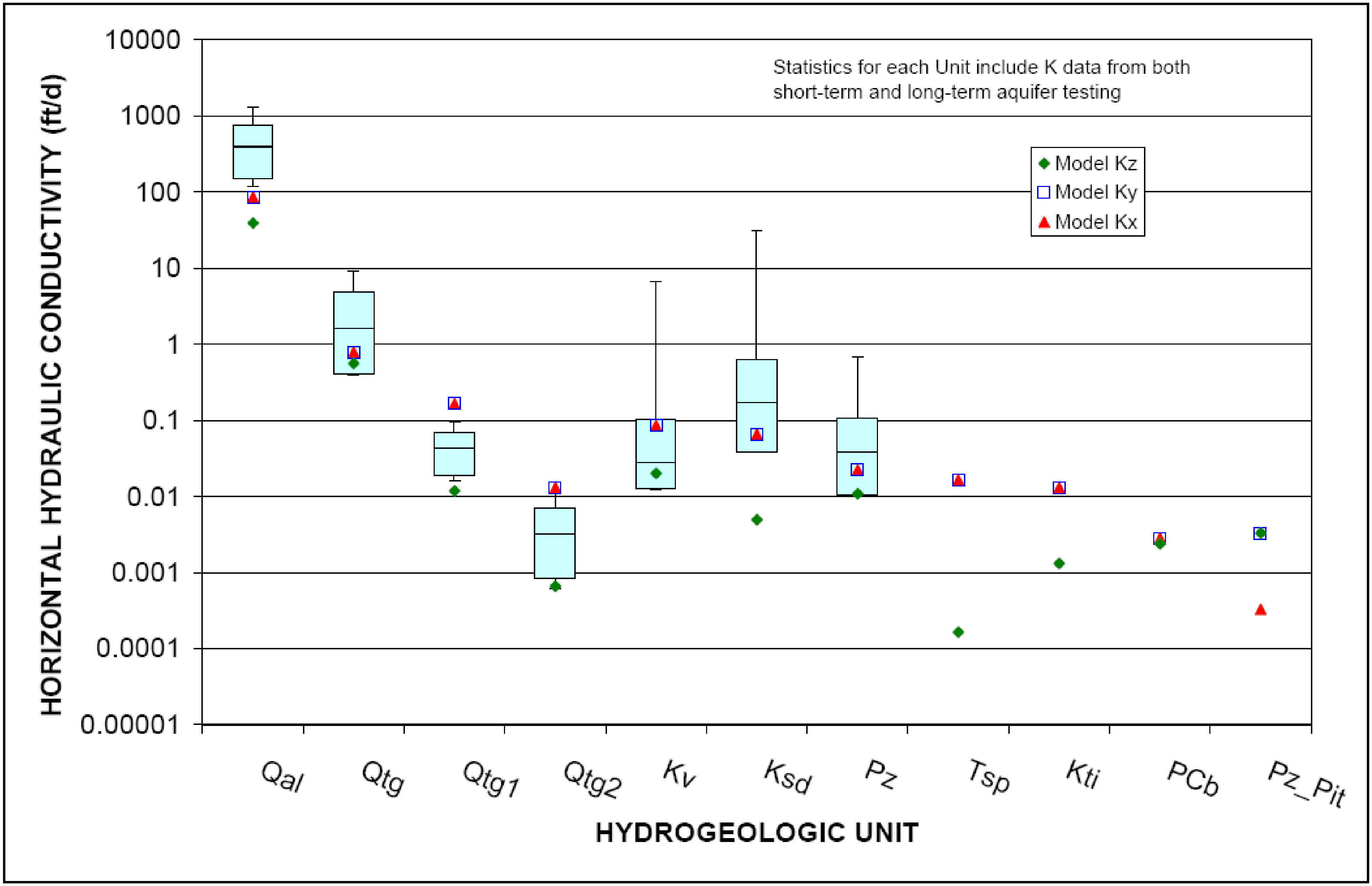

Project No: 114-320874

July 2010

Figure 13
Observed and Simulated Hydraulic Conductivity Values

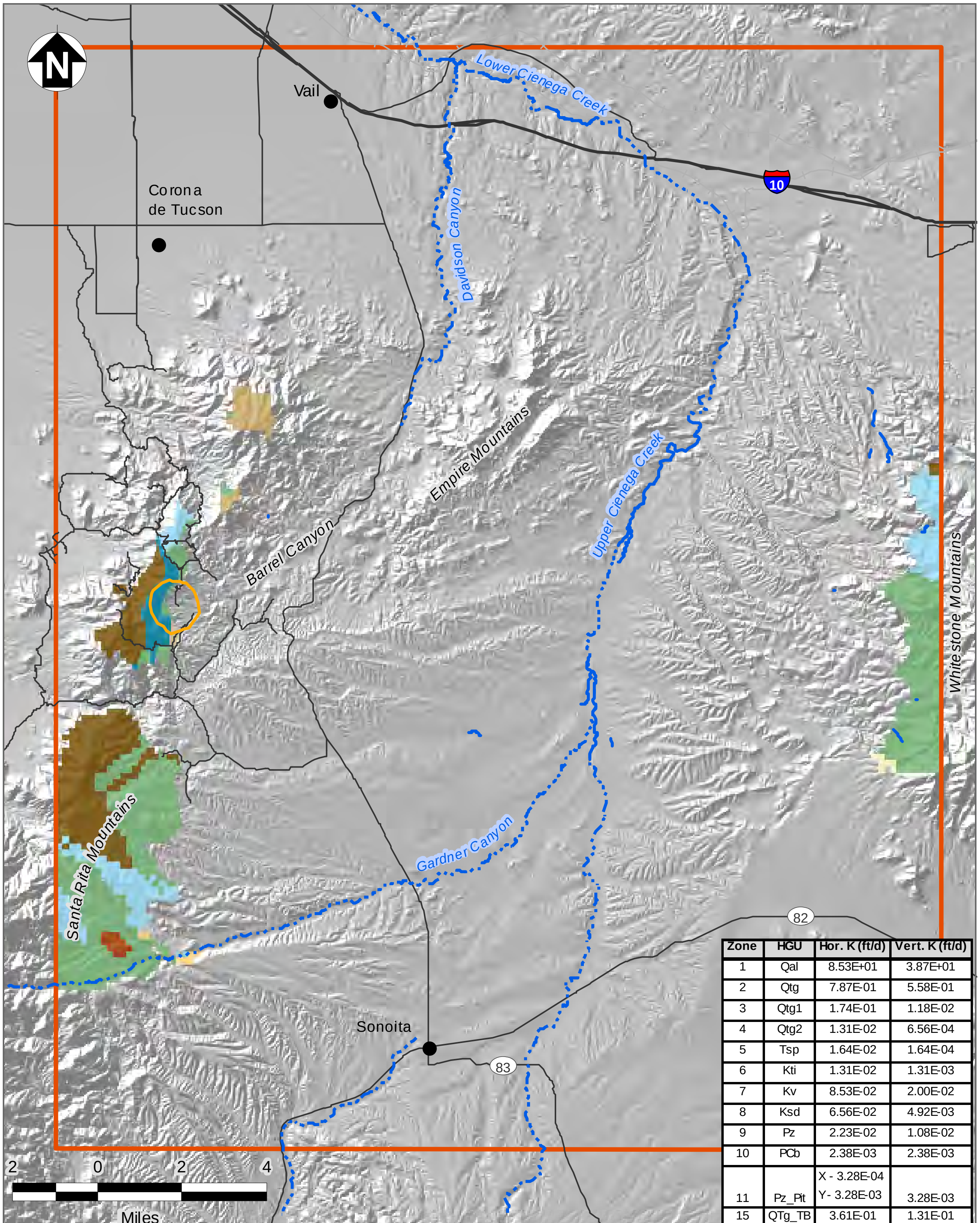

Zone	HGU	Hor. K (ft/d)	Vert. K (ft/d)
1	Qal	8.53E+01	3.87E+01
2	Qtg	7.87E-01	5.58E-01
3	Qtg1	1.74E-01	1.18E-02
4	Qtg2	1.31E-02	6.56E-04
5	Tsp	1.64E-02	1.64E-04
6	Kti	1.31E-02	1.31E-03
7	Kv	8.53E-02	2.00E-02
8	Ksd	6.56E-02	4.92E-03
9	Pz	2.23E-02	1.08E-02
10	PCb	2.38E-03	2.38E-03
11	Pz_Pit	X - 3.28E-04 Y- 3.28E-03	3.28E-03
15	QTg_TB	3.61E-01	1.31E-01

Legend

Perennial Stream
Ephemeral Drainage
Railroad
Roads
Proposed Rosemont Open Pit
Towns

Geology

Qal
QTg
QTg_TB
QTg1
QTg2
Tsp
KTi
Kv
Ksd
Pz
Pz_Pit
PCb

TETRA TECH

ROSEMONT COPPER

FIGURE 14. MODEL LAYER 1 HYDRAULIC CONDUCTIVITY DISTRIBUTION

2010-07-16

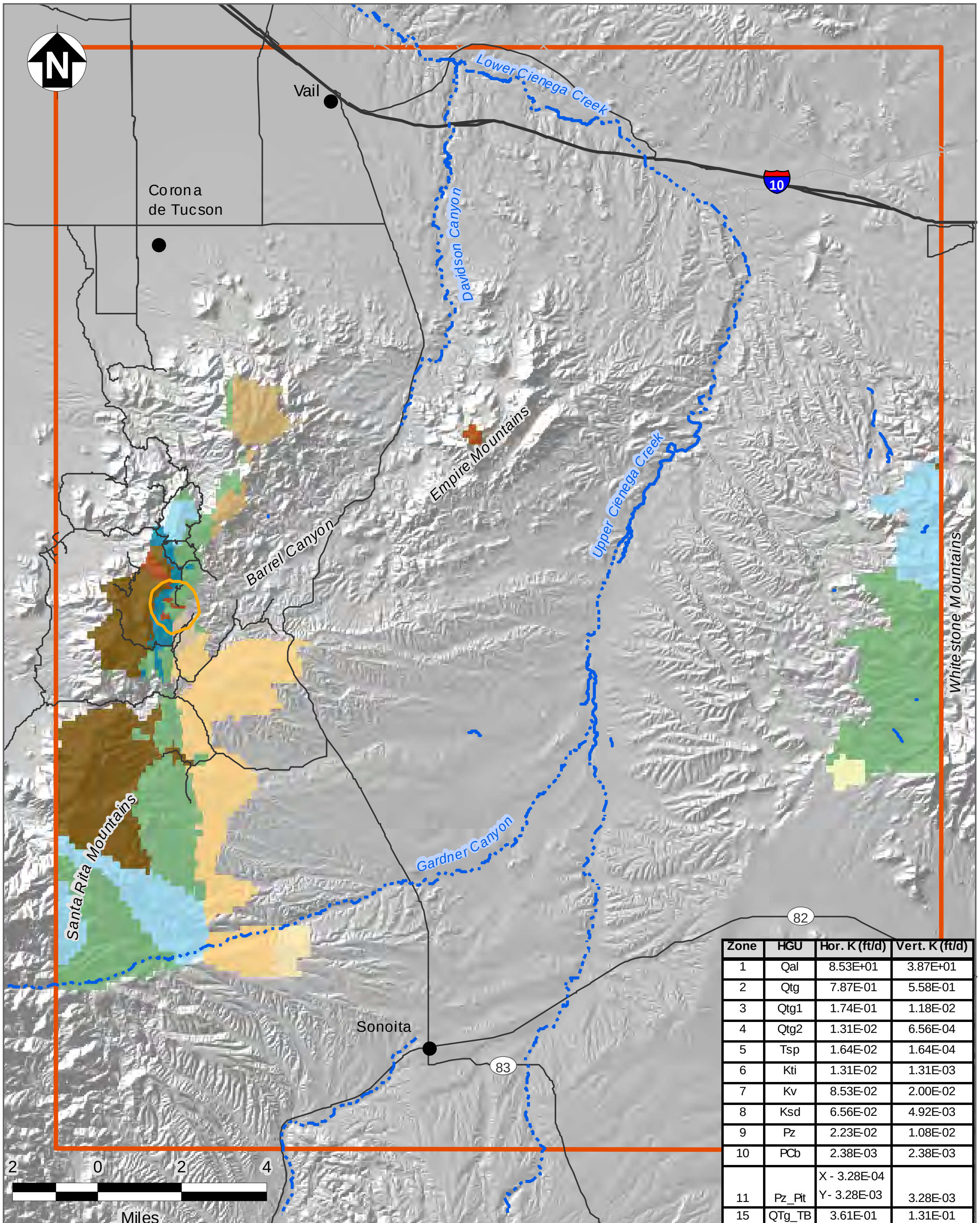

Zone	HGU	Hor. K (ft/d)	Vert. K (ft/d)
1	Qal	8.53E+01	3.87E+01
2	Qtg	7.87E-01	5.58E-01
3	Qtg1	1.74E-01	1.18E-02
4	Qtg2	1.31E-02	6.56E-04
5	Tsp	1.64E-02	1.64E-04
6	Kti	1.31E-02	1.31E-03
7	Kv	8.53E-02	2.00E-02
8	Ksd	6.56E-02	4.92E-03
9	Pz	2.23E-02	1.08E-02
10	PCb	2.38E-03	2.38E-03
11	Pz_Pit	X - 3.28E-04 Y- 3.28E-03	3.28E-03
15	QTg_TB	3.61E-01	1.31E-01

Legend

Perennial Stream
Ephemeral Drainage
Railroad
Roads
Proposed Rosemont Open Pit
Towns

Geology

Qal
QTg
QTg_TB
QTg1
QTg2
Tsp
KTi
Kv
Ksd
Pz
Pz_Pit
PCb

TETRA TECH

ROSEMONT COPPER

FIGURE 15. MODEL LAYER 2 HYDRAULIC CONDUCTIVITY DISTRIBUTION

2010-07-16

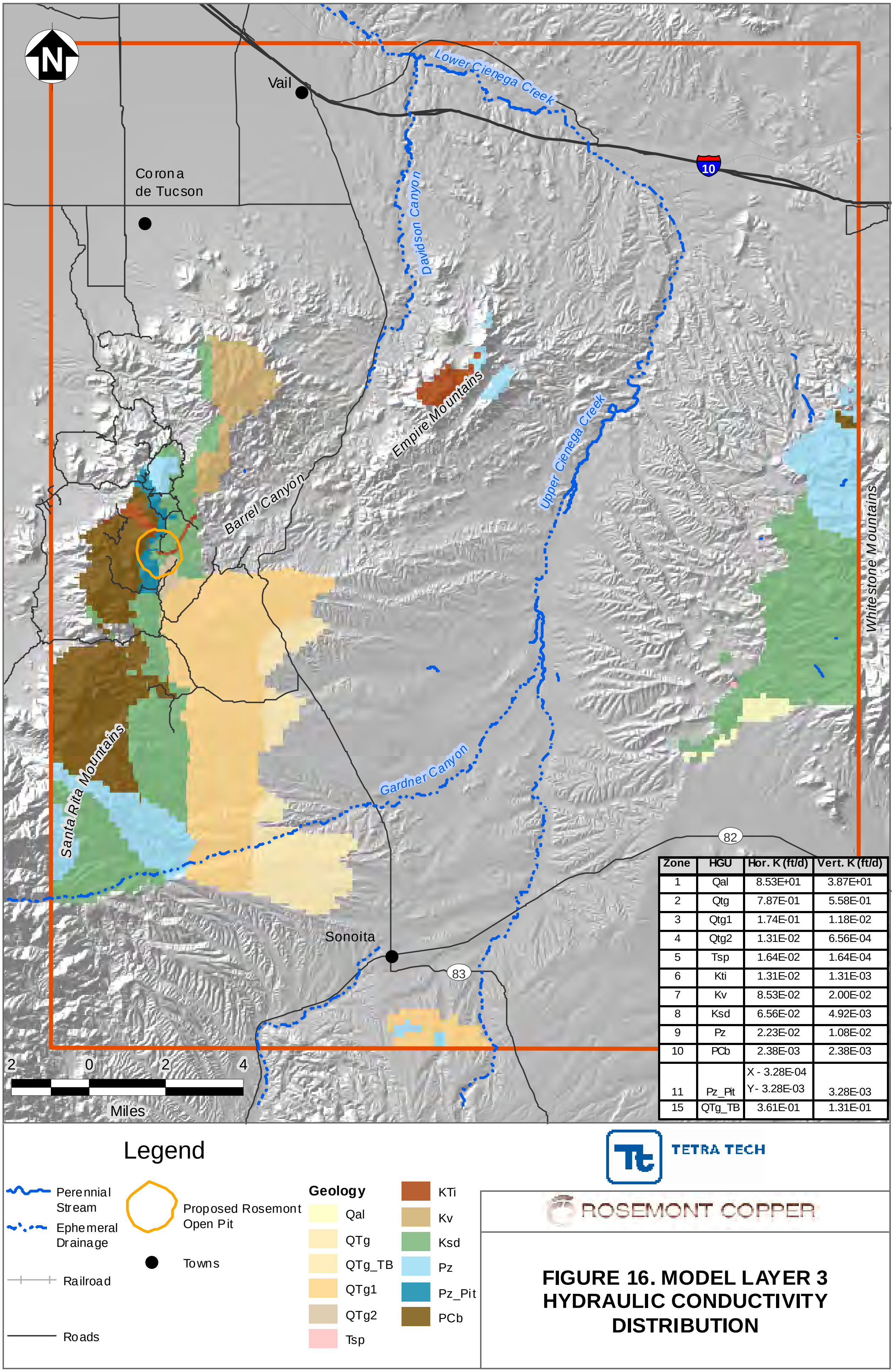

Zone	HGU	Hor. K (ft/d)	Vert. K (ft/d)
1	Qal	8.53E+01	3.87E+01
2	Qtg	7.87E-01	5.58E-01
3	Qtg1	1.74E-01	1.18E-02
4	Qtg2	1.31E-02	6.56E-04
5	Tsp	1.64E-02	1.64E-04
6	Kti	1.31E-02	1.31E-03
7	Kv	8.53E-02	2.00E-02
8	Ksd	6.56E-02	4.92E-03
9	Pz	2.23E-02	1.08E-02
10	PCb	2.38E-03	2.38E-03
11	Pz_Pit	X - 3.28E-04 Y- 3.28E-03	3.28E-03
15	QTg_TB	3.61E-01	1.31E-01

TETRA TECH

ROSEMONT COPPER

FIGURE 16. MODEL LAYER 3 HYDRAULIC CONDUCTIVITY DISTRIBUTION

2010-07-16

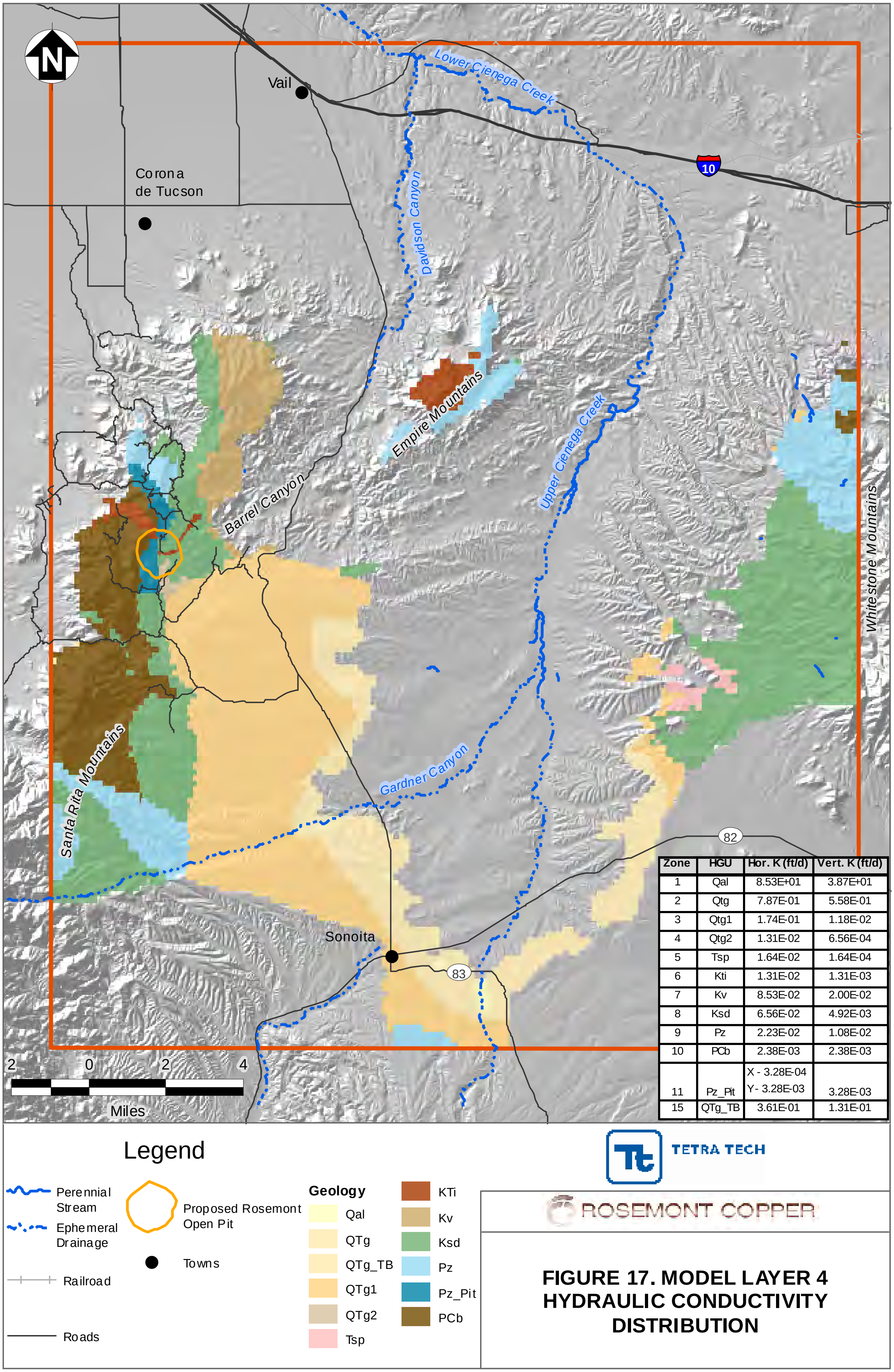

Zone	HGU	Hor. K (ft/d)	Vert. K (ft/d)
1	Qal	8.53E+01	3.87E+01
2	Qtg	7.87E-01	5.58E-01
3	Qtg1	1.74E-01	1.18E-02
4	Qtg2	1.31E-02	6.56E-04
5	Tsp	1.64E-02	1.64E-04
6	Kti	1.31E-02	1.31E-03
7	Kv	8.53E-02	2.00E-02
8	Ksd	6.56E-02	4.92E-03
9	Pz	2.23E-02	1.08E-02
10	PCb	2.38E-03	2.38E-03
11	Pz_Pit	X - 3.28E-04 Y - 3.28E-03	3.28E-03
15	QTg_TB	3.61E-01	1.31E-01

TETRA TECH

ROSEMONT COPPER

FIGURE 17. MODEL LAYER 4 HYDRAULIC CONDUCTIVITY DISTRIBUTION

2010-07-16

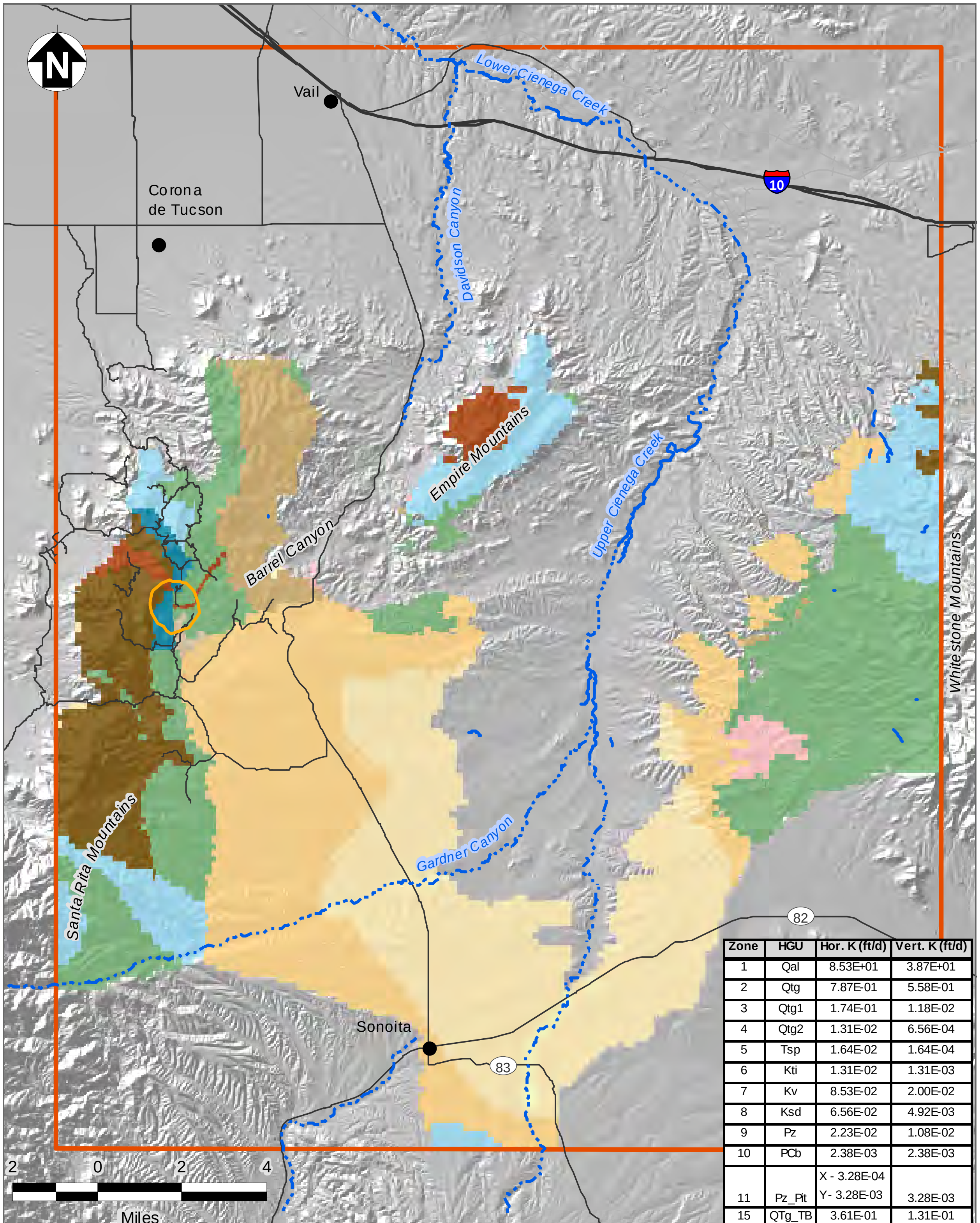

Zone	HGU	Hor. K (ft/d)	Vert. K (ft/d)
1	Qal	8.53E+01	3.87E+01
2	Qtg	7.87E-01	5.58E-01
3	Qtg1	1.74E-01	1.18E-02
4	Qtg2	1.31E-02	6.56E-04
5	Tsp	1.64E-02	1.64E-04
6	Kti	1.31E-02	1.31E-03
7	Kv	8.53E-02	2.00E-02
8	Ksd	6.56E-02	4.92E-03
9	Pz	2.23E-02	1.08E-02
10	PCb	2.38E-03	2.38E-03
11	Pz_Pit	X - 3.28E-04 Y- 3.28E-03	3.28E-03
15	QTg_TB	3.61E-01	1.31E-01

Legend

Perennial Stream
Ephemeral Drainage
Railroad
Roads
Proposed Rosemont Open Pit
Towns

Geology

Qal
QTg
QTg_TB
QTg1
QTg2
Tsp
KTi
Kv
Ksd
Pz
Pz_Pit
PCb

TETRA TECH

ROSEMONT COPPER

FIGURE 18. MODEL LAYER 5 HYDRAULIC CONDUCTIVITY DISTRIBUTION

2010-07-16

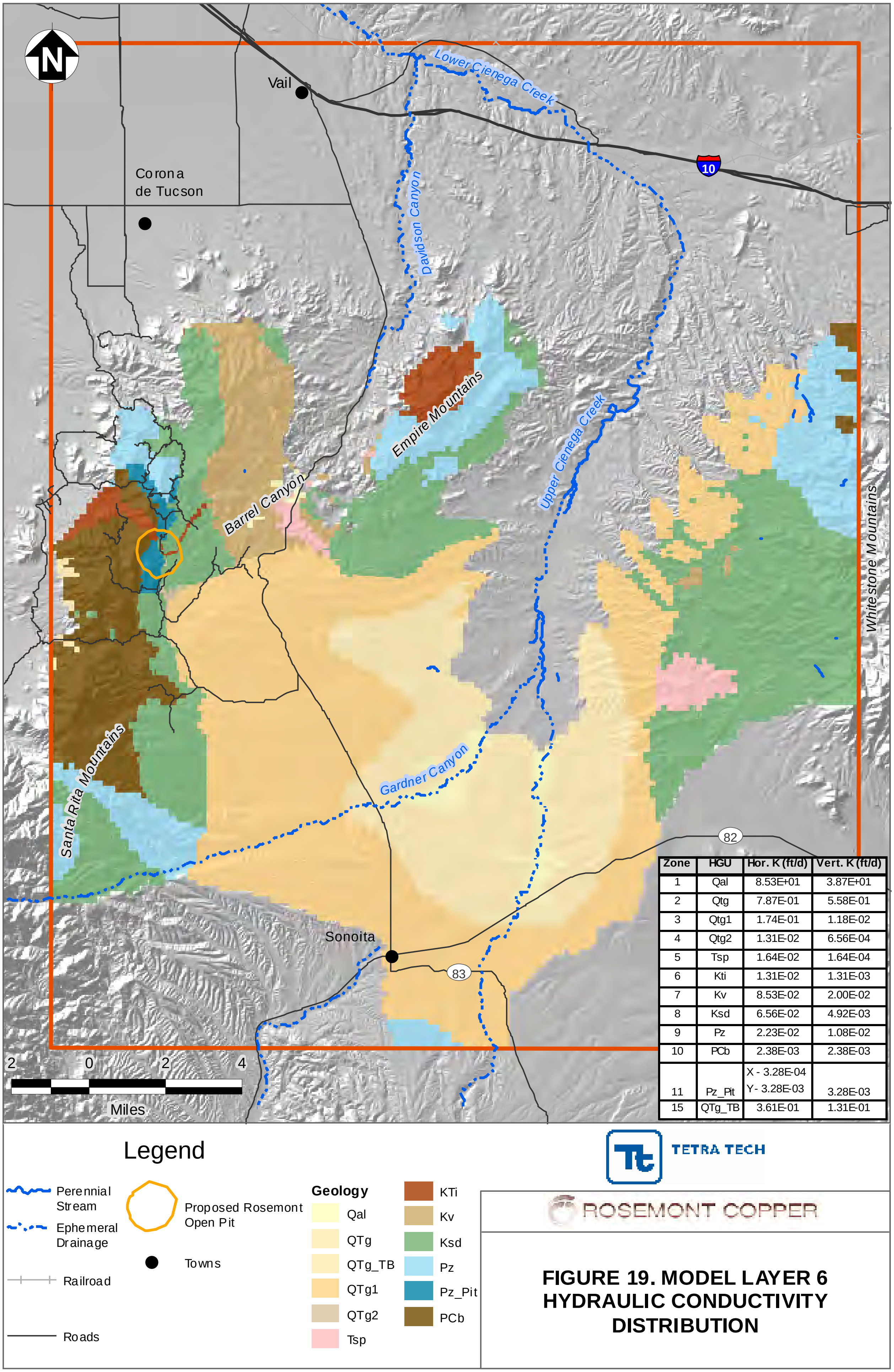

Zone	HGU	Hor. K (ft/d)	Vert. K (ft/d)
1	Qal	8.53E+01	3.87E+01
2	Qtg	7.87E-01	5.58E-01
3	Qtg1	1.74E-01	1.18E-02
4	Qtg2	1.31E-02	6.56E-04
5	Tsp	1.64E-02	1.64E-04
6	Kti	1.31E-02	1.31E-03
7	Kv	8.53E-02	2.00E-02
8	Ksd	6.56E-02	4.92E-03
9	Pz	2.23E-02	1.08E-02
10	PCb	2.38E-03	2.38E-03
11	Pz_Pit	X - 3.28E-04 Y - 3.28E-03	3.28E-03
15	QTg_TB	3.61E-01	1.31E-01

FIGURE 19. MODEL LAYER 6 HYDRAULIC CONDUCTIVITY DISTRIBUTION

2010-07-16

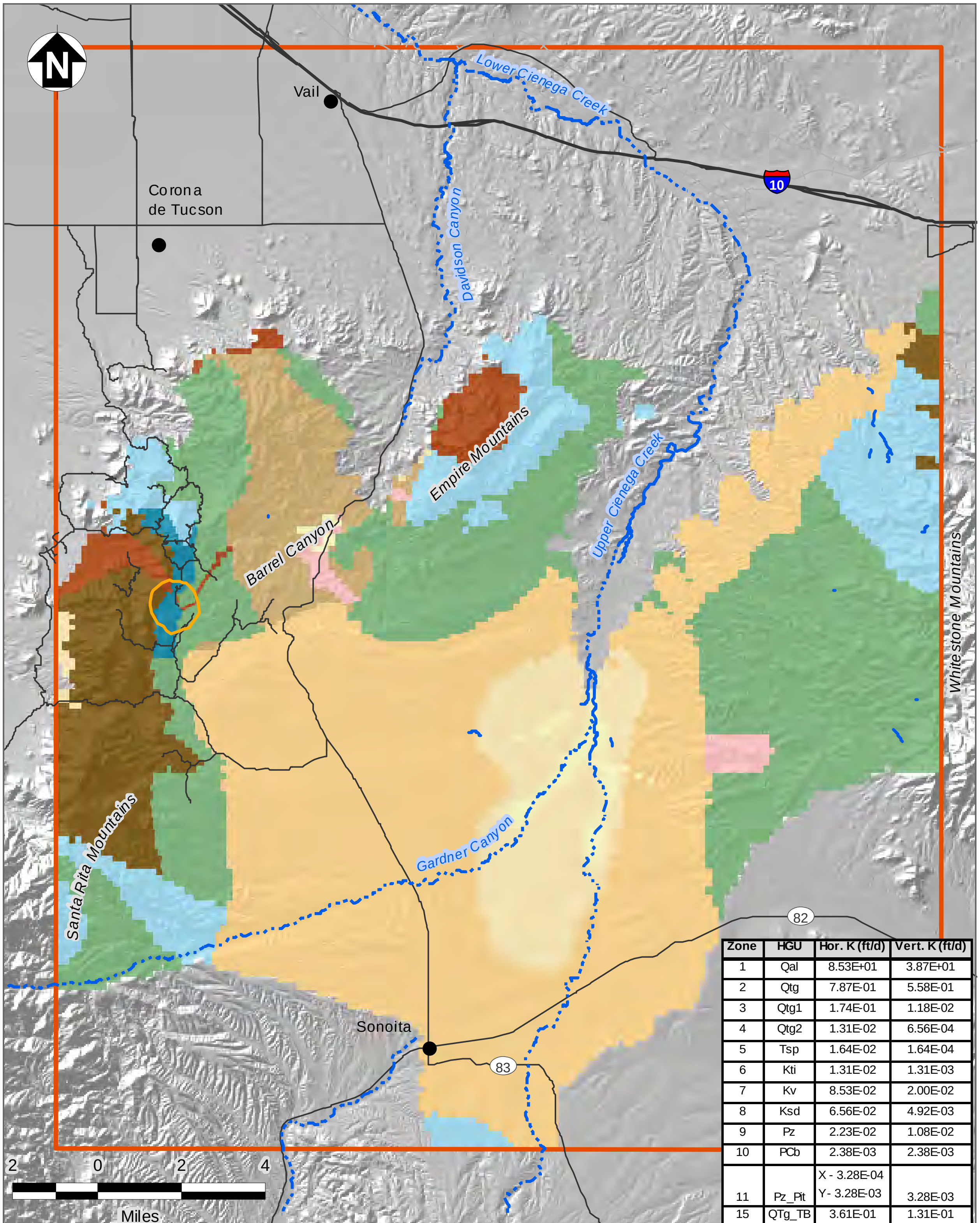

Zone	HGU	Hor. K (ft/d)	Vert. K (ft/d)
1	Qal	8.53E+01	3.87E+01
2	Qtg	7.87E-01	5.58E-01
3	Qtg1	1.74E-01	1.18E-02
4	Qtg2	1.31E-02	6.56E-04
5	Tsp	1.64E-02	1.64E-04
6	Kti	1.31E-02	1.31E-03
7	Kv	8.53E-02	2.00E-02
8	Ksd	6.56E-02	4.92E-03
9	Pz	2.23E-02	1.08E-02
10	PCb	2.38E-03	2.38E-03
11	Pz_Pit	X - 3.28E-04 Y - 3.28E-03	3.28E-03
15	QTg_TB	3.61E-01	1.31E-01

Legend

Perennial Stream
Ephemeral Drainage
Railroad
Roads
Proposed Rosemont Open Pit
Towns

Geology

Qal
QTg
QTg_TB
QTg1
QTg2
Tsp
KTi
Kv
Ksd
Pz
Pz_Pit
PCb

TETRA TECH
ROSEMONT COPPER

FIGURE 20. MODEL LAYER 7 HYDRAULIC CONDUCTIVITY DISTRIBUTION

2010-07-16

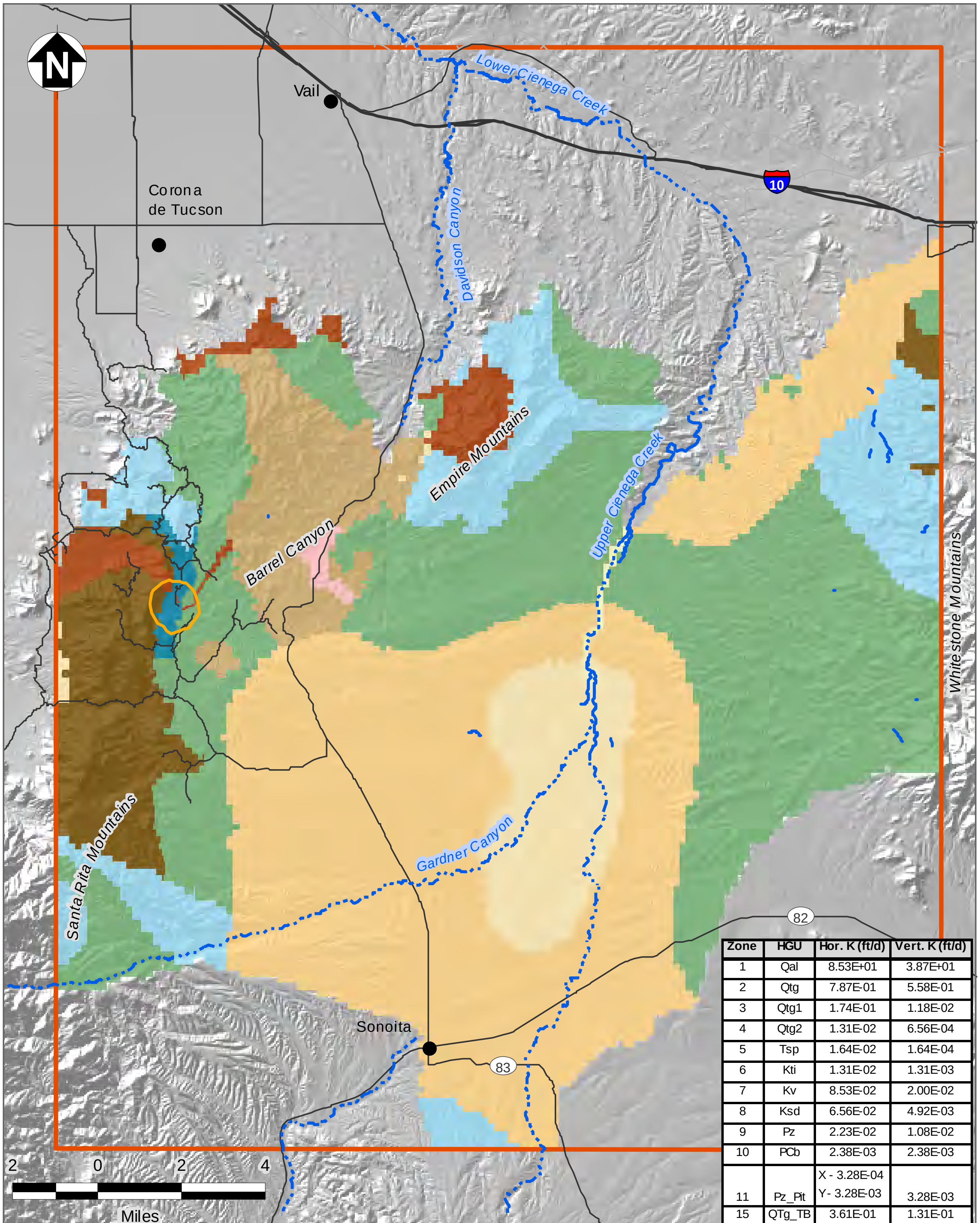

Zone	HGU	Hor. K (ft/d)	Vert. K (ft/d)
1	Qal	8.53E+01	3.87E+01
2	Qtg	7.87E-01	5.58E-01
3	Qtg1	1.74E-01	1.18E-02
4	Qtg2	1.31E-02	6.56E-04
5	Tsp	1.64E-02	1.64E-04
6	Kti	1.31E-02	1.31E-03
7	Kv	8.53E-02	2.00E-02
8	Ksd	6.56E-02	4.92E-03
9	Pz	2.23E-02	1.08E-02
10	PCb	2.38E-03	2.38E-03
11	Pz_Pit	X - 3.28E-04 Y - 3.28E-03	3.28E-03
15	QTg_TB	3.61E-01	1.31E-01

Legend

Perennial Stream
Ephemeral Drainage
Railroad
Roads
Proposed Rosemont Open Pit
Towns

Geology

Qal
QTg
QTg_TB
QTg1
QTg2
Tsp
KTi
Kv
Ksd
Pz
Pz_Pit
PCb

TETRA TECH

ROSEMONT COPPER

FIGURE 21. MODEL LAYER 8 HYDRAULIC CONDUCTIVITY DISTRIBUTION

2010-07-16

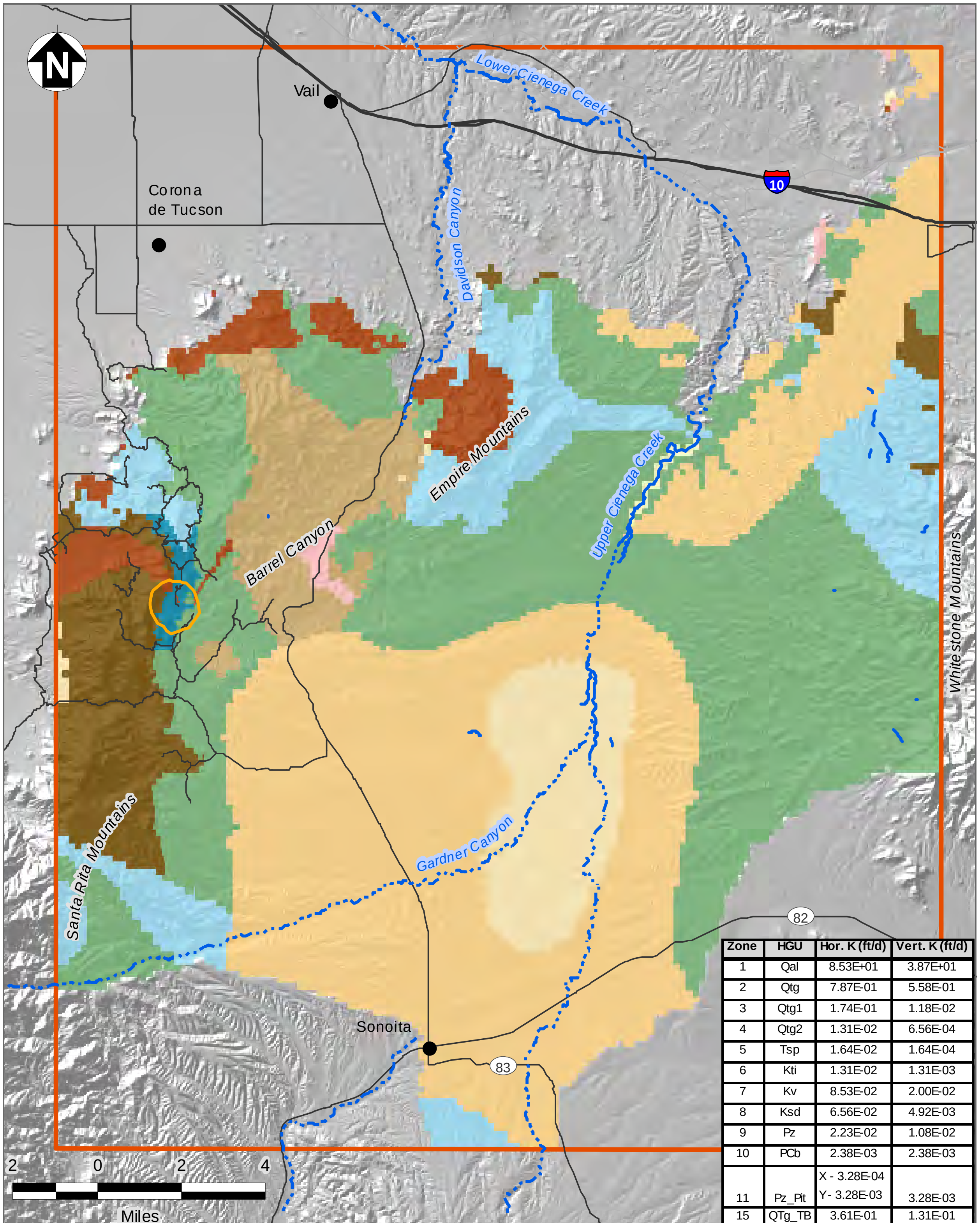

Zone	HGU	Hor. K (ft/d)	Vert. K (ft/d)
1	Qal	8.53E+01	3.87E+01
2	Qtg	7.87E-01	5.58E-01
3	Qtg1	1.74E-01	1.18E-02
4	Qtg2	1.31E-02	6.56E-04
5	Tsp	1.64E-02	1.64E-04
6	Kti	1.31E-02	1.31E-03
7	Kv	8.53E-02	2.00E-02
8	Ksd	6.56E-02	4.92E-03
9	Pz	2.23E-02	1.08E-02
10	PCb	2.38E-03	2.38E-03
11	Pz_Pit	X - 3.28E-04 Y - 3.28E-03	3.28E-03
15	QTg_TB	3.61E-01	1.31E-01

Legend

Perennial Stream
Ephemeral Drainage
Railroad
Roads
Proposed Rosemont Open Pit
Towns

Geology

Qal
QTg
QTg_TB
QTg1
QTg2
Tsp
KTi
Kv
Ksd
Pz
Pz_Pit
PCb

TETRA TECH

ROSEMONT COPPER

FIGURE 22. MODEL LAYER 9 HYDRAULIC CONDUCTIVITY DISTRIBUTION

2010-07-16

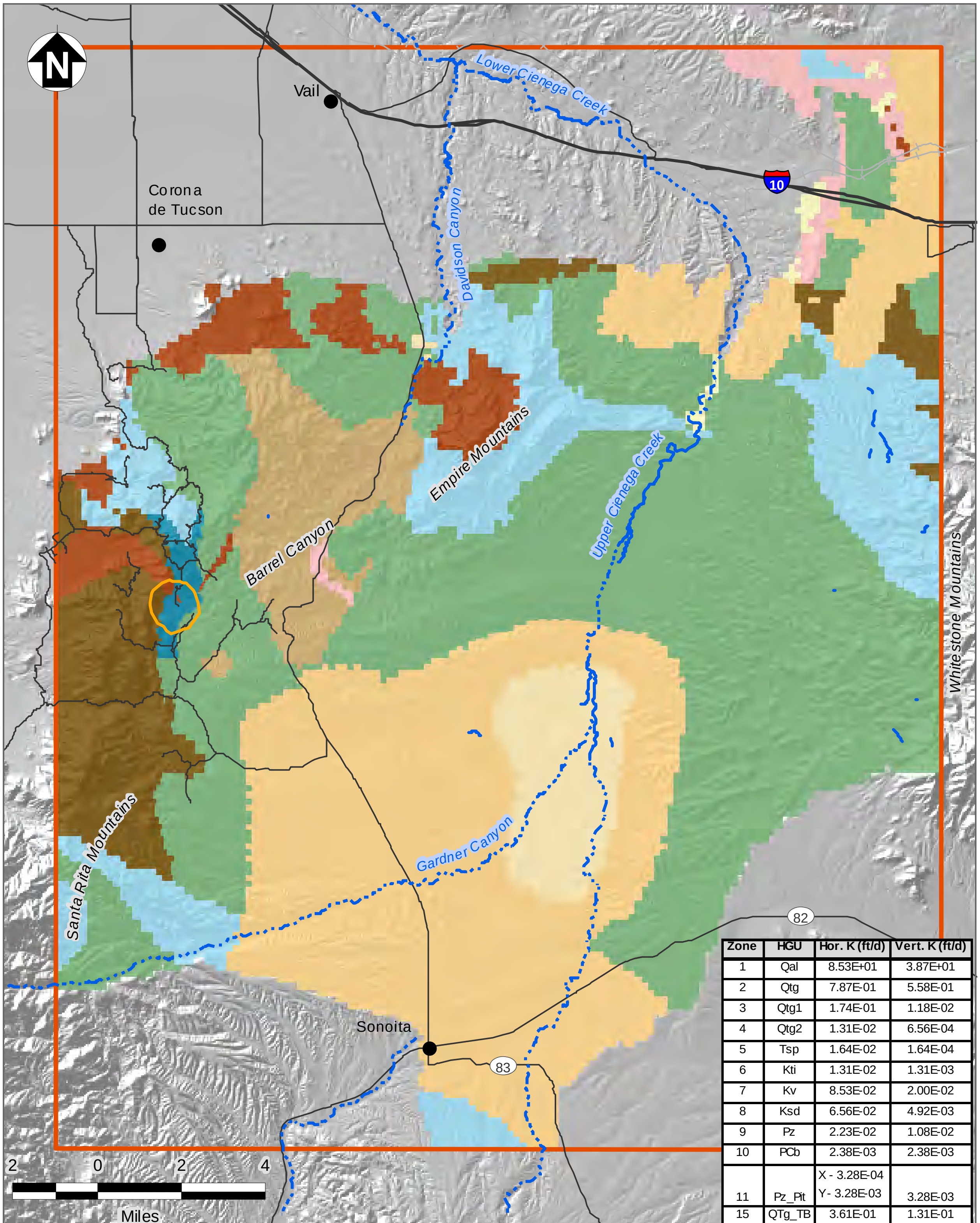

Zone	HGU	Hor. K (ft/d)	Vert. K (ft/d)
1	Qal	8.53E+01	3.87E+01
2	Qtg	7.87E-01	5.58E-01
3	Qtg1	1.74E-01	1.18E-02
4	Qtg2	1.31E-02	6.56E-04
5	Tsp	1.64E-02	1.64E-04
6	Kti	1.31E-02	1.31E-03
7	Kv	8.53E-02	2.00E-02
8	Ksd	6.56E-02	4.92E-03
9	Pz	2.23E-02	1.08E-02
10	PCb	2.38E-03	2.38E-03
11	Pz_Pit	X - 3.28E-04 Y - 3.28E-03	3.28E-03
15	QTg_TB	3.61E-01	1.31E-01

Legend

Perennial Stream
Ephemeral Drainage
Railroad
Roads
Proposed Rosemont Open Pit
Towns

Geology

Qal
QTg
QTg_TB
QTg1
QTg2
Tsp
KTi
Kv
Ksd
Pz
Pz_Pit
PCb

TETRA TECH

ROSEMONT COPPER

FIGURE 23. MODEL LAYER 10 HYDRAULIC CONDUCTIVITY DISTRIBUTION

2010-07-16

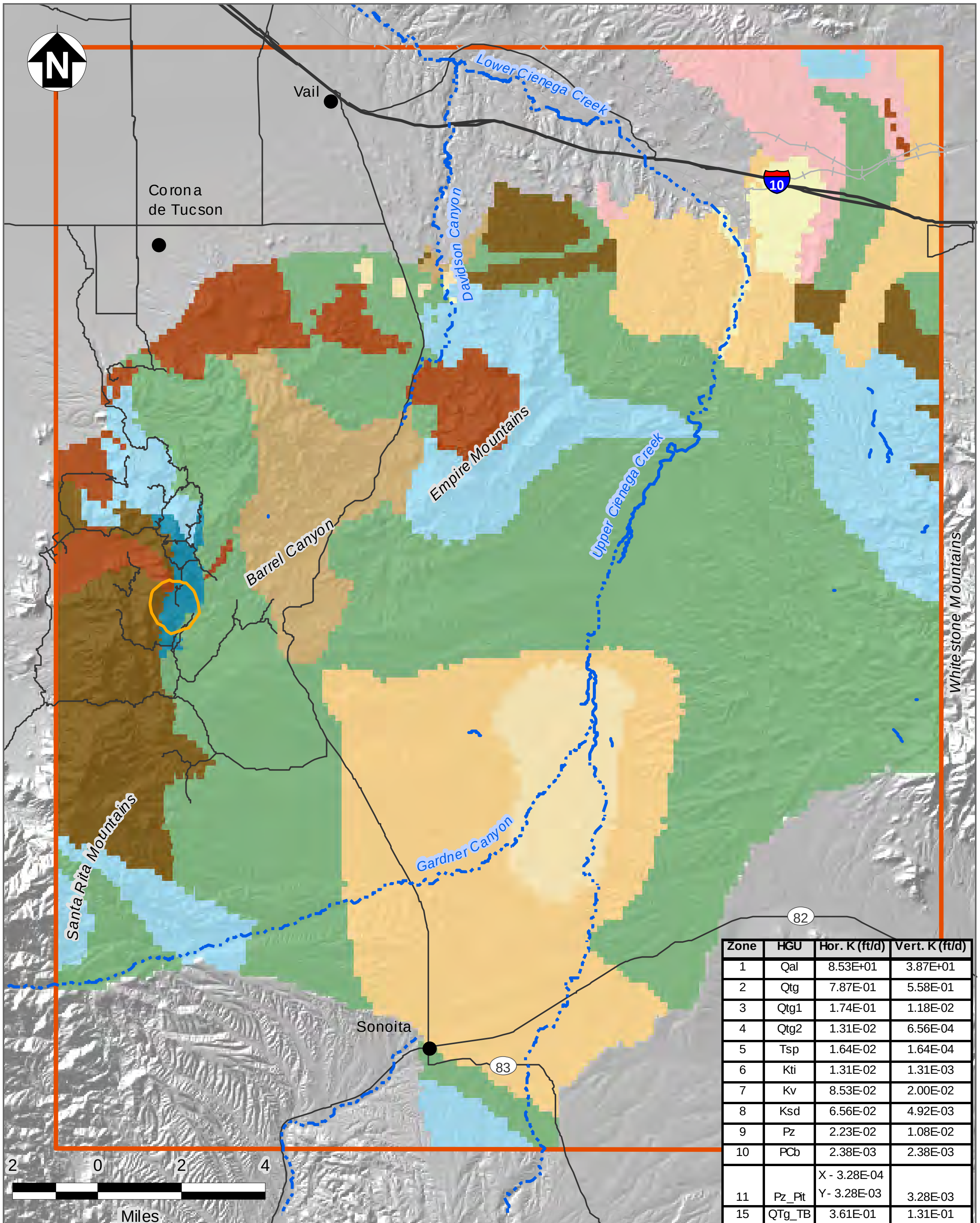

Zone	HGU	Hor. K (ft/d)	Vert. K (ft/d)
1	Qal	8.53E+01	3.87E+01
2	Qtg	7.87E-01	5.58E-01
3	Qtg1	1.74E-01	1.18E-02
4	Qtg2	1.31E-02	6.56E-04
5	Tsp	1.64E-02	1.64E-04
6	Kti	1.31E-02	1.31E-03
7	Kv	8.53E-02	2.00E-02
8	Ksd	6.56E-02	4.92E-03
9	Pz	2.23E-02	1.08E-02
10	PCb	2.38E-03	2.38E-03
11	Pz_Pit	X - 3.28E-04 Y - 3.28E-03	3.28E-03
15	QTg_TB	3.61E-01	1.31E-01

Legend

Perennial Stream

Ephemeral Drainage

Railroad

Roads

Proposed Rosemont Open Pit

Towns

Geology

Qal

QTg

QTg_TB

QTg1

QTg2

Tsp

KTi

Kv

Ksd

Pz

Pz_Pit

PCb

TETRA TECH

ROSEMONT COPPER

FIGURE 24. MODEL LAYER 11 HYDRAULIC CONDUCTIVITY DISTRIBUTION

2010-07-16

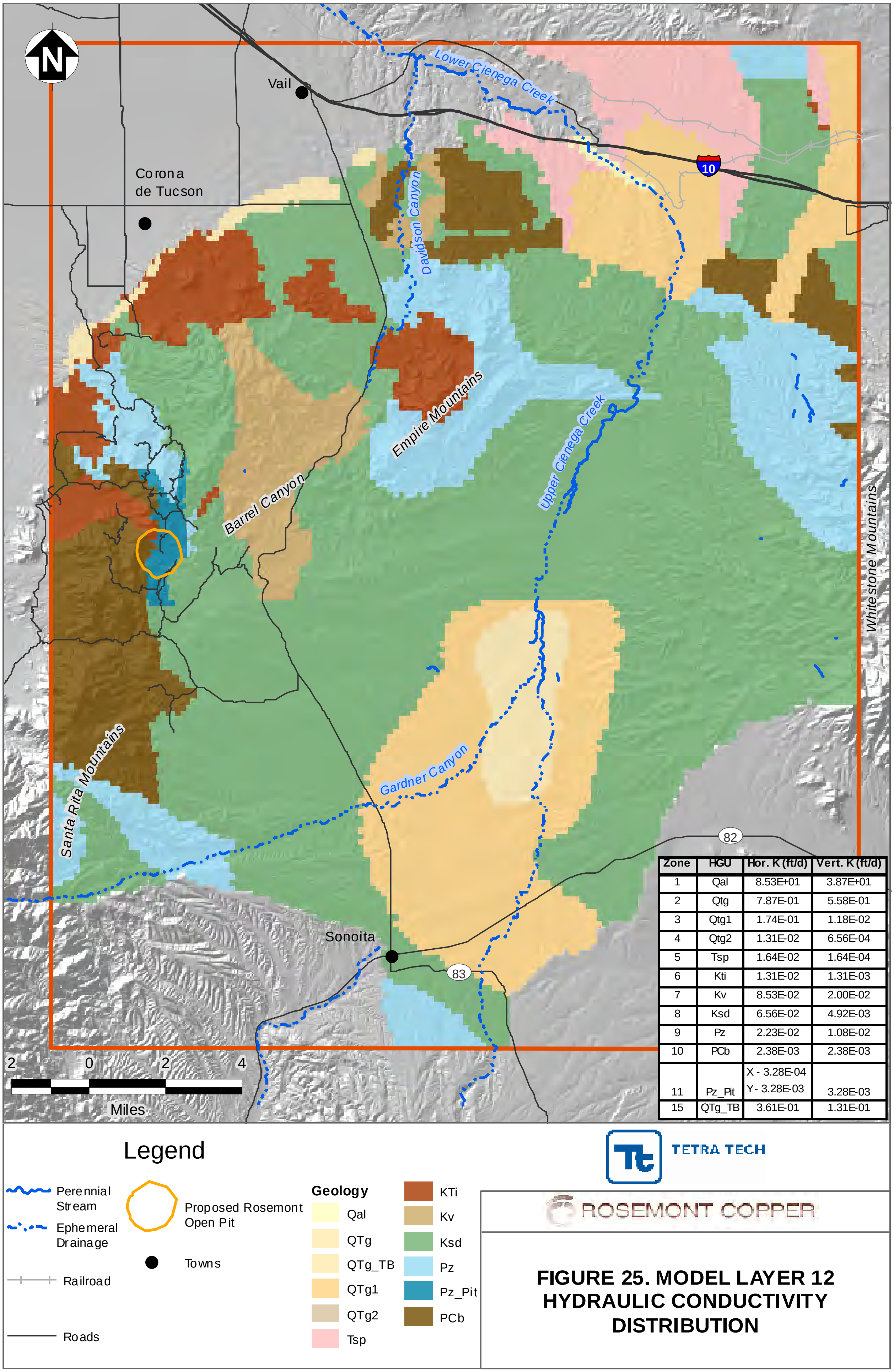

Zone	HGU	Hor. K (ft/d)	Vert. K (ft/d)
1	Qal	8.53E+01	3.87E+01
2	Qtg	7.87E-01	5.58E-01
3	Qtg1	1.74E-01	1.18E-02
4	Qtg2	1.31E-02	6.56E-04
5	Tsp	1.64E-02	1.64E-04
6	Kti	1.31E-02	1.31E-03
7	Kv	8.53E-02	2.00E-02
8	Ksd	6.56E-02	4.92E-03
9	Pz	2.23E-02	1.08E-02
10	PCb	2.38E-03	2.38E-03
11	Pz_Pit	X - 3.28E-04 Y - 3.28E-03	3.28E-03
15	QTg_TB	3.61E-01	1.31E-01

TETRA TECH

ROSEMONT COPPER

FIGURE 25. MODEL LAYER 12 HYDRAULIC CONDUCTIVITY DISTRIBUTION

2010-07-16

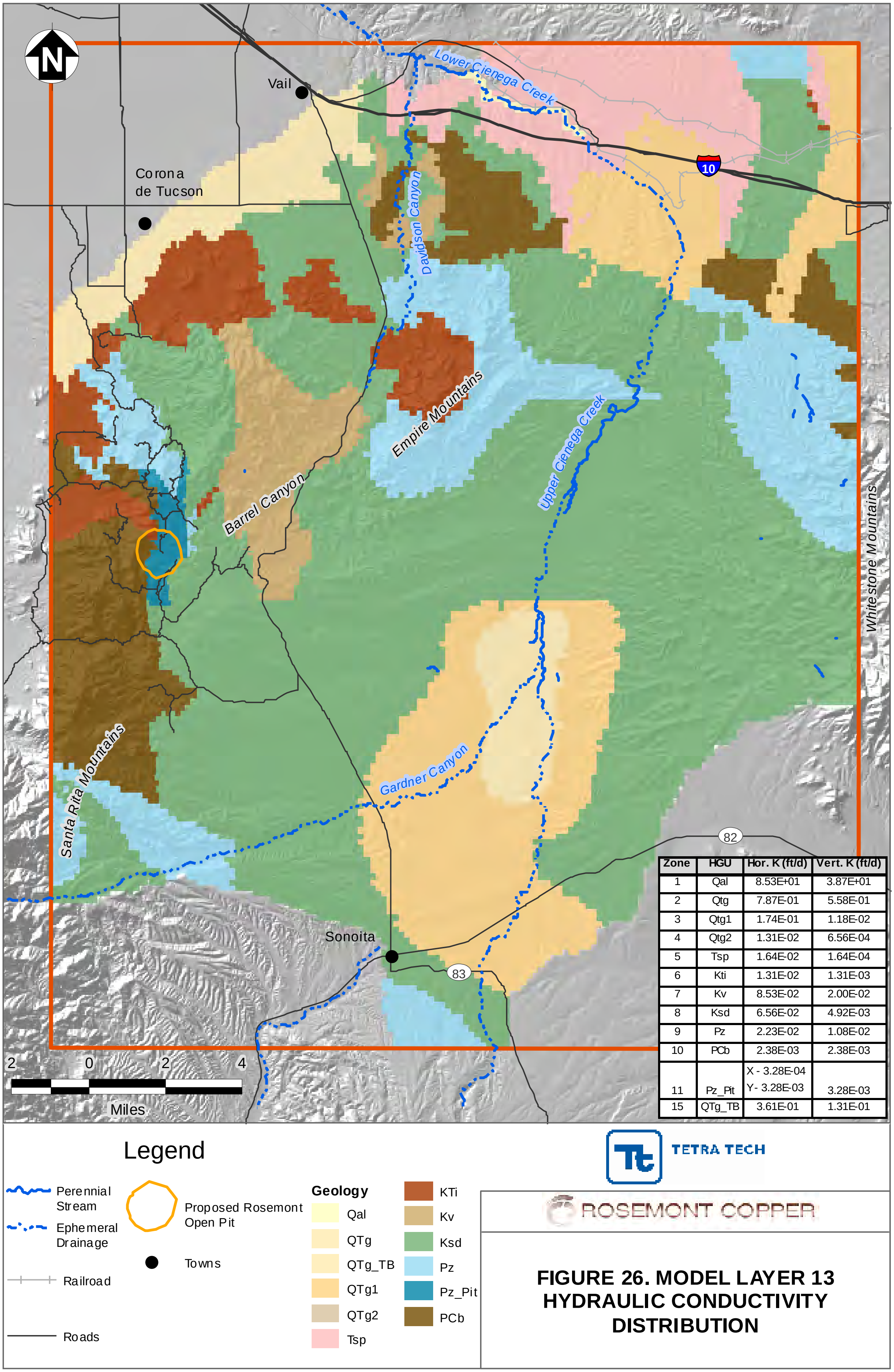

Zone	HGU	Hor. K (ft/d)	Vert. K (ft/d)
1	Qal	8.53E+01	3.87E+01
2	Qtg	7.87E-01	5.58E-01
3	Qtg1	1.74E-01	1.18E-02
4	Qtg2	1.31E-02	6.56E-04
5	Tsp	1.64E-02	1.64E-04
6	Kti	1.31E-02	1.31E-03
7	Kv	8.53E-02	2.00E-02
8	Ksd	6.56E-02	4.92E-03
9	Pz	2.23E-02	1.08E-02
10	PCb	2.38E-03	2.38E-03
11	Pz_Pit	X - 3.28E-04 Y- 3.28E-03	3.28E-03
15	QTg_TB	3.61E-01	1.31E-01

TETRA TECH

ROSEMONT COPPER

FIGURE 26. MODEL LAYER 13 HYDRAULIC CONDUCTIVITY DISTRIBUTION

2010-07-16

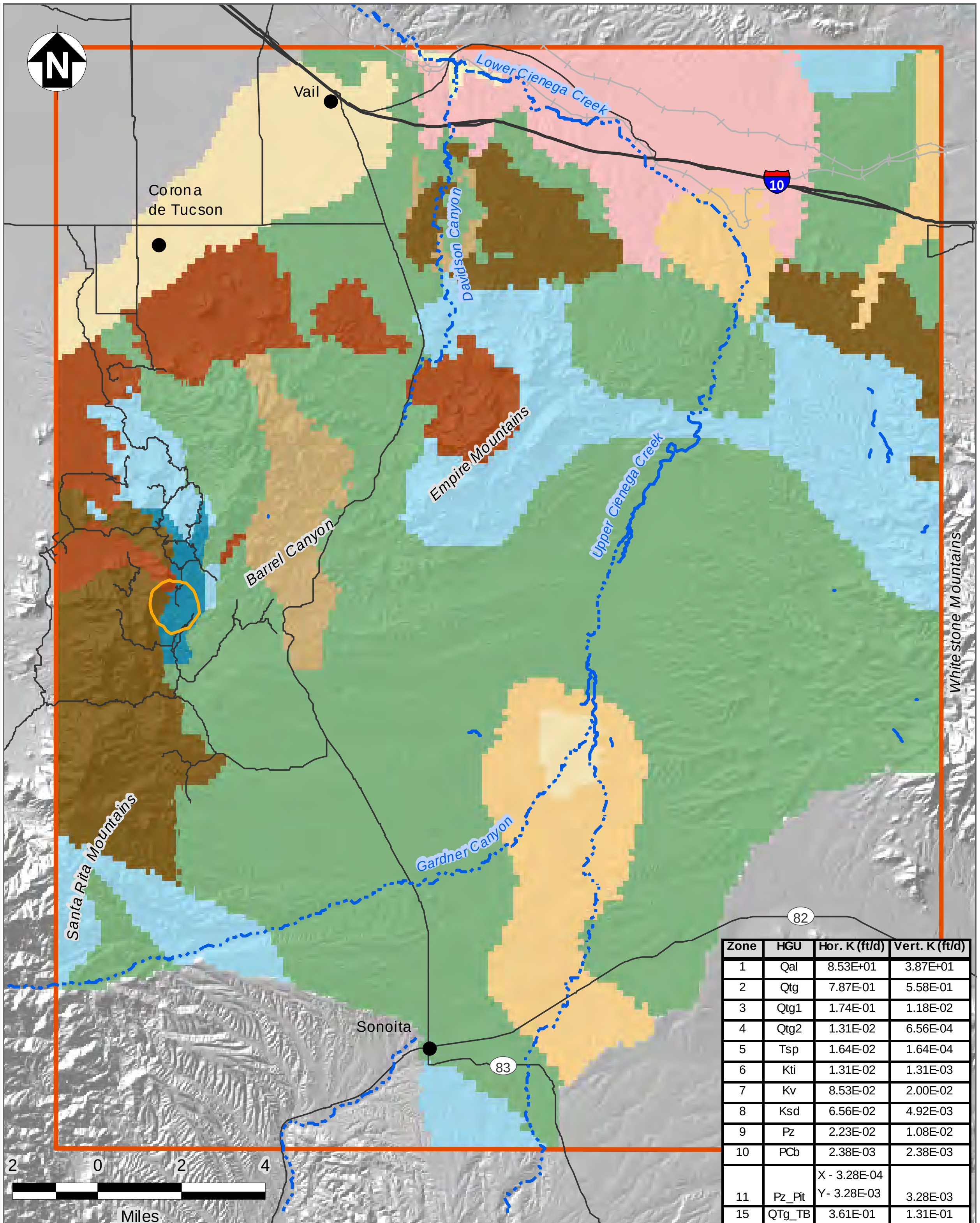

Zone	HGU	Hor. K (ft/d)	Vert. K (ft/d)
1	Qal	8.53E+01	3.87E+01
2	Qtg	7.87E-01	5.58E-01
3	Qtg1	1.74E-01	1.18E-02
4	Qtg2	1.31E-02	6.56E-04
5	Tsp	1.64E-02	1.64E-04
6	Kti	1.31E-02	1.31E-03
7	Kv	8.53E-02	2.00E-02
8	Ksd	6.56E-02	4.92E-03
9	Pz	2.23E-02	1.08E-02
10	PCb	2.38E-03	2.38E-03
11	Pz_Pit	X - 3.28E-04 Y - 3.28E-03	3.28E-03
15	QTg_TB	3.61E-01	1.31E-01

Legend

Perennial Stream
Ephemeral Drainage
Railroad
Roads
Proposed Rosemont Open Pit
Towns

Geology

Qal
QTg
QTg_TB
QTg1
QTg2
Tsp
KTi
Kv
Ksd
Pz
Pz_Pit
PCb

TETRA TECH

ROSEMONT COPPER

FIGURE 27. MODEL LAYER 14 HYDRAULIC CONDUCTIVITY DISTRIBUTION

2010-07-16

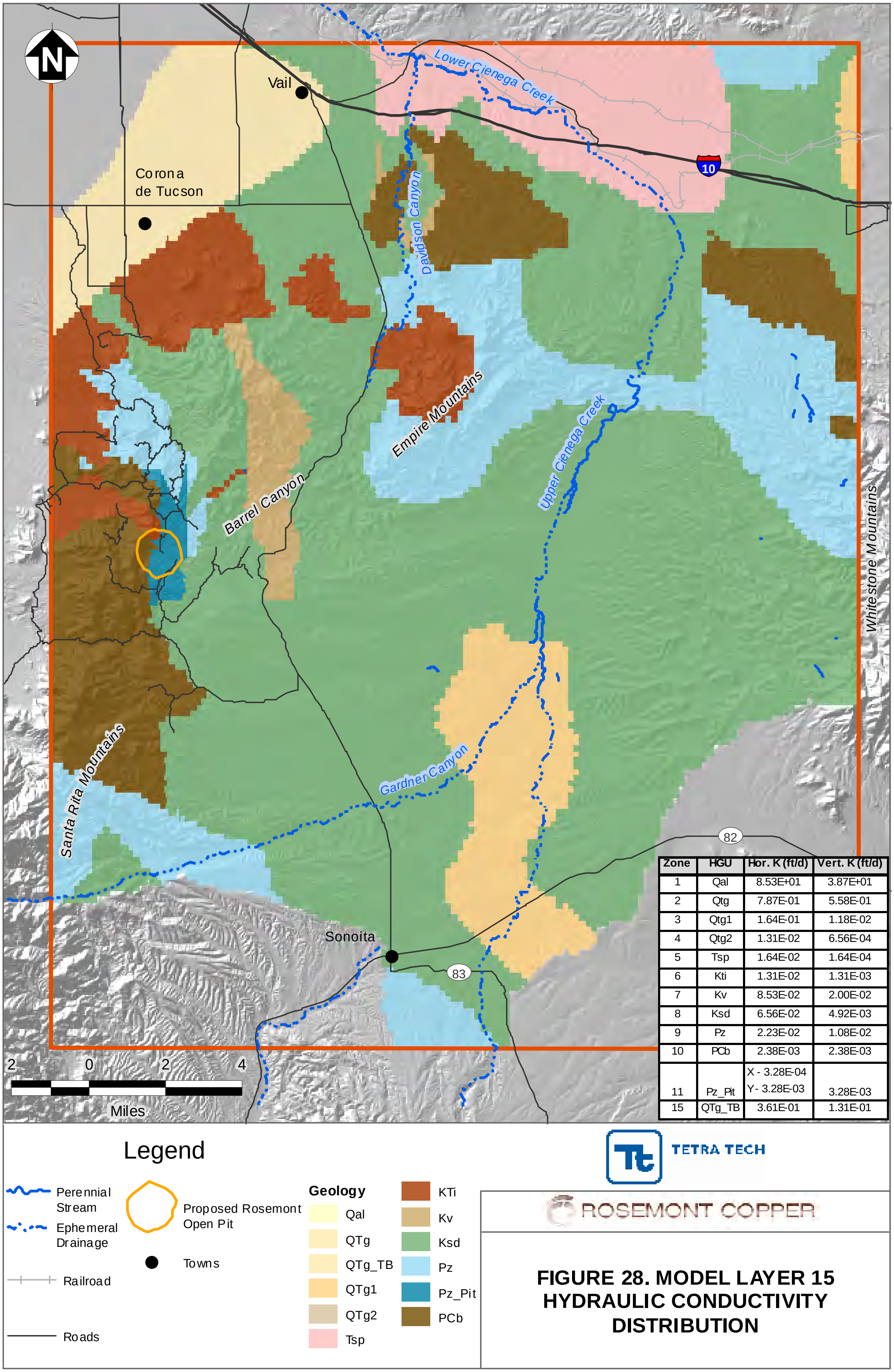

Zone	HGU	Hor. K (ft/d)	Vert. K (ft/d)
1	Qal	8.53E+01	3.87E+01
2	Qtg	7.87E-01	5.58E-01
3	Qtg1	1.64E-01	1.18E-02
4	Qtg2	1.31E-02	6.56E-04
5	Tsp	1.64E-02	1.64E-04
6	Kti	1.31E-02	1.31E-03
7	Kv	8.53E-02	2.00E-02
8	Ksd	6.56E-02	4.92E-03
9	Pz	2.23E-02	1.08E-02
10	PCb	2.38E-03	2.38E-03
11	Pz_Pit	X - 3.28E-04 Y- 3.28E-03	3.28E-03
15	QTg_TB	3.61E-01	1.31E-01

FIGURE 28. MODEL LAYER 15 HYDRAULIC CONDUCTIVITY DISTRIBUTION

2010-07-16

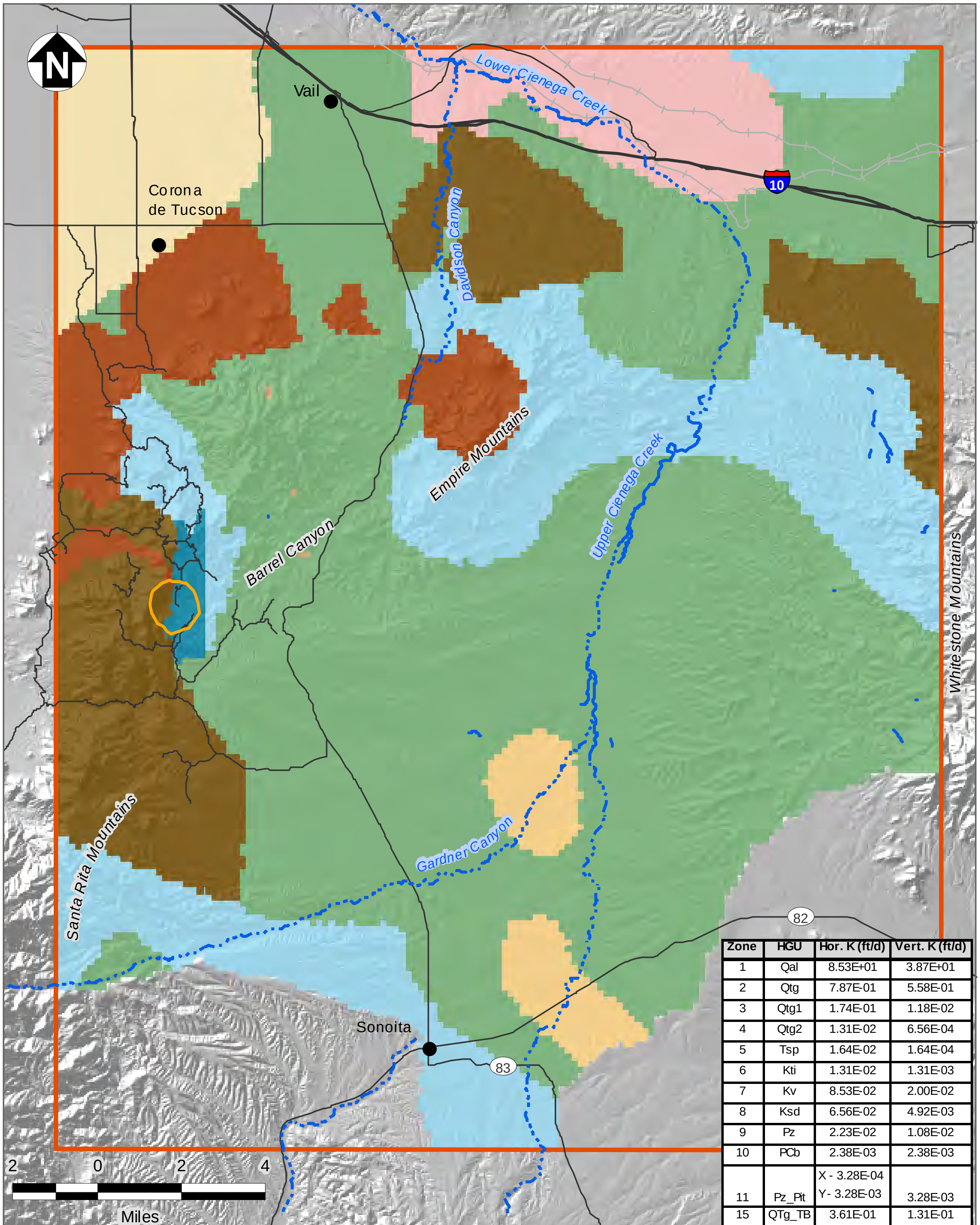

Zone	HGU	Hor. K (ft/d)	Vert. K (ft/d)
1	Qal	8.53E+01	3.87E+01
2	Qtg	7.87E-01	5.58E-01
3	Qtg1	1.74E-01	1.18E-02
4	Qtg2	1.31E-02	6.56E-04
5	Tsp	1.64E-02	1.64E-04
6	Kti	1.31E-02	1.31E-03
7	Kv	8.53E-02	2.00E-02
8	Ksd	6.56E-02	4.92E-03
9	Pz	2.23E-02	1.08E-02
10	PCb	2.38E-03	2.38E-03
11	Pz_Pit	X - 3.28E-04 Y - 3.28E-03	3.28E-03
15	QTg_TB	3.61E-01	1.31E-01

Legend

Perennial Stream
Ephemeral Drainage
Railroad
Roads
Proposed Rosemont Open Pit
Towns

Geology

Qal
QTg
QTg_TB
QTg1
QTg2
Tsp
KTi
Kv
Ksd
Pz
Pz_Pit
PCb

TETRA TECH

ROSEMONT COPPER

FIGURE 29. MODEL LAYER 16 HYDRAULIC CONDUCTIVITY DISTRIBUTION

2010-07-16

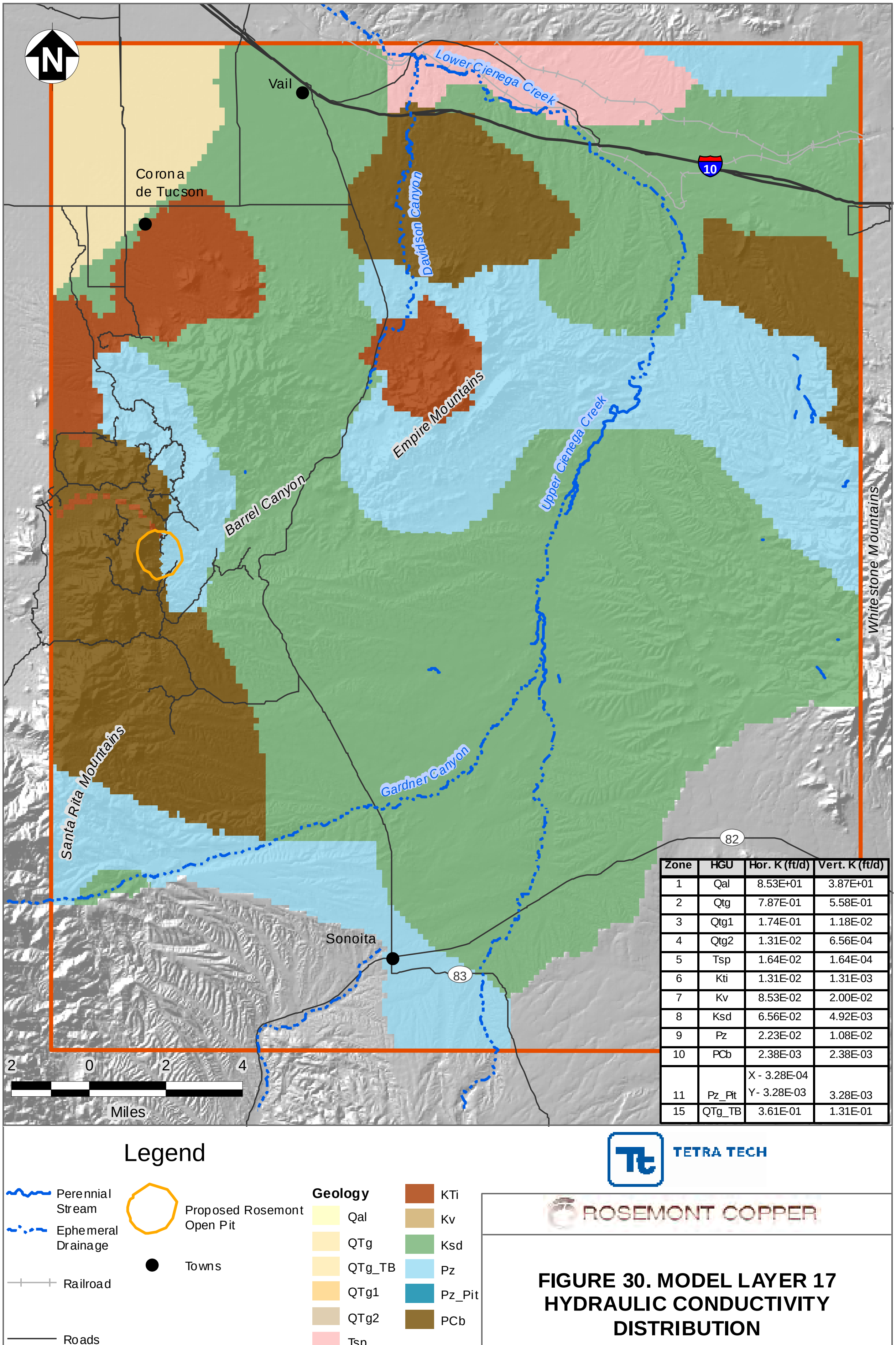

Zone	HGU	Hor. K (ft/d)	Vert. K (ft/d)
1	Qal	8.53E+01	3.87E+01
2	Qtg	7.87E-01	5.58E-01
3	Qtg1	1.74E-01	1.18E-02
4	Qtg2	1.31E-02	6.56E-04
5	Tsp	1.64E-02	1.64E-04
6	Kti	1.31E-02	1.31E-03
7	Kv	8.53E-02	2.00E-02
8	Ksd	6.56E-02	4.92E-03
9	Pz	2.23E-02	1.08E-02
10	PCb	2.38E-03	2.38E-03
11	Pz_Pit	X - 3.28E-04 Y - 3.28E-03	3.28E-03
15	QTg_TB	3.61E-01	1.31E-01

TETRA TECH

ROSEMONT COPPER

FIGURE 30. MODEL LAYER 17 HYDRAULIC CONDUCTIVITY DISTRIBUTION

2010-07-16

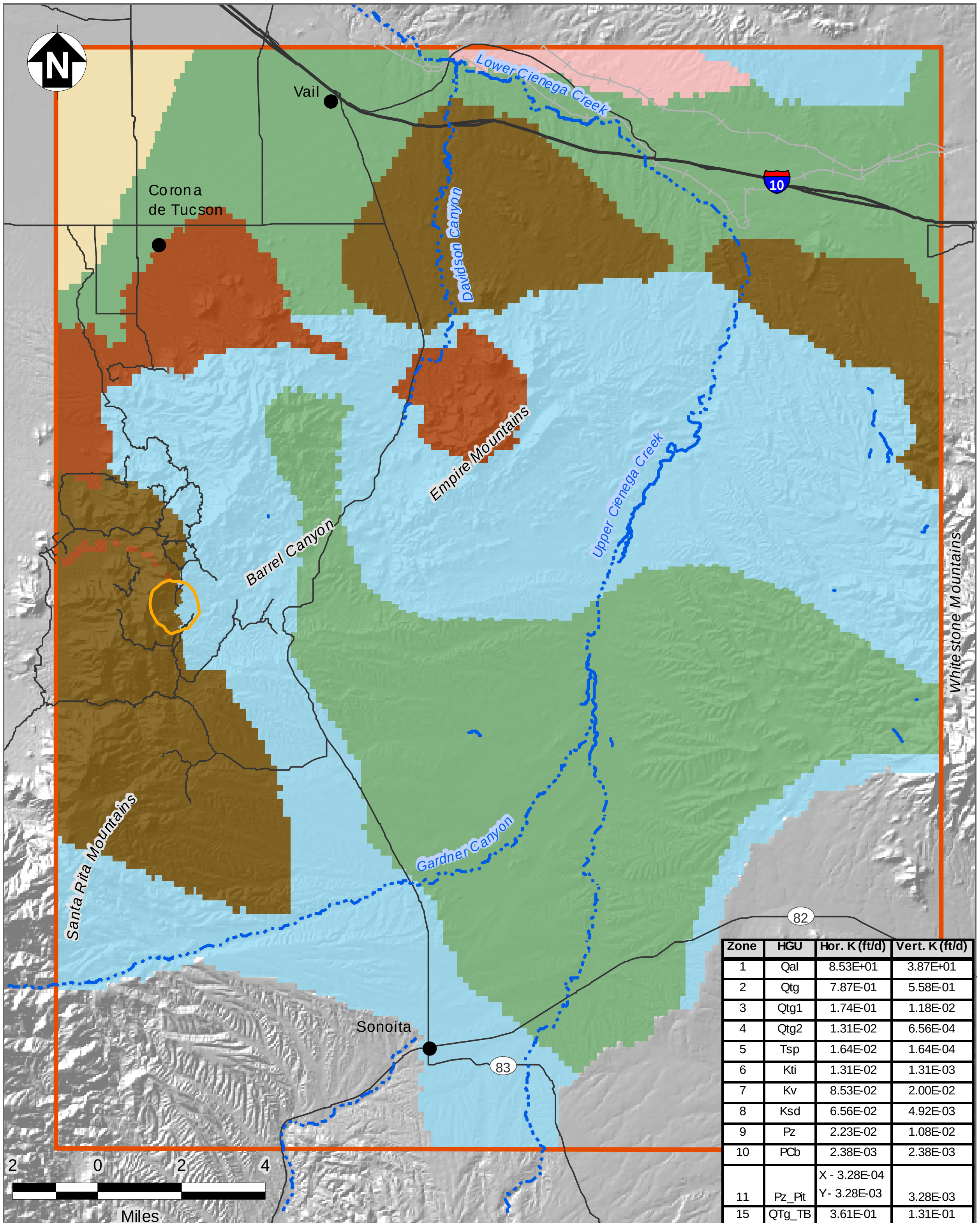

Zone	HGU	Hor. K (ft/d)	Vert. K (ft/d)
1	Qal	8.53E+01	3.87E+01
2	Qtg	7.87E-01	5.58E-01
3	Qtg1	1.74E-01	1.18E-02
4	Qtg2	1.31E-02	6.56E-04
5	Tsp	1.64E-02	1.64E-04
6	Kti	1.31E-02	1.31E-03
7	Kv	8.53E-02	2.00E-02
8	Ksd	6.56E-02	4.92E-03
9	Pz	2.23E-02	1.08E-02
10	PCb	2.38E-03	2.38E-03
11	Pz_Pit	X - 3.28E-04 Y- 3.28E-03	3.28E-03
15	QTg_TB	3.61E-01	1.31E-01

Legend

Perennial Stream

Ephemeral Drainage

Railroad

Roads

Proposed Rosemont Open Pit

Towns

Geology

Qal

QTg

QTg_TB

QTg1

QTg2

Tsp

KTi

Kv

Ksd

Pz

Pz_Pit

PCb

TETRA TECH

ROSEMONT COPPER

FIGURE 31. MODEL LAYER 18 HYDRAULIC CONDUCTIVITY DISTRIBUTION

2010-07-16

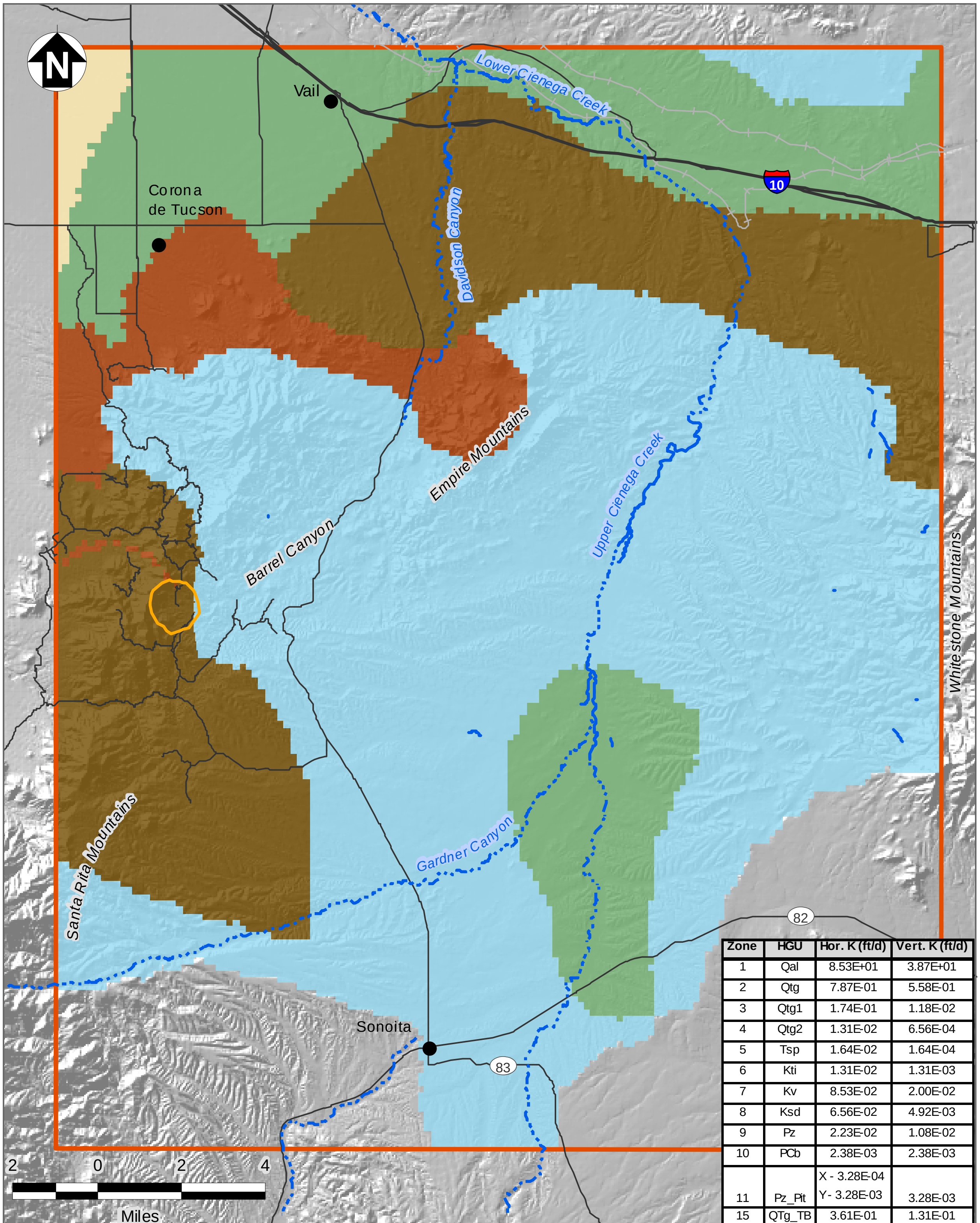

Zone	HGU	Hor. K (ft/d)	Vert. K (ft/d)
1	Qal	8.53E+01	3.87E+01
2	Qtg	7.87E-01	5.58E-01
3	Qtg1	1.74E-01	1.18E-02
4	Qtg2	1.31E-02	6.56E-04
5	Tsp	1.64E-02	1.64E-04
6	Kti	1.31E-02	1.31E-03
7	Kv	8.53E-02	2.00E-02
8	Ksd	6.56E-02	4.92E-03
9	Pz	2.23E-02	1.08E-02
10	PCb	2.38E-03	2.38E-03
11	Pz_Pit	X - 3.28E-04 Y - 3.28E-03	3.28E-03
15	QTg_TB	3.61E-01	1.31E-01

Legend

Perennial Stream
Ephemeral Drainage
Railroad
Roads
Proposed Rosemont Open Pit
Towns

Geology

Qal
QTg
QTg_TB
QTg1
QTg2
Tsp
KTi
Kv
Ksd
Pz
Pz_Pit
PCb

TETRA TECH

ROSEMONT COPPER

FIGURE 32. MODEL LAYER 19 HYDRAULIC CONDUCTIVITY DISTRIBUTION

2010-07-16

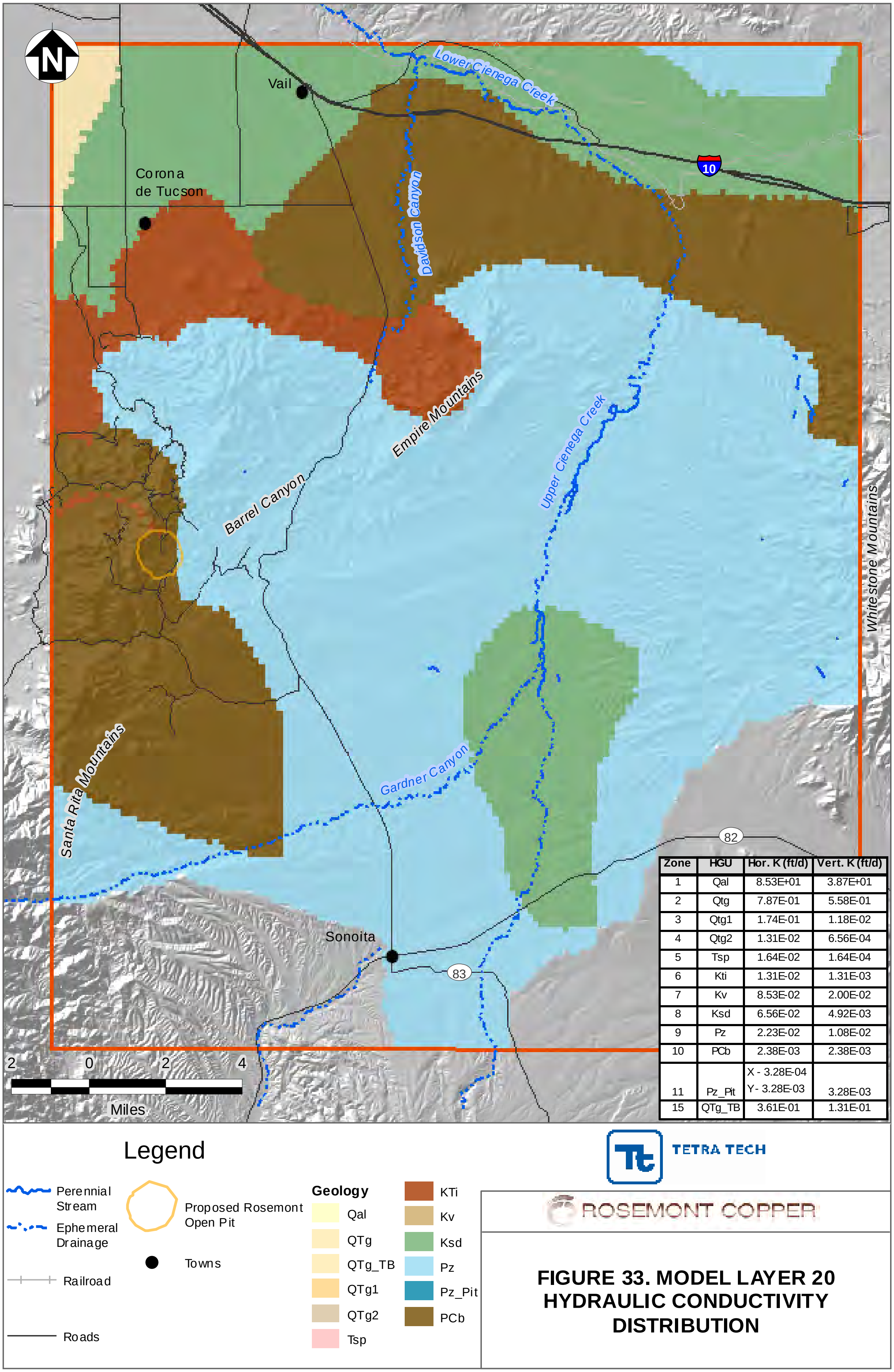

Zone	HGU	Hor. K (ft/d)	Vert. K (ft/d)
1	Qal	8.53E+01	3.87E+01
2	Qtg	7.87E-01	5.58E-01
3	Qtg1	1.74E-01	1.18E-02
4	Qtg2	1.31E-02	6.56E-04
5	Tsp	1.64E-02	1.64E-04
6	Kti	1.31E-02	1.31E-03
7	Kv	8.53E-02	2.00E-02
8	Ksd	6.56E-02	4.92E-03
9	Pz	2.23E-02	1.08E-02
10	PCb	2.38E-03	2.38E-03
11	Pz_Pit	X - 3.28E-04 Y - 3.28E-03	3.28E-03
15	QTg_TB	3.61E-01	1.31E-01

FIGURE 33. MODEL LAYER 20 HYDRAULIC CONDUCTIVITY DISTRIBUTION

2010-07-16

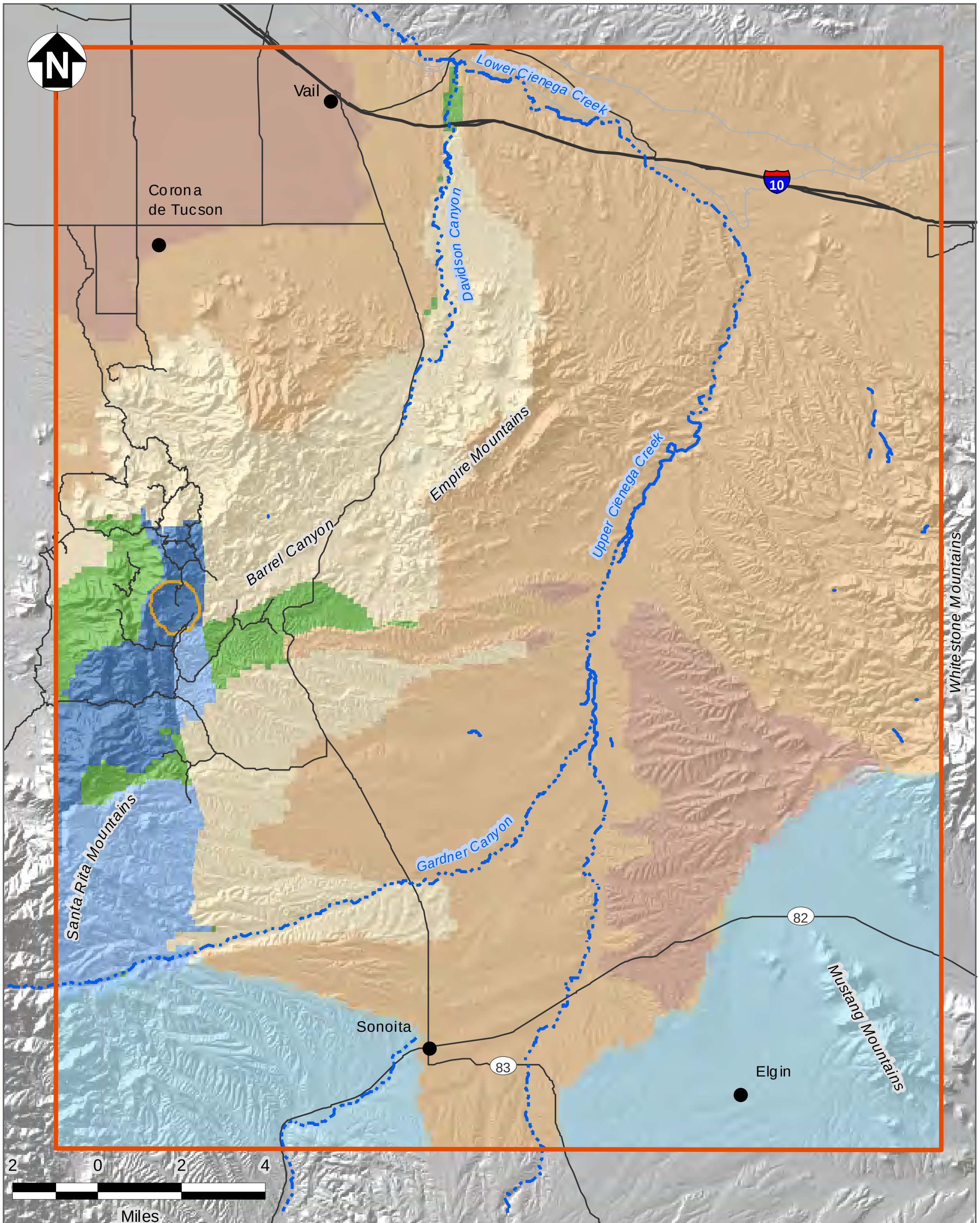

Legend

Perennial Stream
Ephemeral Drainage
No Flow Cells
Extent of Model Domain
Railroad
Proposed Rosemont Open Pit
Roads
Towns

Recharge (in/yr)
0.33
0.37
0.42
0.53
0.68
1.31

TETRA TECH

ROSEMONT COPPER

FIGURE 34. SIMULATED RECHARGE

2010-07-16

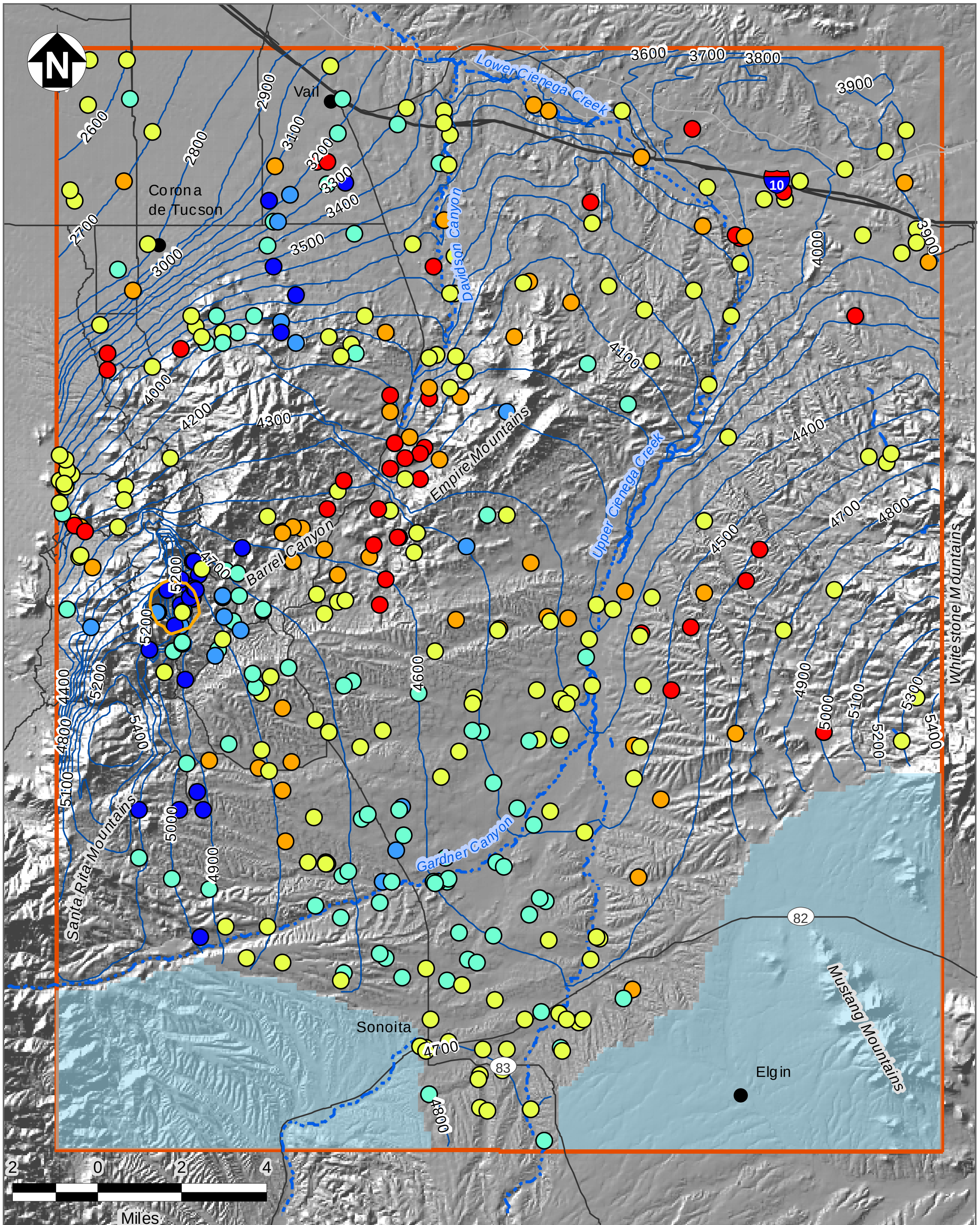

Legend

- Perennial Stream
- Ephemeral Drainage
- No Flow Cells
- Extent of Model Domain
- Railroad
- Roads
- Proposed Rosemont Open Pit
- Towns
- Water-Level Contours (ft)

Weighted Residuals (ft)

Residual

- -334 - -100
- -99 - -50
- -49 - 0
- 1 - 50
- 51 - 100
- 101 - 465

TETRA TECH

ROSEMONT COPPER

FIGURE 35. WEIGHTED WATER-LEVEL RESIDUALS FOR CALIBRATED STEADY-STATE MODEL

2010-07-16

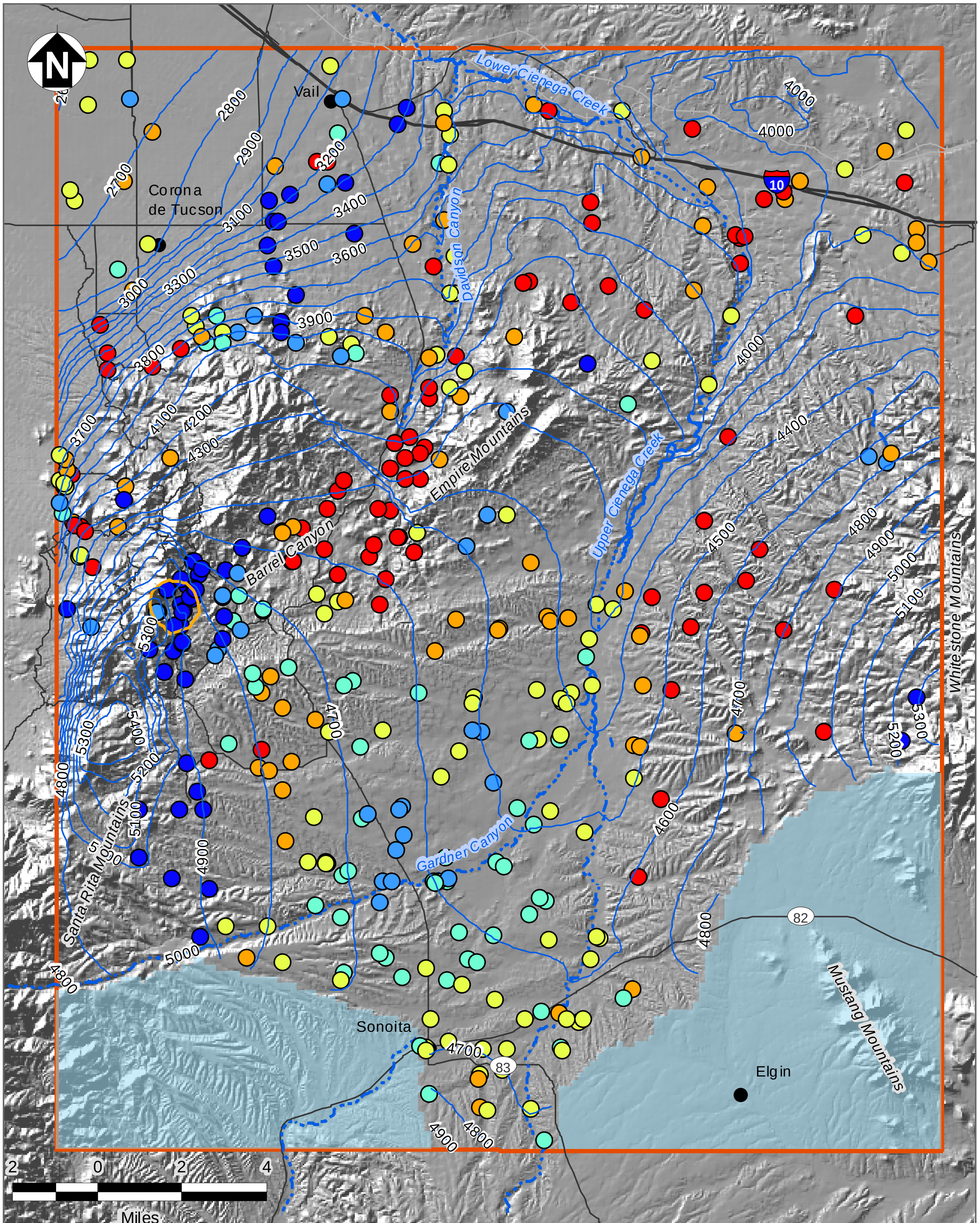

Legend

Perennial Stream
Ephemeral Drainage
No Flow Cells
Extent of Model Domain
Railroad
Roads
Proposed Rosemont Open Pit
Towns
Water-Level Contours (ft)

Unweighted Residuals (ft)

Residual

- -334 - -100
- -99 - -50
- -49 - 0
- 1 - 50
- 51 - 100
- 101 - 465

TETRA TECH

ROSEMONT COPPER

FIGURE 36. UNWEIGHTED WATER-LEVEL RESIDUALS FOR CALIBRATED STEADY-STATE MODEL

2010-07-16

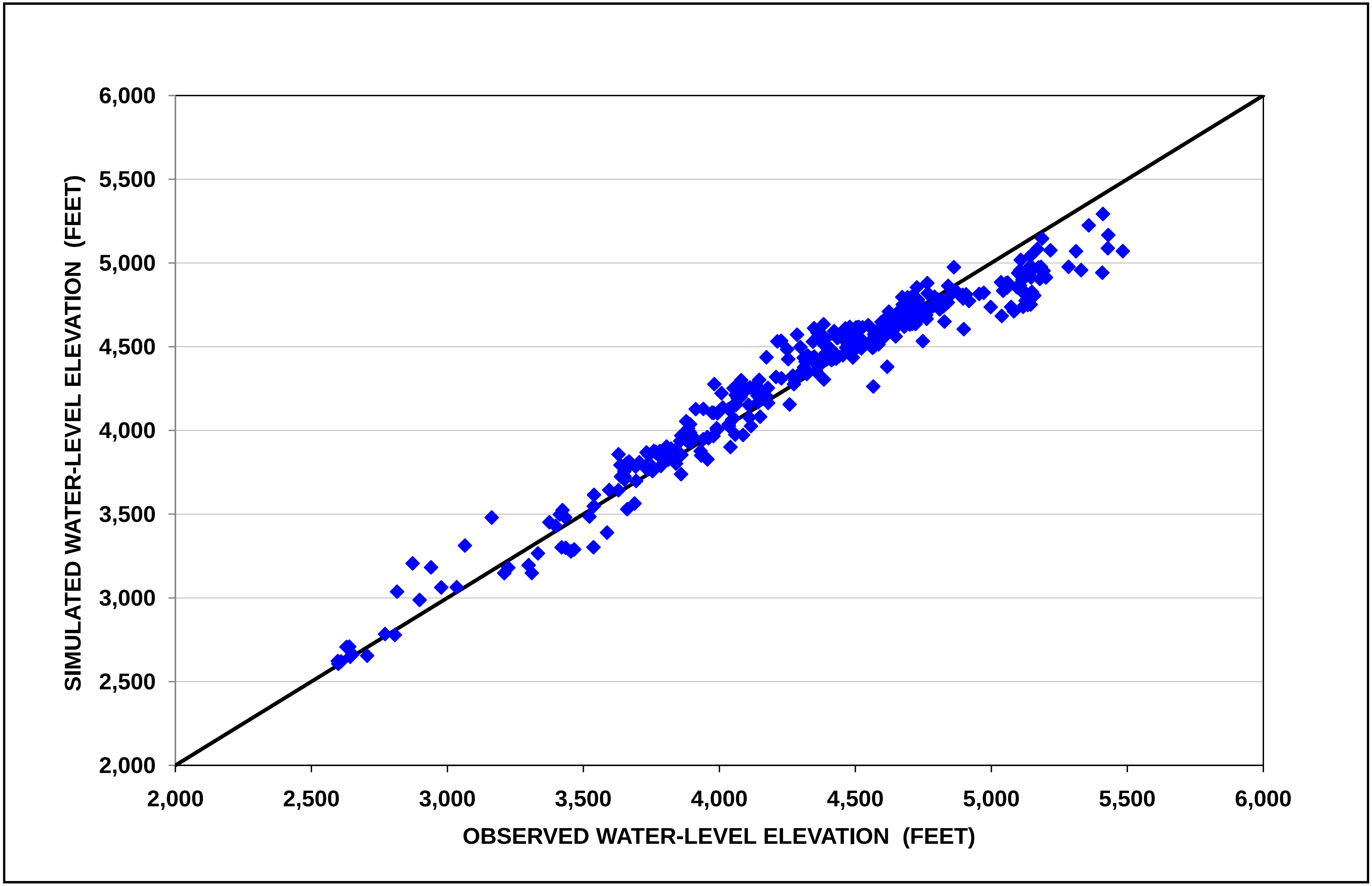

Project No: 114-320874

July 2010

Figure 37
Observed versus Simulated Water Levels

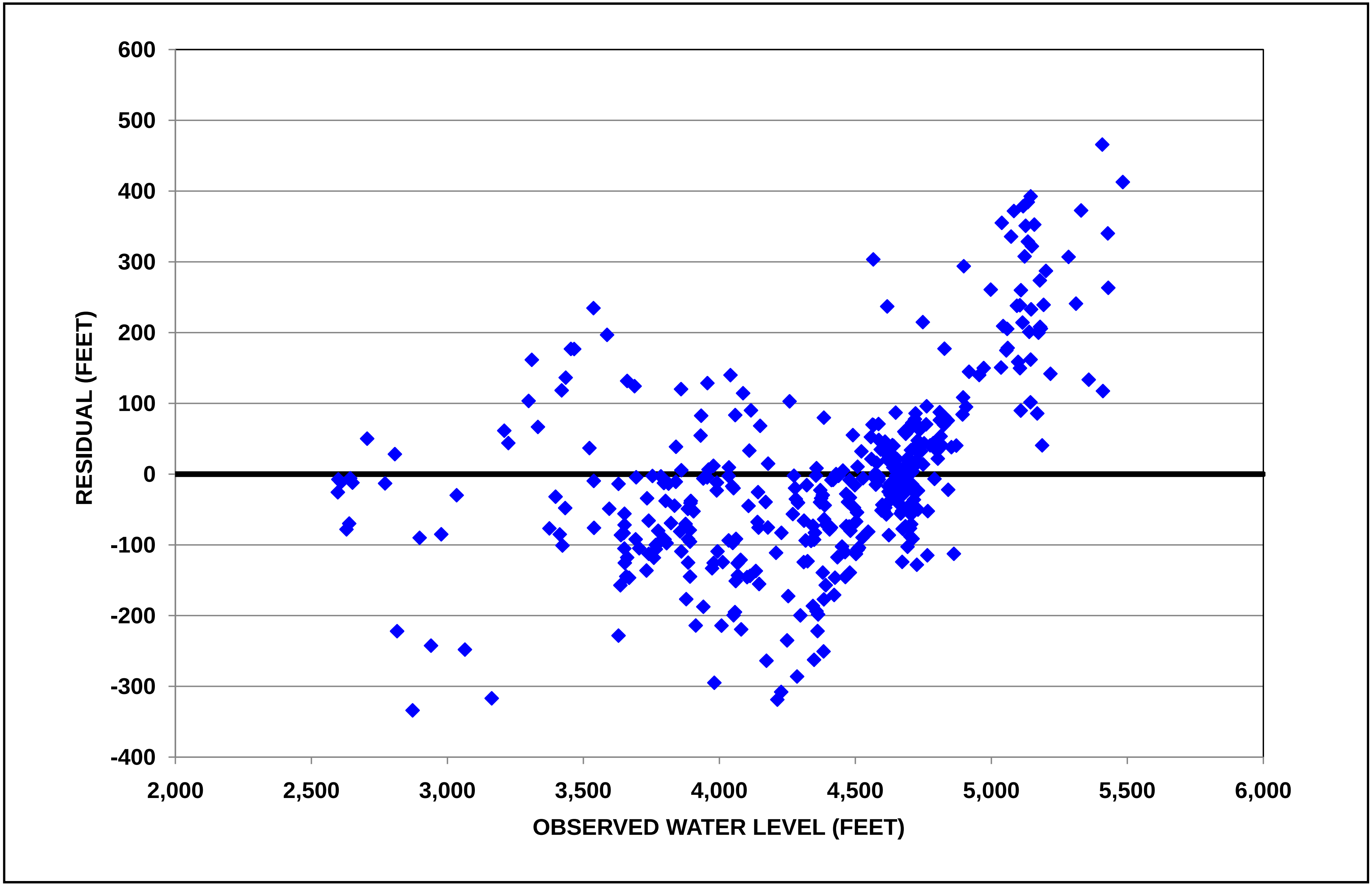

Project No: 114-320874

July 2010

Figure 38
Observed versus Unweighted Residuals

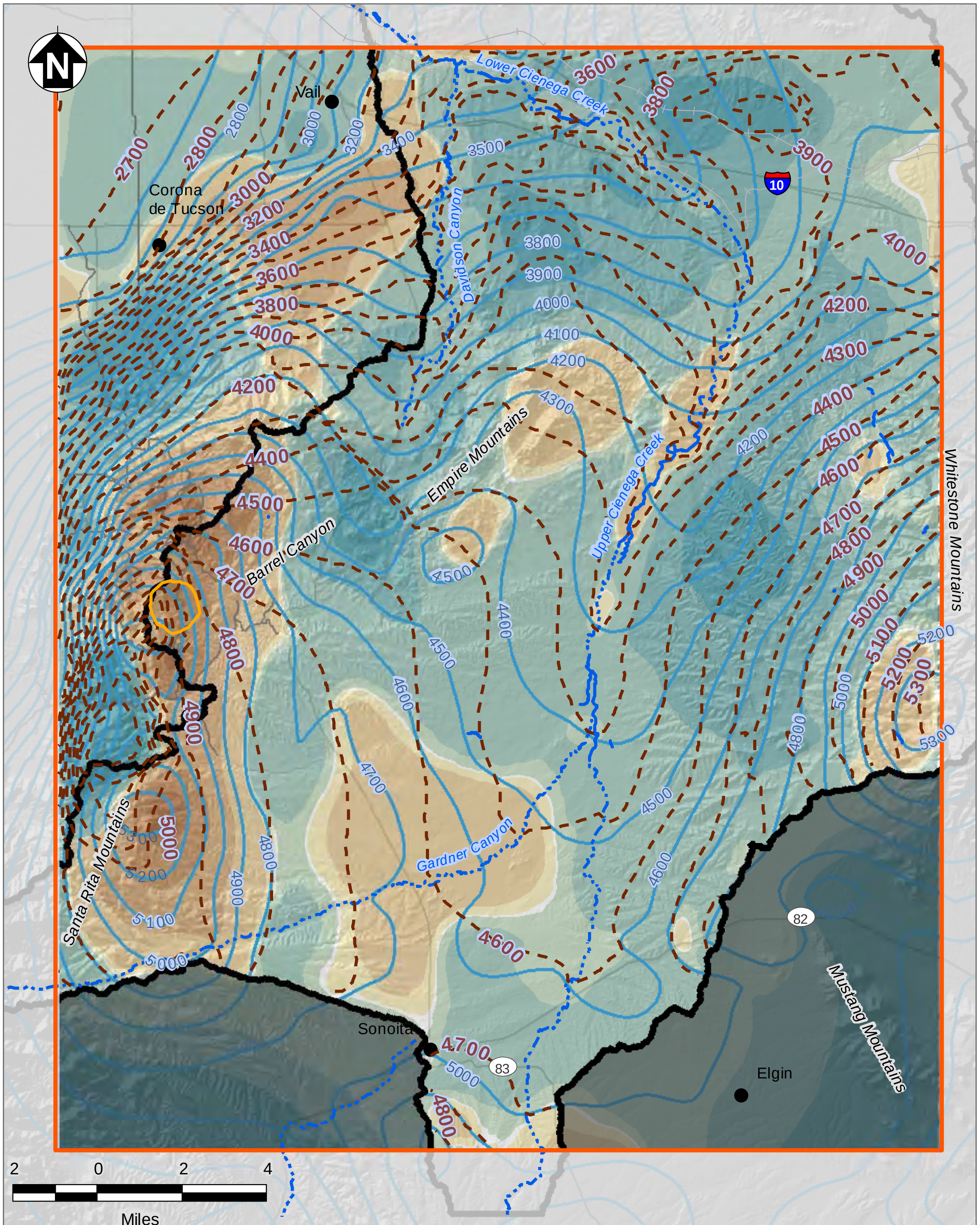

Legend

Perennial Stream

Ephemeral Drainage

No Flow Cells

Railroad

Roads

Towns

Cienega Creek Watershed

Simulated Water Levels (ft)

Observed Water Levels (ft)

Proposed Rosemont Open Pit

Water-Level Residuals

Model Underpredicts by 300 ft

Zero Residual

Model Overpredicts by 300 ft

TETRA TECH

ROSEMONT COPPER

FIGURE 39. SIMULATED VERSUS OBSERVED POTENTIOMETRIC SURFACE MAP

2010-07-16

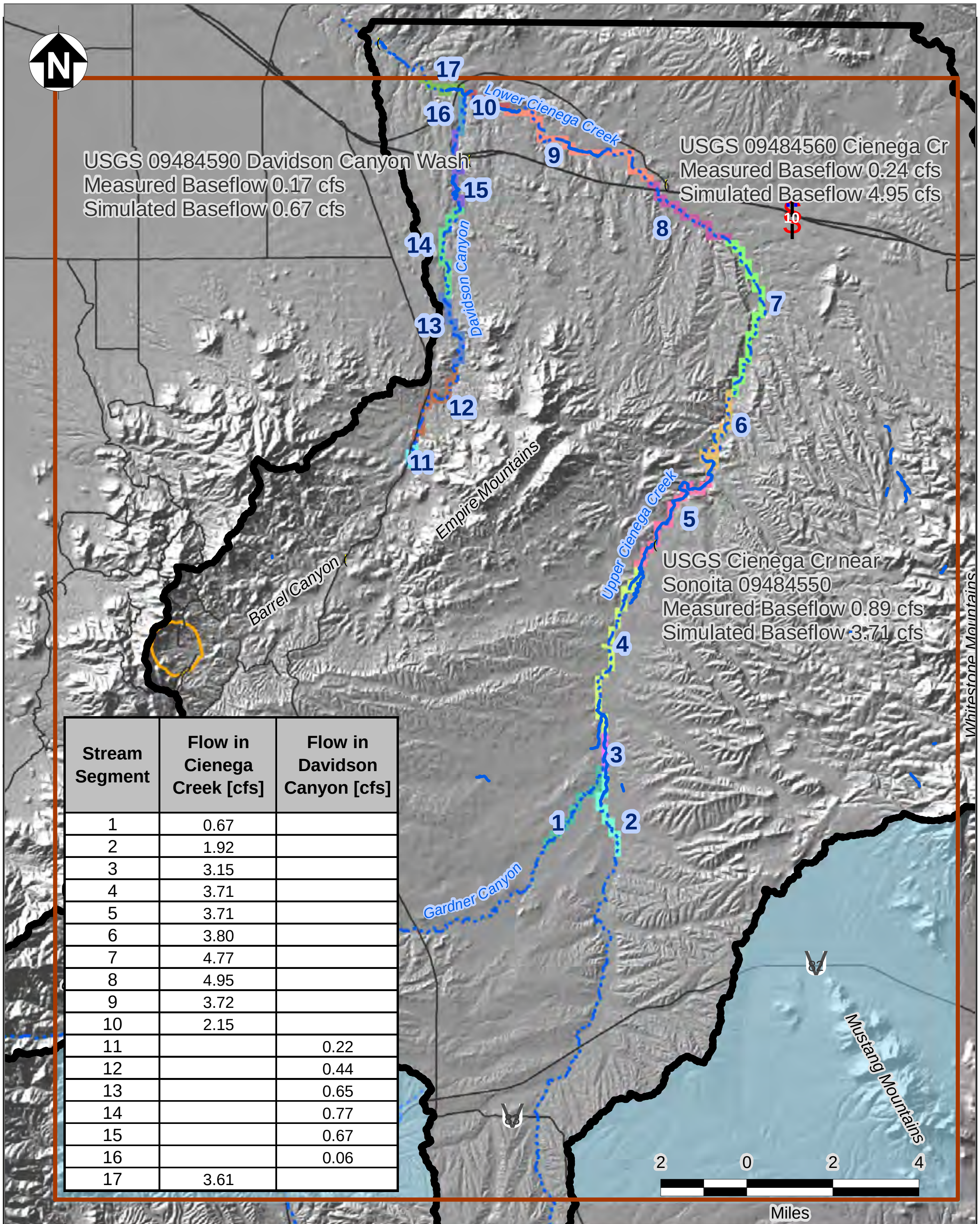

Stream Segment	Flow in Cienega Creek [cfs]	Flow in Davidson Canyon [cfs]
1	0.67	
2	1.92	
3	3.15	
4	3.71	
5	3.71	
6	3.80	
7	4.77	
8	4.95	
9	3.72	
10	2.15	
11		0.22
12		0.44
13		0.65
14		0.77
15		0.67
16		0.06
17	3.61	

Legend

- Proposed Rosemont Open Pit
- Cienega Creek Watershed
- Ephemeral Drainage
- Perennial Stream
- Stream Gage
- No Flow Cells
- Stream Cells

ROSEMONT COPPER

FIGURE 40. SIMULATED STEADY-STATE STREAM FLOWS

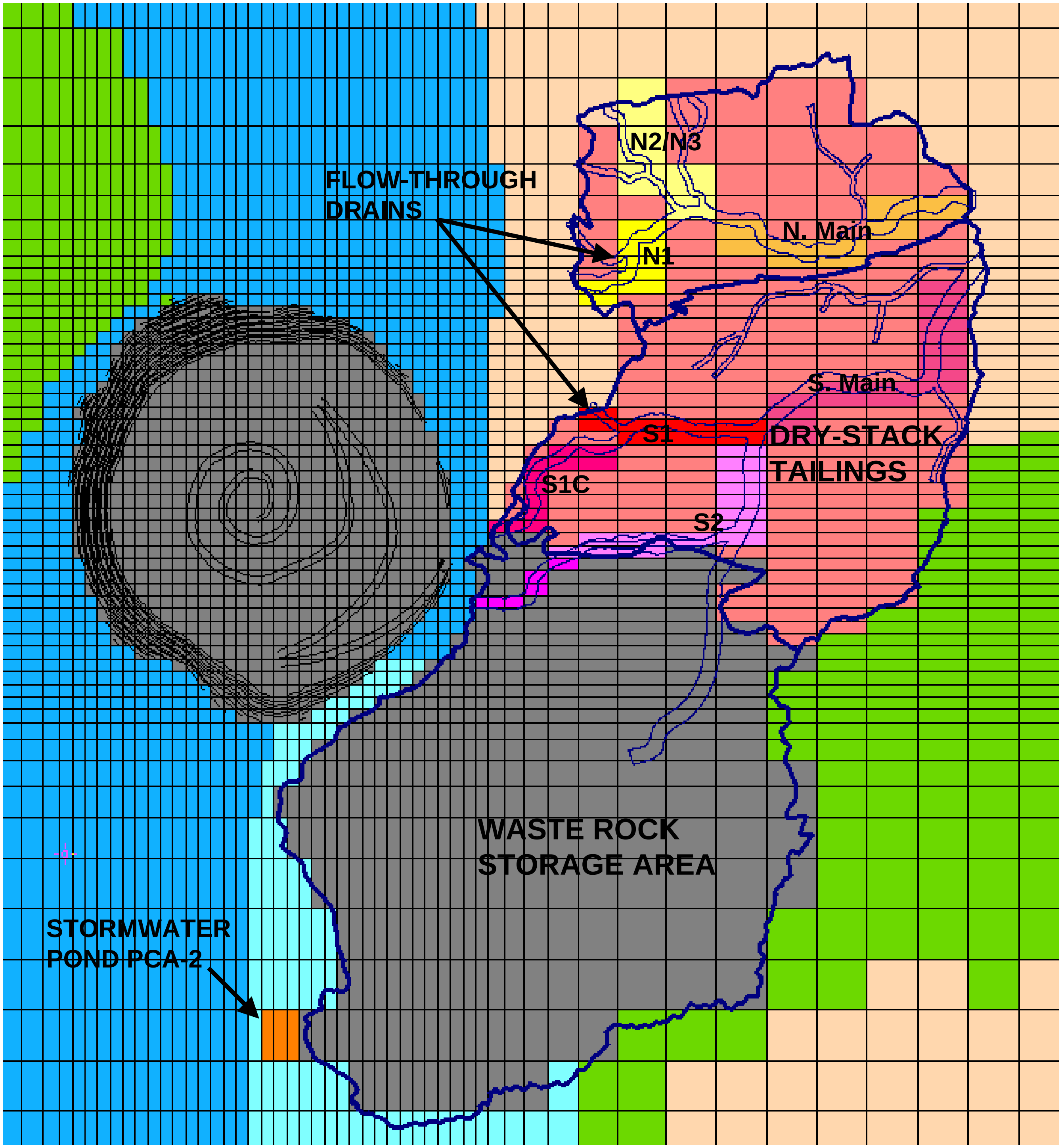

Recharge Zone	Recharge Value	Recharge Zone	Recharge Value	Recharge Zone	Recharge Value
1	0.00	7	1.31	13	6.53
2	0.33	8	0.14	14	1.70
3	0.37	9	61.12	15	3.54
4	0.42	10	19.27	16	3.47
5	0.53	11	4.96	17	8.08
6	0.68	12	31.06		

Recharge values in in/yr
Applicable to start of post-mining

Project No. 114-320874

July 2010

Figure 41
Post-Mining Recharge in Mine Facilities Areas

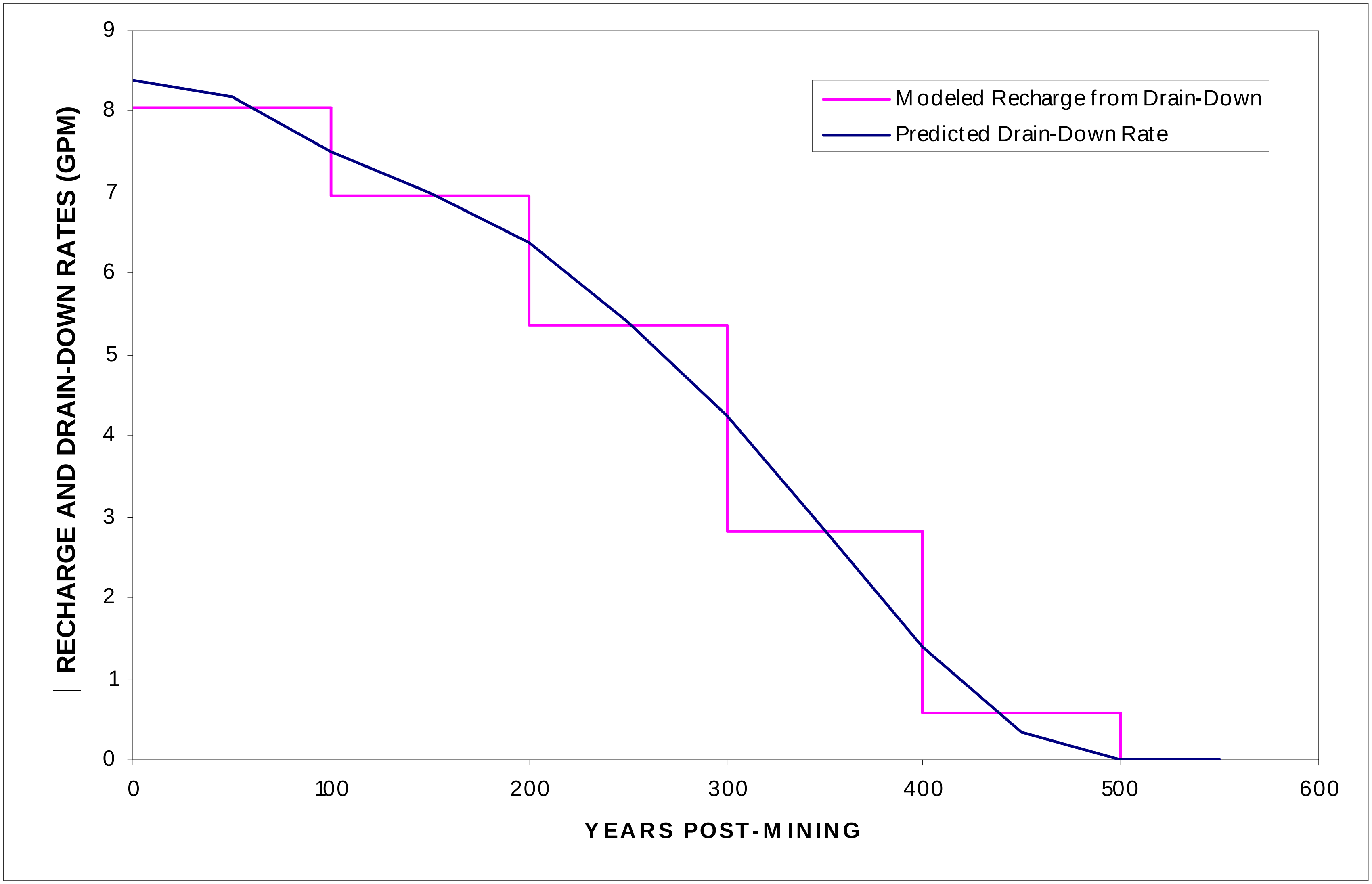

Figure 42
Post-Mining Recharge from Dry-Stack Tailings Drain-Down

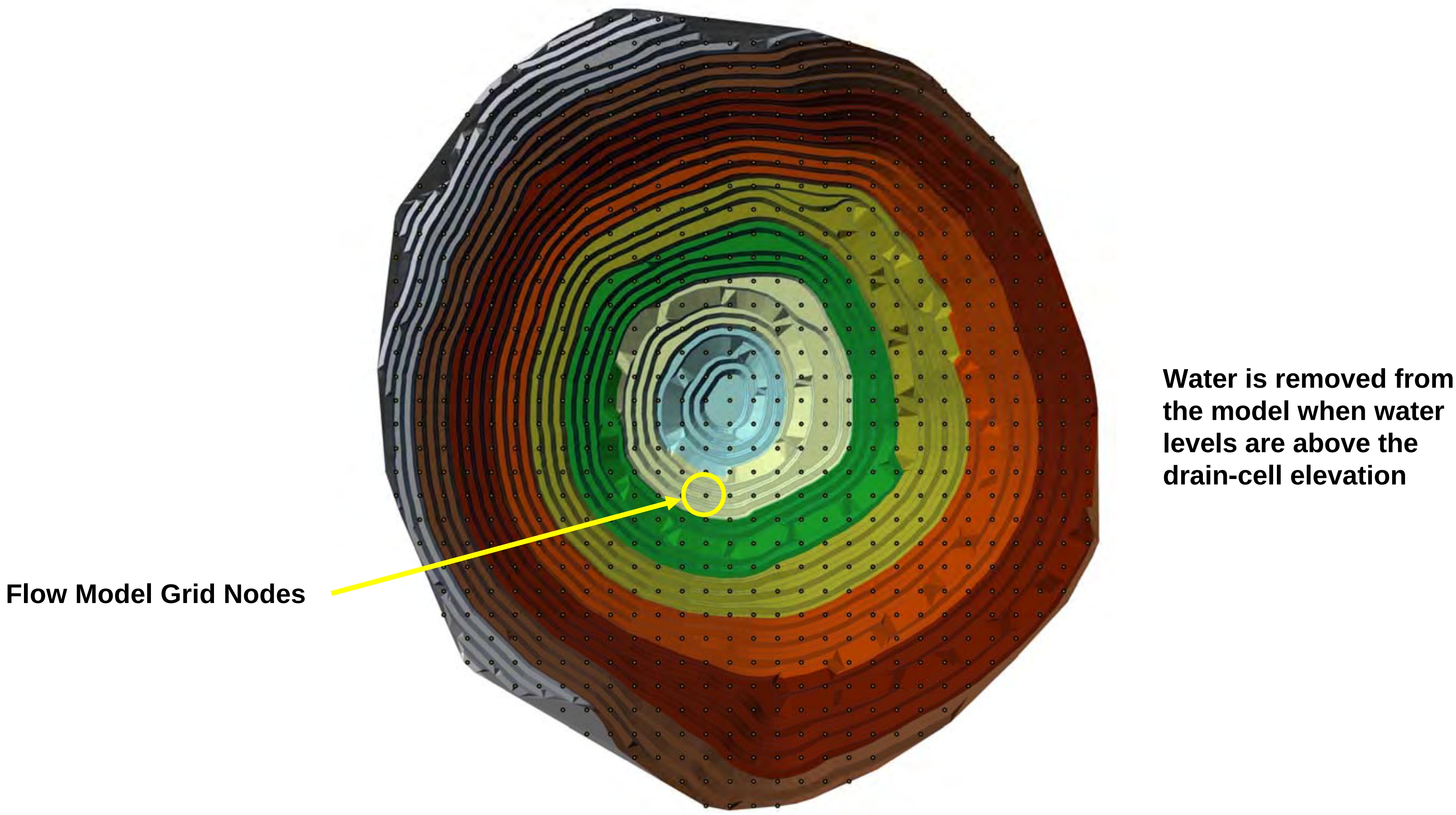

Year 2032 Pit Shell

Figure 43
Simulated Drain Cell Nodes in the 2032 Pit Shell

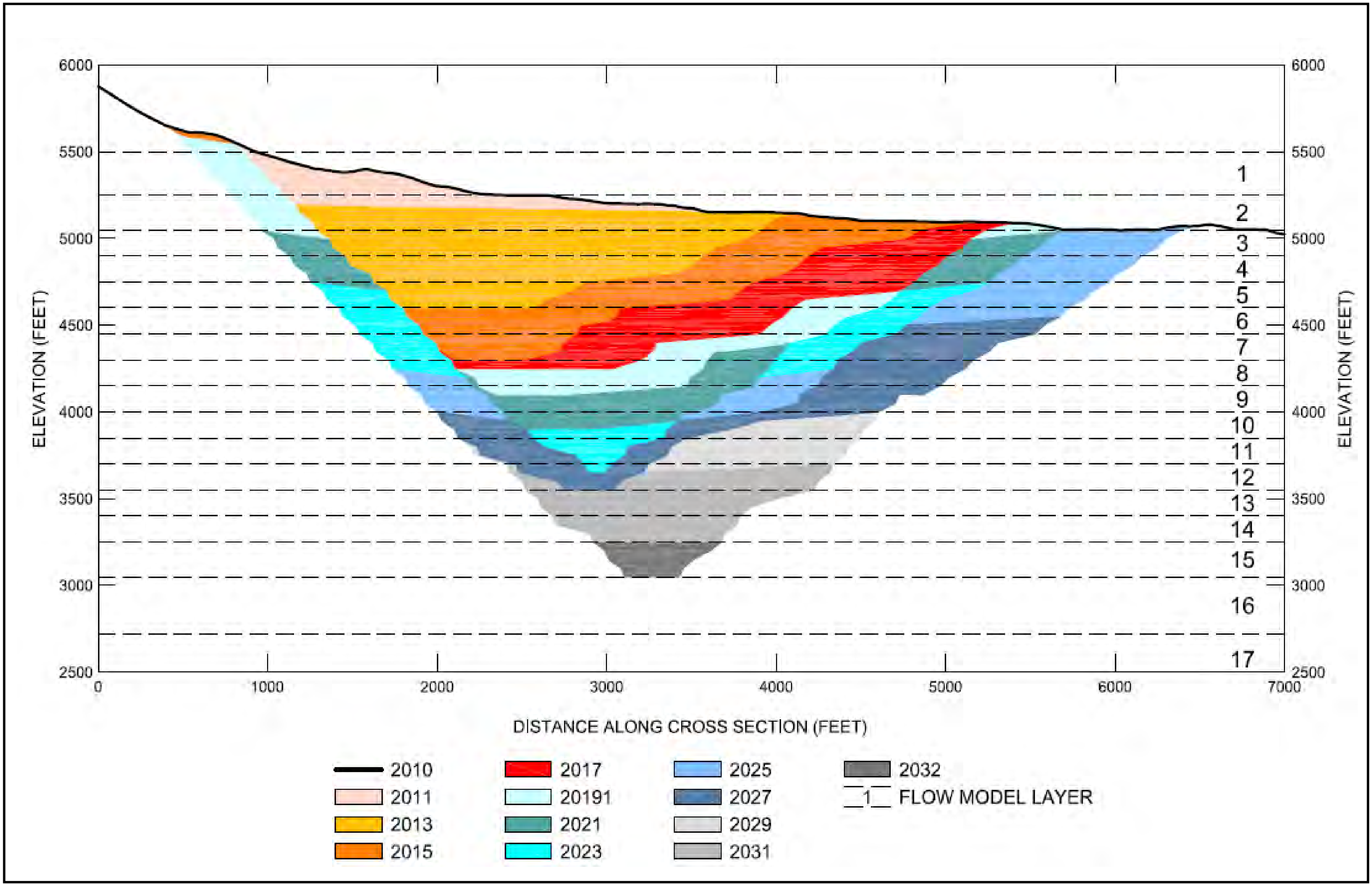

Project No: 114-320874

July 2010

Figure 44
Simulated Progression of Open Pit Development

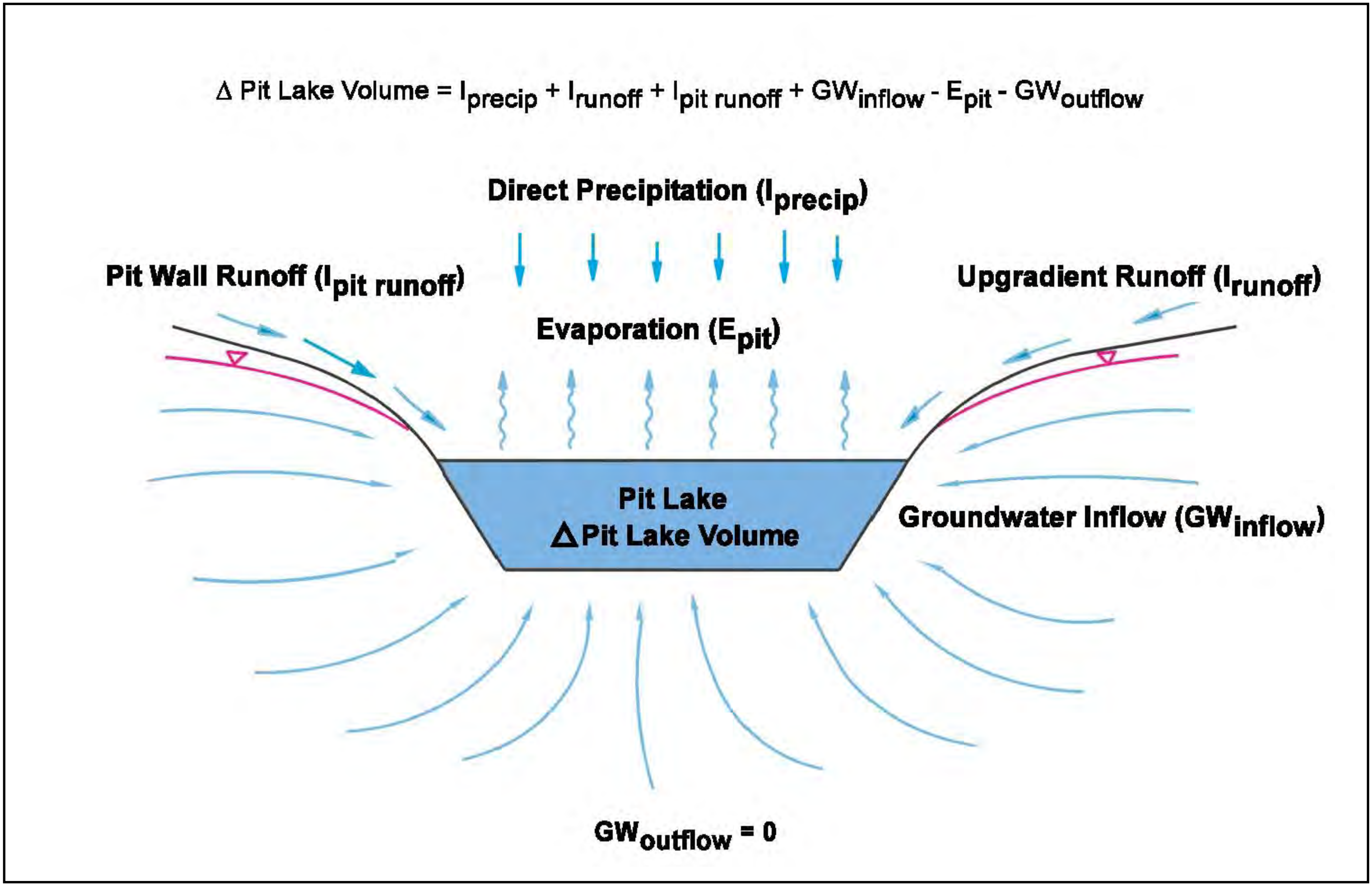

Project No: 114-320874

July 2010

Figure 45
Conceptual Hydrologic Model of the Rosemont Pit Lake

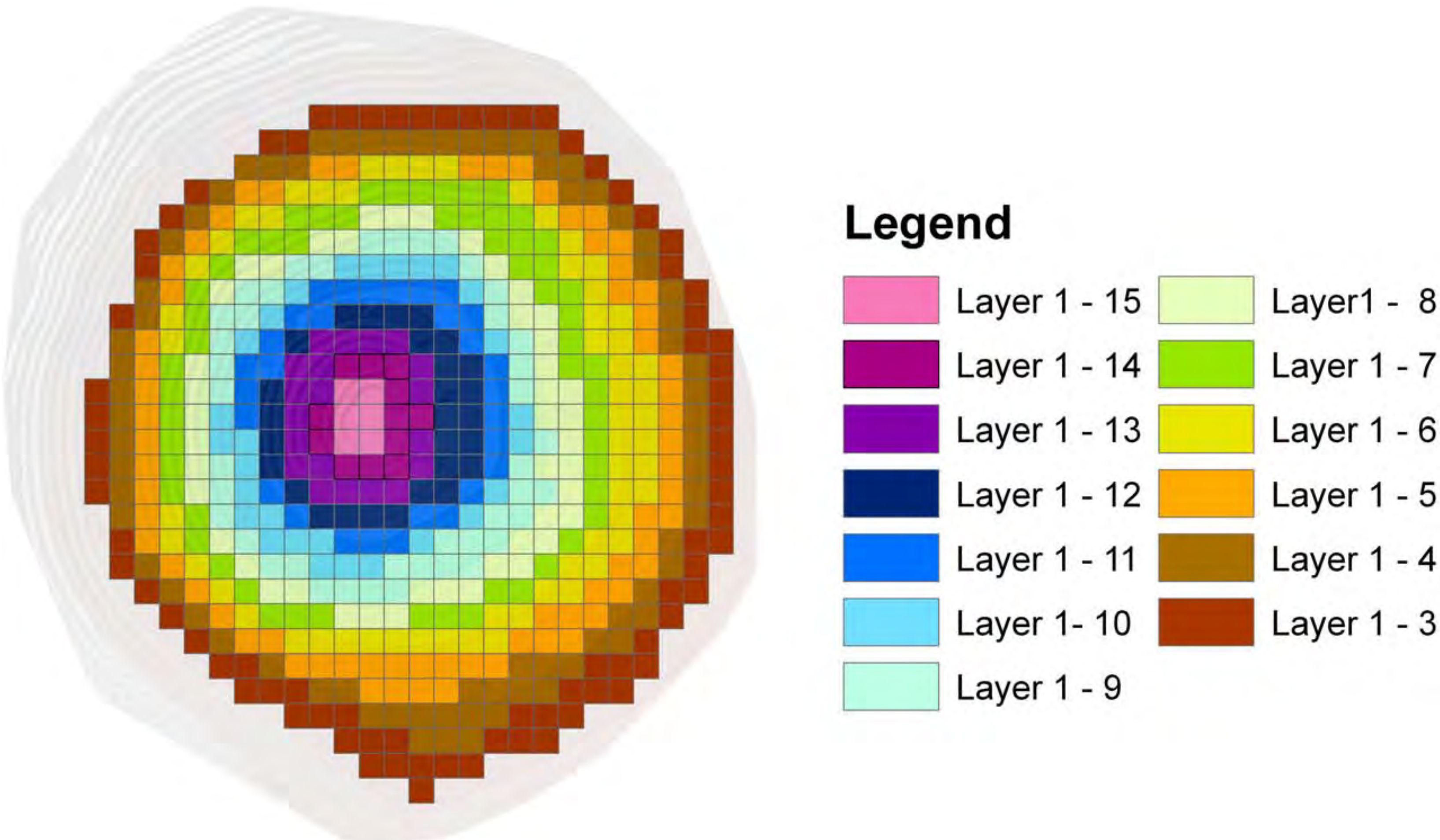

Note: Spill elevation is below layer 3. Cells in layers 1 through 3 must have the same configuration.

Project No: 114-310874

July 2010

Figure 46
Lake Package Configuration For Bottom Cells

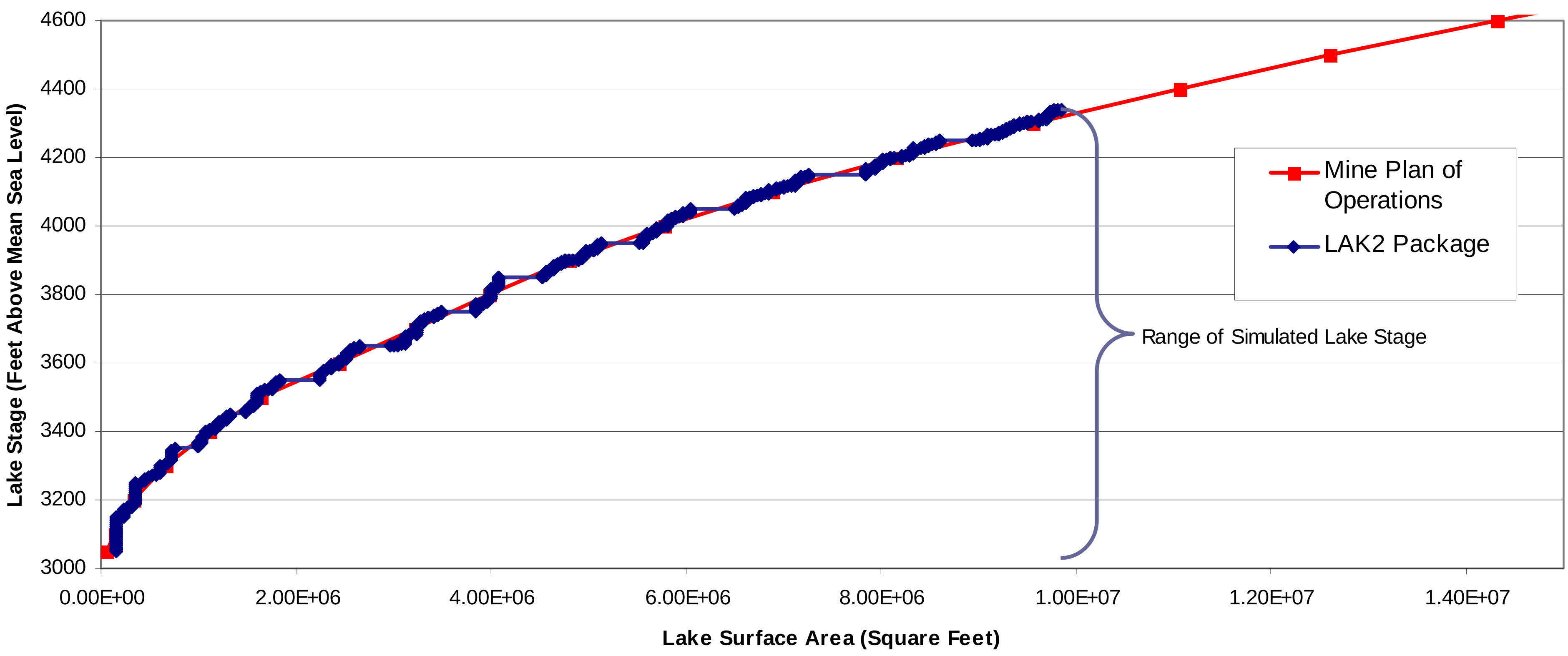

Figure 47
Stage – Area Relationship in the Lake Package

ATTACHMENT 1

RECHARGE ESTIMATES

Estimated Distribution and Rates of Recharge for the Groundwater Flow Model Domain

Sub-Watershed	Sub-Basin		Area (acres)	Average Annual Precip. (in/yr)	Average Annual Precip. Volume (ac-ft/yr)	Annual Runoff Volume (ac-ft/yr)	Potential Recharge (ac-ft/yr)	Change in Potential Recharge (%)	Normalized Recharge (ac-ft/yr)	Normalized Recharge (in/yr)
1	1a	Bedrock	11,725	6.98	6,816	85	6,731	-1.2%	362	0.370
	1b	Fan	5,880	6.74	3,304	48	3,341	1.1%	179	0.366
	1c	Valley	7,004	6.68	3,898	90	3,946	1.2%	212	0.363
2	2a	Bedrock	3,646	7.30	2,218	27	2,191	-1.2%	118	0.387
	2b	Fan	6,965	6.82	3,960	57	3,930	-0.8%	211	0.364
	2c	Valley	560	6.81	317	7	375	18.0%	20	0.432
3	3a	Bedrock	5,241	7.11	3,105	38	3,066	-1.2%	165	0.377
	3b	Fan	5,108	6.95	2,956	43	2,952	-0.2%	159	0.372
	3c	Valley	2,688	6.80	1,524	33	1,567	2.8%	84	0.376
4	4a	Bedrock	28,948	8.17	19,712	246	19,466	-1.2%	1,046	0.433
	4b	Fan	3,933	8.67	2,840	40	3,046	7.3%	164	0.499
	4c	Valley	0							
5	5a	Bedrock	10,046	6.92	5,797	72	5,725	-1.2%	308	0.367
	5b	Fan	6,112	6.70	3,410	49	3,433	0.7%	184	0.362
	5c	Valley	1,045	6.67	581	13	630	8.4%	34	0.389
6	6a	Bedrock	9,438	7.52	5,917	73	5,844	-1.2%	314	0.399
	6b	Fan	3,945	7.65	2,513	35	2,552	1.5%	137	0.417
	6c	Valley	635	6.83	361	8	396	9.7%	21	0.402
7	7a	Bedrock	1,956	6.57	1,070	13	1,057	-1.2%	57	0.348
	7b	Fan	5,238	6.58	2,870	41	2,843	-1.0%	153	0.350
	7c	Valley	3,290	6.65	1,822	42	1,863	2.2%	100	0.365
8	8a	Bedrock	1,316	6.57	721	9	712	-1.2%	38	0.349
	8b	Fan	8,383	6.45	4,507	65	4,451	-1.2%	239	0.342
	8c	Valley	2,228	6.52	1,211	30	1,276	5.4%	69	0.369
9	9a	Bedrock	0							
	9b	Fan	2,236	7.56	1,409	20	1,389	-1.4%	75	0.400
	9c	Valley	6,045	6.77	3,408	74	3,428	0.6%	184	0.366
10	10a	Bedrock	9,328	9.93	7,721	98	7,623	-1.3%	409	0.527
	10b	Fan	8,038	8.32	5,575	78	5,595	0.4%	301	0.449
	10c	Valley	11,487	7.42	7,106	172	7,184	1.1%	386	0.403
11	11a	Bedrock	73	7.15	43	1	43	-1.2%	2	0.379
	11b	Fan	7,691	7.40	4,742	68	4,675	-1.4%	251	0.392
	11c	Valley	5,490	7.06	3,228	76	3,296	2.1%	177	0.387
12	12a	Bedrock	14,349	6.78	8,111	99	8,013	-1.2%	430	0.360
	12b	Fan	1,919	6.65	1,063	15	1,147	7.9%	62	0.385
	12c	Valley	0							
13	13a	Bedrock	6,979	7.19	4,181	52	4,129	-1.2%	222	0.381

Estimated Distribution and Rates of Recharge for the Groundwater Flow Model Domain

Sub-Watershed	Sub-Basin		Area (acres)	Average Annual Precip. (in/yr)	Average Annual Precip. Volume (ac-ft/yr)	Annual Runoff Volume (ac-ft/yr)	Potential Recharge (ac-ft/yr)	Change in Potential Recharge (%)	Normalized Recharge (ac-ft/yr)	Normalized Recharge (in/yr)
	13b	Fan	10,442	6.83	5,944	86	5,910	-0.6%	317	0.365
	13c	Valley	0							
14	14a	Bedrock	1,492	10.22	1,272	16	1,256	-1.2%	67	0.542
	14b	Fan	7,899	8.60	5,658	81	5,593	-1.1%	300	0.456
	14c	Valley	10,670	7.41	6,590	159	6,671	1.2%	358	0.403
15	15a	Bedrock	219	6.93	126	2	125	-1.2%	7	0.368
	15b	Fan	1,698	6.70	948	14	936	-1.3%	50	0.355
	15c	Valley	878	6.54	479	11	492	2.8%	26	0.361
16	16a	Bedrock	300	7.00	175	2	173	-1.2%	9	0.371
	16b	Fan	534	6.91	307	5	305	-0.8%	16	0.368
	16c	Valley	4,945	6.43	2,651	64	2,656	0.2%	143	0.346
17	17a	Bedrock	6,410	7.75	4,138	51	4,087	-1.2%	220	0.411
	17b	Fan	2,505	7.11	1,484	21	1,514	2.0%	81	0.390
	17c	Valley	7,987	6.43	4,279	103	4,300	0.5%	231	0.347
18	18a	Bedrock	2,786	8.08	1,877	23	1,853	-1.2%	100	0.429
	18b	Fan	1,921	6.92	1,108	16	1,115	0.6%	60	0.374
	18c	Valley	7,265	6.25	3,781	85	3,797	0.4%	204	0.337
19	19a	Bedrock	9,241	8.48	6,534	82	6,452	-1.3%	347	0.450
	19b	Fan	3,744	6.99	2,181	32	2,231	2.3%	120	0.384
	19c	Valley	2,761	6.39	1,471	35	1,503	2.2%	81	0.351
20	20a	Bedrock	2,750	9.29	2,129	26	2,103	-1.2%	113	0.493
	20b	Fan	1,131	8.13	767	11	782	2.0%	42	0.446
	20c	Valley	0							
21	21a	Bedrock	6,821	10.04	5,706	73	5,634	-1.3%	303	0.532
	21b	Fan	382	9.49	302	4	371	22.8%	20	0.626
	21c	Valley	348	8.97	260	7	264	1.5%	14	0.489
TOTALS			304,092		188,187	2,922	188,035	-0.1%	10,100	

TETRA TECH

ATTACHMENT 2

STEADY-STATE CALIBRATION HEAD TARGETS

Steady-State Calibration Head Targets

Target Name	UTM X Coordinate (NAD83, meters)	UTM Y Coordinate (NAD83, meters)	Target Head (ft msl)	Layer	Row	Column	Weight	Group	Model Layer Midpoint Elevation (ft msl)	Target Approach
(D-18-16)13aab	532324	3526650	4208.18	10	68	88	1	1	3925.97	PerfMid
D01601523CCC	519745	3542650	2598.98	17	3	6	0.9	2	2506.53	PerfMid
D01601523DDD	521161	3542653	2608.99	17	3	12	0.9	2	2506.53	PerfMid
D01601526DDD	521243	3541144	2704.99	17	9	12	0.4	9	2506.53	PerfMid
D01601534AAA	519643	3540956	2597.02	17	9	6	0	8	2506.53	TD-WL
D01601536CAD	522112	3539914	2629.00	17	14	20	0.5	9	2506.53	TD-WL
D01601626CCC	529376	3541164	3209.02	15	9	76	0.5	9	3150.62	TD-WL
D01601627ABD	528901	3542395	3033.99	16	4	74	0.9	2	2885.69	PerfMid
D01601634DAD	529197	3539840	3224.01	16	14	75	0.9	2	2885.69	TD-WL
D01601636ABC	531844	3540833	3420.00	13	10	86	0	7	3476.17	WL
D01601636CAB	531505	3540185	3435.00	13	13	84	0.2	5	3476.17	WL
D016017031BAD	533260	3540715	3397.76	14	10	92	0.5	9	3326.24	TD-WL
D01601731BDD	533262	3540253	3374.99	14	12	92	0.5	9	3326.24	PerfMid
D01601731DCB	533474	3539791	3433.00	13	14	93	0.9	2	3476.17	TD-WL
D01601733AAD	537276	3540698	3422.99	14	11	108	0.5	9	3326.24	PerfMid
D01601733ABB	536697	3540942	3413.02	14	10	106	0.9	2	3326.24	TD-WL
D01601735ACA	540057	3540677	3595.00	13	11	120	0.5	9	3476.17	TD-WL
D01601831CAD	542762	3540011	3636.01	15	13	131	0.8	3	3150.62	PerfMid
D01601836CDA	550897	3539987	3884.01	10	13	164	0.2	5	3925.97	WL
D017015010ACC	519168	3537261	2651.02	17	25	4	1	1	2506.53	PerfMid
D017015010BAD	518964	3537673	2642.68	17	23	3	1	1	2506.53	PerfMid

Steady-State Calibration Head Targets

Target Name	UTM X Coordinate (NAD83, meters)	UTM Y Coordinate (NAD83, meters)	Target Head (ft msl)	Layer	Row	Column	Weight	Group	Model Layer Midpoint Elevation (ft msl)	Target Approach
D017015023ABB	520790	3534633	2806.79	17	35	10	0.9	2	2506.53	PerfMid
D017015023DAA	521395	3533840	2897.83	16	39	13	0.9	2	2885.69	PerfMid
D01701502DCD	521040	3538003	2639.01	17	22	11	1	1	2506.53	PerfMid
D017015035BAB	520392	3531433	3064.40	17	49	9	1	1	2506.53	PerfMid
D017015035BDC	520392	3530842	3162.89	17	51	9	0.5	9	2506.53	PerfMid
D01701513BDC	521963	3535604	2770.80	17	31	17	0	8	2506.53	TD-WL
D01701526BCA	520132	3532552	2814.99	16	44	8	0.2	5	2885.69	WL
D01701536BDA	522105	3530955	3628.99	12	50	19	0	6	3626.10	WL
D017016003BDC	528384	3538786	2939.73	16	18	72	1	1	2885.69	PerfMid
D017016004CAB	526781	3538607	2977.36	16	19	65	1	1	2885.69	PerfMid
D017016009ACA	527386	3537487	3298.75	15	24	68	0.9	2	3150.62	PerfMid
D017016009BCD	526583	3537288	3310.20	16	25	64	1	1	2885.69	PerfMid
D017016010ABB	528788	3537890	3332.74	16	22	73	0.5	9	2885.69	PerfMid
D017016016CBA	526499	3535537	3586.90	12	32	64	0.2	5	3626.10	WL
D017016021DAC	527603	3533657	3859.01	13	39	68	1	1	3476.17	TD-WL
D017016026BAD	530212	3532851	3798.25	13	43	79	0.4	9	3476.17	PerfMid
D017016026DAA	531021	3532254	3855.76	12	45	82	1	1	3626.10	PerfMid
D017016028BDA	527004	3532648	4040.60	12	44	66	0.4	4	3626.10	PerfMid
D017016028CAA	527006	3532249	4086.99	11	45	66	1	1	3776.04	PerfMid
D017016028DDB	527614	3531852	4115.99	11	47	69	1	1	3776.04	PerfMid
D017016029AAC	525997	3532847	3930.99	12	43	62	0.4	4	3626.10	PerfMid
D017016029CAA	525397	3532247	4058.15	12	45	59	0.4	4	3626.10	TD-WL
D017016029CBB	524797	3532247	3940.77	12	45	57	1	1	3626.10	PerfMid
D017016029CCB	524799	3531845	4034.99	12	47	57	0.2	9	3626.10	PerfMid

Steady-State Calibration Head Targets

Target Name	UTM X Coordinate (NAD83, meters)	UTM Y Coordinate (NAD83, meters)	Target Head (ft msl)	Layer	Row	Column	Weight	Group	Model Layer Midpoint Elevation (ft msl)	Target Approach
D017016030AAD	524595	3532849	3840.41	13	43	56	0.4	4	3476.17	TD-WL
D017016030BAC	523604	3532846	3693.98	13	43	44	0.9	2	3476.17	PerfMid
D017016030BDD	523802	3532445	3785.09	14	44	47	1	1	3326.24	PerfMid
D017016030CCC	523198	3531639	3759.01	13	48	37	1	1	3476.17	PerfMid
D017016030DBC	524002	3532044	3822.00	14	46	50	0.4	4	3326.24	PerfMid
D017016030DCA	524202	3531843	3959.89	14	47	53	1	1	3326.24	PerfMid
D017016034AAC	529330	3531325	4149.79	9	49	76	0	8	4075.90	TD-WL
D01701603DBB	528806	3538761	2872.01	16	18	73	1	1	2885.69	PerfMid
D01701609CDC1	526896	3536447	3466.00	14	28	66	0.4	4	3326.24	TD-WL
D01701609CDC2	526739	3536446	3453.99	13	28	65	0.2	5	3476.17	WL
D01701610AAA	529464	3537932	3537.00	16	22	76	1	1	2885.69	PerfMid
D01701613ACD	532070	3535630	3651.01	12	31	87	0.5	9	3626.10	TD-WL
D01701614BBD	529811	3536024	3661.01	12	30	78	0.2	5	3626.10	WL
D01701616CDC	526743	3534753	3688.01	12	35	65	0.9	2	3626.10	PerfMid
D01701626CCA	529692	3531805	4047.00	9	47	77	0.2	5	4075.90	WL
D01701627DBC	528877	3532080	4034.01	9	46	74	0.2	5	4075.90	WL
D01701635BBA	529903	3531467	4109.99	9	48	78	0.2	5	4075.90	WL
D017017006BDC	533075	3538720	3522.17	16	19	91	0.9	2	2885.69	PerfMid
D017017007CDA	533272	3536531	3651.20	14	28	92	1	1	3326.24	PerfMid
D017017010DDD	538893	3536397	3732.01	13	28	115	0.2	9	3476.17	TD-WL
D017017018CCD	532885	3534737	3650.58	14	35	90	1	1	3326.24	PerfMid
D017017018DBD	533674	3535136	3733.91	13	33	93	0.9	2	3476.17	PerfMid
D017017019DBA	533684	3533740	3839.85	13	39	93	1	1	3476.17	PerfMid
D017017019DBB	533485	3533740	3795.95	11	39	93	0.5	9	3776.04	TD-WL

Steady-State Calibration Head Targets

Target Name	UTM X Coordinate (NAD83, meters)	UTM Y Coordinate (NAD83, meters)	Target Head (ft msl)	Layer	Row	Column	Weight	Group	Model Layer Midpoint Elevation (ft msl)	Target Approach
D01701701BCA	540798	3538956	3539.00	13	18	123	1	1	3476.17	PerfMid
D017017022CDA	538094	3533373	3993.16	12	41	111	0.9	2	3626.10	PerfMid
D017017031CCB	532703	3530145	3973.02	11	54	89	0.4	4	3776.04	PerfMid
D017017031DCB	533486	3530157	4142.01	10	54	93	0.9	2	3925.97	PerfMid
D01701710ADD	538837	3537193	3668.00	14	25	115	0.9	2	3326.24	PerfMid
D01701721BDA	536512	3534198	3941.00	11	37	105	0.4	4	3776.04	TD-WL
D01701723BDC	539532	3533994	3892.01	10	38	117	0.2	5	3925.97	WL
D01701725BBA	540927	3533076	3884.99	10	42	123	0.2	5	3925.97	WL
D01701728CBB	535968	3532072	4049.00	10	46	103	0.9	2	3925.97	PerfMid
D01701731AAB	533738	3531325	3878.00	10	49	94	0.1	9	3925.97	WL
D01701731ADD	534081	3530772	4107.00	9	51	95	0.5	9	4075.90	PerfMid
D01701731BBA	532976	3531384	3895.00	10	49	91	1	1	3925.97	TD-WL
D01701734ADB	538729	3531066	4257.99	8	50	114	0.2	5	4225.83	WL
D01701736BAC	541224	3531137	4051.98	9	50	124	0.2	5	4075.90	WL
D017018017CDD	544571	3534895	3705.24	14	34	138	0.4	4	3326.24	PerfMid
D017018018ABB	543134	3536281	3692.05	14	29	132	0.9	2	3326.24	PerfMid
D01701802ADA	550140	3539182	3905.01	10	17	161	0.9	2	3925.97	PerfMid
D01701803DAD	548569	3538467	3955.00	10	20	154	0.2	5	3925.97	WL
D01701804DDC	546839	3537997	3780.99	13	22	147	0.4	4	3476.17	PerfMid
D01701807ABA	543323	3537796	3647.99	12	22	133	0.2	5	3626.10	WL
D01701809ACB	546263	3537625	3766.00	14	23	145	1	1	3326.24	PerfMid
D01701809ACC	546264	3537317	3774.99	13	24	145	0.4	4	3476.17	PerfMid
D01701809BCC	545477	3537344	3740.01	11	24	142	0	7	3776.04	WL
D01701812BAA	550855	3537954	3859.99	11	22	164	0.5	9	3776.04	PerfMid

Steady-State Calibration Head Targets

Target Name	UTM X Coordinate (NAD83, meters)	UTM Y Coordinate (NAD83, meters)	Target Head (ft msl)	Layer	Row	Column	Weight	Group	Model Layer Midpoint Elevation (ft msl)	Target Approach
D01701813ABD	551310	3536171	3891.00	10	29	166	0.2	5	3925.97	WL
D01701813ACD	551338	3535678	3884.99	11	31	166	0.5	9	3776.04	PerfMid
D01701813BAD	550763	3535244	3990.01	10	33	163	0.5	9	3925.97	PerfMid
D01701813DDD	551762	3534911	3892.01	11	34	168	0.9	2	3776.04	TD-WL
D01701814BDA	549289	3535976	3990.99	10	30	157	0.9	2	3925.97	PerfMid
D01701817BDA	544565	3535831	3651.99	12	31	138	1	1	3626.10	TD-WL
D01701817BDB	544380	3535984	3661.01	13	30	137	0.9	2	3476.17	PerfMid
D01701819CAB	542788	3533853	3805.99	11	39	131	0.2	5	3776.04	WL
D01701829BBD	544210	3532874	3813.01	11	43	137	0.9	2	3776.04	TD-WL
D018015012DAB	522818	3527418	4178.13	11	65	31	0.2	9	3776.04	TD-WL
D018015022ABD	519371	3524832	4112.55	9	76	4	0.5	9	4075.90	TD-WL
D018015023ABC_OldDick	520828	3524790	4348.31	7	76	10	0.2	5	4375.77	WL
D018015025DBD1_PC-7	522666	3522436	5146.03	7	95	29	0.4	4	4375.77	PerfMid
D018015034DAA	519775	3521000	4826.48	4	119	6	1	1	4825.56	TD-WL
D018015035ABC_1445	520721	3521673	5407.64	2	108	10	1	1	5150.53	TD-WL
D018015036ABC1_PC-8	522327	3521582	5217.13	8	109	23	0.4	4	4225.83	PerfMid
D018015036DAA_PC-4	523003	3521024	5108.50	7	118	34	0.4	4	4375.77	PerfMid
D01801510BCD	518562	3527530	3628.99	12	65	1	0	11	3626.10	WL
D01801510CAB	518776	3527408	3638.01	12	65	2	0.1	9	3626.10	WL
D01801510CDA	518855	3527007	3740.01	11	67	2	0.1	9	3776.04	WL
D01801514AAC1	521090	3526365	4170.00	9	69	12	0.5	9	4075.90	PerfMid
D01801514AAC2	521064	3526365	4140.01	9	69	11	0.5	9	4075.90	TD-WL
D01801515BAA2	519013	3526792	3766.00	11	68	3	0.2	5	3776.04	WL
D01801515BAC	518725	3526330	3859.99	10	69	2	0.1	9	3925.97	WL

Steady-State Calibration Head Targets

Target Name	UTM X Coordinate (NAD83, meters)	UTM Y Coordinate (NAD83, meters)	Target Head (ft msl)	Layer	Row	Column	Weight	Group	Model Layer Midpoint Elevation (ft msl)	Target Approach
D01801515BAC2	518830	3526361	3834.99	11	69	2	0.2	5	3776.04	WL
D01801515BAC3	518751	3526484	3801.99	11	69	2	0.2	5	3776.04	WL
D01801515BBA	518562	3526606	3753.99	11	68	1	0	11	3776.04	WL
D01801515CAC	518699	3526484	3955.99	10	69	2	0.1	9	3925.97	WL
D01801515CBD	518562	3525744	3932.99	10	72	1	0	11	3925.97	WL
D01801515CDB	518701	3525314	3978.00	10	74	2	0.1	9	3925.97	WL
D01801522ABB	519069	3524976	4061.01	9	75	3	0.1	9	4075.90	WL
D01801522ABC	519148	3524853	4078.00	9	75	4	1	1	4075.90	TD-WL
D01801522ADB	519569	3524669	4146.01	9	76	5	1	1	4075.90	TD-WL
D01801522DCA	519361	3523745	4280.98	9	80	4	1	1	4075.90	PerfMid
D01801522DCD	519335	3523652	4288.99	8	80	4	0.9	2	4225.83	PerfMid
D01801527AAD	519835	3523284	4253.00	9	83	6	0.4	4	4075.90	PerfMid
D01801534BAA	518839	3521681	4617.00	6	107	2	0.2	5	4525.70	WL
D018016001BBB	531223	3529839	3978.99	11	55	83	1	1	3776.04	PerfMid
D018016001BCC	531220	3529240	4034.01	12	58	83	1	1	3626.10	PerfMid
D018016012ABB	531956	3528237	4067.01	10	62	86	0.5	9	3925.97	PerfMid
D018016012ADA	532511	3527838	4101.82	10	63	89	1	1	3925.97	PerfMid
D018016012ADC	532325	3527641	4052.08	10	64	88	1	1	3925.97	PerfMid
D018016012CAA	531771	3527443	4057.23	12	65	86	1	1	3626.10	PerfMid
D018016012CCB	531217	3527044	4134.00	9	67	83	1	1	4075.90	PerfMid
D018016014DAC	530772	3525510	4213.01	8	73	81	0.9	2	4225.83	TD-WL
D018016015AAA_RP-7	529460	3526589	4248.83	9	68	76	0.9	2	4075.90	PerfMid
D018016015ADB_Mulberry Stock	529212	3526209	4297.68	8	70	75	0.2	5	4225.83	WL

Steady-State Calibration Head Targets

Target Name	UTM X Coordinate (NAD83, meters)	UTM Y Coordinate (NAD83, meters)	Target Head (ft msl)	Layer	Row	Column	Weight	Group	Model Layer Midpoint Elevation (ft msl)	Target Approach
D018016015DBC_RP-6	528799	3525495	4343.78	8	73	73	0.9	2	4225.83	PerfMid
D018016020DBC1_HC-4A	525545	3524038	4898.37	5	79	60	0.4	4	4675.63	PerfMid
D018016021ABD_HV-2	527498	3524802	4477.01	8	76	68	0.9	2	4225.83	PerfMid
D018016021ACB_HV-1	527110	3524608	4481.64	8	76	66	0.8	3	4225.83	PerfMid
D018016021ADA_Hidden Valley Stock	527812	3524734	4450.86	7	76	69	0.9	2	4375.77	TD-WL
D018016021BDA_DH-1455	527103	3524624	4505.98	9	76	66	0.4	4	4075.90	TD-WL
D018016021DCD	527503	3523526	4526.19	6	81	68	0.2	5	4525.70	WL
D018016022DBC_DH-1494_(East of Rest Area)	528679	3523958	4425.04	8	79	73	0.4	4	4225.83	TD-WL
D018016023DBA_RP-8	530575	3524114	4285.48	8	79	81	0.9	2	4225.83	PerfMid
D018016023DCC2	530391	3523668	4360.77	9	80	80	0.4	4	4075.90	TD-WL
D018016024DCA	532111	3523835	4433.94	7	80	87	0.2	5	4375.77	WL
D018016026ADD	531026	3522828	4421.83	8	89	83	0.9	2	4225.83	PerfMid
D018016027ADB_DH-1490	529212	3523010	4463.27	8	86	75	0.4	4	4225.83	TD-WL
D018016027DDC_RP-9	529215	3521929	4609.95	6	103	75	0.9	2	4525.70	PerfMid
D018016028ABA1_RP-2A	527460	3523501	4513.10	6	81	68	1	1	4525.70	PerfMid
D018016028ABA2_RP-2B	527459	3523511	4508.80	7	81	68	0.9	2	4375.77	PerfMid
D018016028ABA3_RP-2C	527461	3523520	4507.46	8	81	68	0.8	3	4225.83	PerfMid
D018016029BBD_P-899	524939	3523178	4827.40	15	84	58	0.2	4	3150.62	TD-WL
D018016029BDA_C-13	525398	3523031	4734.19	5	85	59	0.2	5	4675.63	WL
D018016029CCB1_HC-3A	524808	3522153	4823.24	4	100	57	1	1	4825.56	PerfMid
D018016029CCB2_HC-3B	524814	3522160	4810.34	6	100	57	0.9	2	4525.70	PerfMid
D018016029CCB3_HC-3C	524819	3522162	4809.92	9	100	57	0.4	4	4075.90	PerfMid
D018016029CDA__G-35	525449	3522203	4740.85	6	99	60	0.4	4	4525.70	TD-WL

Steady-State Calibration Head Targets

Target Name	UTM X Coordinate (NAD83, meters)	UTM Y Coordinate (NAD83, meters)	Target Head (ft msl)	Layer	Row	Column	Weight	Group	Model Layer Midpoint Elevation (ft msl)	Target Approach
D018016030BAB1_HC-5A	523686	3523492	5082.71	4	81	45	0.8	3	4825.56	PerfMid
D018016030BAB2_HC-5B	523691	3523484	5038.16	7	81	45	0.8	3	4375.77	PerfMid
D018016030BCC_PC-6	523194	3522830	5148.79	8	89	37	0.4	4	4225.83	PerfMid
D018016030BDA_C-1	523873	3522993	5072.44	6	86	48	0.4	4	4525.70	TD-WL
D018016030CAD1_PC-5	523745	3522451	5144.39	9	95	46	0.4	4	4075.90	PerfMid
D018016030CBA_PC-1	523425	3522568	5134.03	5	93	41	0.4	4	4675.63	PerfMid
D018016030CDC_PC-2	523520	3522142	5157.78	7	100	43	0.4	4	4375.77	PerfMid
D018016030CDD_A-886	523683	3522088	5058.04	3	101	45	0.0	10	4975.50	TD-WL
D018016031BBB_9-7	523202	3521850	5122.02	10	105	37	0.4	4	3925.97	TD-WL
D018016031BBD_AR-2050	523309	3521601	5043.25	6	109	39	0.0	10	4525.70	TD-WL
D018016031CBB_AH-8	523196	3521056	5054.83	4	118	37	0.4	4	4825.56	TD-WL
D018016032BDC1_Gayler	525188	3521229	4813.29	6	115	59	0.4	4	4525.70	TD-WL
D018016032BDC2_Gayler2	525178	3521231	4800.76	4	115	59	0.2	5	4825.56	WL
D018016032CAD1_RP-4A	525486	3520871	4839.77	5	121	60	0.8	3	4675.63	PerfMid
D018016032CAD2_RP-4B	525484	3520862	4825.60	8	121	60	0.8	3	4225.83	PerfMid
D018016032CCB_DH-1537	524822	3520542	4895.97	8	125	57	0	7	4225.83	TD-WL
D018016033BBC1_RP-3A	526328	3521634	4752.44	6	108	63	0.8	3	4525.70	PerfMid
D018016033BBC2_RP-3B	526332	3521643	4724.71	8	108	63	0.9	2	4225.83	PerfMid
D018016034BDA_DH-1497	528705	3521480	4645.19	8	111	73	0.4	4	4225.83	TD-WL
D018016035AAB	530823	3521815	4479.31	7	105	82	0.9	2	4375.77	PerfMid
D01801612BBD1	531358	3527992	4068.00	9	63	84	0.9	2	4075.90	TD-WL
D01801612BBD2	531358	3527992	4059.99	9	63	84	0.2	5	4075.90	WL
D01801613BAA	531756	3526670	4080.00	10	68	86	0.2	9	3925.97	PerfMid
D01801621DDC	527509	3523517	4511.99	6	81	68	0.2	5	4525.70	WL

TETRA TECH

Steady-State Calibration Head Targets

Target Name	UTM X Coordinate (NAD83, meters)	UTM Y Coordinate (NAD83, meters)	Target Head (ft msl)	Layer	Row	Column	Weight	Group	Model Layer Midpoint Elevation (ft msl)	Target Approach
D01801624ADB	532210	3524608	4528.00	6	76	87	1	1	4525.70	TD-WL
D01801624BDC1	531553	3524422	4384.00	7	77	85	1	1	4375.77	TD-WL
D01801624BDC2	531501	3524421	4363.00	7	77	84	0.9	2	4375.77	PerfMid
D01801627CDB3	528432	3522226	4619.01	5	98	72	0.2	5	4675.63	WL
D01801631CCC1	523232	3520397	5173.00	2	126	38	0.2	5	5150.53	WL
D01801631CCC2	523258	3520366	5179.01	2	126	38	0.2	5	5150.53	WL
D01801632CCC	524652	3520154	4906.99	3	127	56	0.2	5	4975.50	WL
D018017005ADD	535656	3529195	4384.00	8	58	101	0.9	2	4225.83	PerfMid
D018017006AAB	533881	3529769	4144.01	10	55	94	0.9	2	3925.97	PerfMid
D018017006BBB	532707	3529756	4012.22	12	55	89	1	1	3626.10	PerfMid
D018017007CAB	533100	3527397	4228.00	10	65	91	1	1	3925.97	PerfMid
D018017017CDD	534893	3525253	4490.73	7	74	98	0.2	9	4375.77	TD-WL
D018017017DDD	535674	3525251	4411.86	7	74	102	1	1	4375.77	PerfMid
D018017019DAD	534110	3524054	4563.04	7	79	95	0.9	2	4375.77	PerfMid
D01801702AAC	540285	3529502	4178.98	8	56	120	0.2	5	4225.83	WL
D018017031ACD	533716	3521258	4466.22	7	114	94	0.8	3	4375.77	PerfMid
D01801725CD	541207	3522147	4324.00	7	100	124	0.1	9	4375.77	WL
D01801726DCA	540155	3522358	4269.99	8	96	120	1	1	4225.83	TD-WL
D01801728BAA	536576	3523422	4336.99	8	82	105	0.9	2	4225.83	TD-WL
D01801732DBA	535349	3520955	4409.00	7	119	100	0.9	2	4375.77	TD-WL
D01801733ADA	537188	3521362	4344.01	7	113	108	1	1	4375.77	TD-WL
D01801734BDC	537977	3521303	4311.00	8	114	111	0.9	2	4225.83	TD-WL
D01801734DDA	538795	3520536	4321.01	10	125	114	0.4	3	3925.97	PerfMid
D01801735BAD	539711	3521648	4278.00	8	108	118	0.2	5	4225.83	WL

Steady-State Calibration Head Targets

Target Name	UTM X Coordinate (NAD83, meters)	UTM Y Coordinate (NAD83, meters)	Target Head (ft msl)	Layer	Row	Column	Weight	Group	Model Layer Midpoint Elevation (ft msl)	Target Approach
D01801736CBC	540792	3520759	4309.99	8	122	123	0.9	2	4225.83	TD-WL
D01801819ABB	543193	3525018	4173.01	9	75	132	0	6	4075.90	TD-WL
D01801820DAD2	545326	3523950	4348.01	8	79	141	0.9	2	4225.83	TD-WL
D01801829ACC	544780	3522747	4382.98	7	90	139	0.9	2	4375.77	TD-WL
D01801830DCB	543231	3522309	4357.00	7	97	133	0.5	9	4375.77	TD-WL
D01801831CAC	542684	3520983	4390.99	7	119	130	0.9	2	4375.77	TD-WL
D01801833CAD	546260	3520844	4671.99	7	121	145	0.4	4	4375.77	TD-WL
D01901501AAA	522943	3520088	5181.99	2	128	33	0.2	5	5150.53	WL
D019015024CCC	521590	3514004	5483.20	2	152	14	1	1	5150.53	PerfMid
D01901536BBB	521619	3512204	5310.99	1	160	14	0.2	5	5375.26	WL
D01901536DAB	522857	3511375	5192.00	2	163	32	0.2	5	5150.53	WL
D019016002CCD_Oaktree WM	529798	3518925	4689.05	5	132	77	1	1	4675.63	TD-WL
D019016004DBB_DH-1541	527310	3519422	4774.78	5	130	67	0.4	4	4675.63	TD-WL
D019016006AAD1_HC-2A	524537	3519926	4955.09	6	128	56	0.4	4	4525.70	PerfMid
D019016006AAD2_HC-2B	524537	3519926	4893.97	9	128	56	0.8	3	4075.90	PerfMid
D019016006CCA_RP-5	523376	3518970	5035.40	4	132	40	0.8	3	4825.56	PerfMid
D019016010AAA_E-6	529422	3518737	4695.42	5	133	76	0.2	5	4675.63	WL
D019016014BDD_WM	530088	3516422	4704.40	5	143	79	0	7	4675.63	TD-WL
D019016016CBB	526276	3516320	4691.68	5	143	63	0.2	5	4675.63	WL
D019016016DDB	527460	3515841	4704.34	5	145	68	0.9	2	4675.63	TD-WL
D019016017DDD	526183	3515603	4710.15	5	146	63	0.9	2	4675.63	TD-WL
D019016018DDB	524294	3515885	4725.89	7	145	54	0.4	4	4375.77	TD-WL
D019016019	523825	3514696	5200.46	2	150	48	0.5	9	5150.53	TD-WL

TETRA TECH

Steady-State Calibration Head Targets

Target Name	UTM X Coordinate (NAD83, meters)	UTM Y Coordinate (NAD83, meters)	Target Head (ft msl)	Layer	Row	Column	Weight	Group	Model Layer Midpoint Elevation (ft msl)	Target Approach
D019016019CCC	523159	3513991	5329.82	2	153	37	0.5	9	5150.53	TD-WL
D01901601BAB1_HC-1A	522015	3520122	5429.56	1	127	18	0.9	2	5375.26	PerfMid
D01901601BAB2_HC-1B	522016	3520113	5427.95	3	127	18	0.4	4	4975.50	PerfMid
D019016021BAB	526601	3515478	4701.65	5	146	64	0.4	4	4675.63	TD-WL
D01901604CDB	526626	3519112	4702.99	6	132	64	0.9	2	4525.70	PerfMid
D01901604DBD	527309	3519422	4710.01	6	130	67	0.4	4	4525.70	TD-WL
D01901605DAC	525942	3519233	4819.00	5	131	62	0.4	4	4675.63	TD-WL
D01901608AAA	526075	3518680	4802.99	5	133	62	0.9	2	4675.63	TD-WL
D01901609BBC	526312	3518495	4705.00	5	134	63	0.2	5	4675.63	WL
D01901609DBB	527103	3517882	4684.00	5	137	66	1	1	4675.63	TD-WL
D01901611BBB	529441	3518750	4696.99	10	133	76	0.4	4	3925.97	PerfMid
D01901615ABA	528867	3516963	4696.99	5	140	74	0	6	4675.63	TD-WL
D01901617BDB	525055	3516553	4871.00	4	142	58	0.1	9	4825.56	WL
D01901618CCA	523426	3515779	5104.99	2	145	41	0.1	9	5150.53	WL
D01901619DC	524035	3513995	5177.99	2	153	51	0.5	9	5150.53	TD-WL
D01901621ACC	527111	3514741	4700.99	5	149	66	0.9	2	4675.63	TD-WL
D01901624CDA	531664	3514139	4700.01	5	152	85	1	1	4675.63	TD-WL
D01901625CAA	531720	3513061	4685.02	5	156	85	0.1	9	4675.63	WL
D01901625CDC	531458	3512475	4721.01	6	159	84	1	1	4525.70	PerfMid
D01901626BAD	530139	3513641	4715.00	5	154	79	1	1	4675.63	TD-WL
D01901627BAC	528298	3513698	4719.99	5	154	71	1	1	4675.63	TD-WL
D01901628DBC	527195	3512802	4729.99	5	157	67	1	1	4675.63	TD-WL
D01901634ABC1	528723	3512036	4705.00	5	161	73	1	1	4675.63	TD-WL
D01901634ABC2	528776	3511975	4709.00	6	161	73	0.8	3	4525.70	PerfMid

Steady-State Calibration Head Targets

Target Name	UTM X Coordinate (NAD83, meters)	UTM Y Coordinate (NAD83, meters)	Target Head (ft msl)	Layer	Row	Column	Weight	Group	Model Layer Midpoint Elevation (ft msl)	Target Approach
D01901634BBD	528066	3512004	4715.00	5	161	70	1	1	4675.63	TD-WL
D01901634DAA	529383	3511484	4710.01	5	163	76	0.2	5	4675.63	WL
D01901635BC	529619	3511669	4731.01	5	162	77	0.1	9	4675.63	WL
D01901635DAA	530936	3511273	4719.00	5	164	82	0.1	9	4675.63	WL
D01901635DAD	530909	3511273	4710.01	5	164	82	1	1	4675.63	TD-WL
D01901636CB	531252	3511243	4700.99	5	164	83	0.5	9	4675.63	TD-WL
D019017006BBD	532925	3520071	4502.90	7	128	90	0.5	9	4375.77	TD-WL
D01901701CCD	540879	3518728	4384.99	12	133	123	0.4	4	3626.10	PerfMid
D019017031BAA	533337	3512156	4606.18	7	160	92	0.2	9	4375.77	TD-WL
D01901703ADB	538666	3519858	4357.00	10	128	114	0.2	4	3925.97	PerfMid
D01901703DDD	538907	3518782	4355.00	8	133	115	0.2	5	4225.83	WL
D01901708BCB	534386	3518273	4473.01	7	135	96	0.9	2	4375.77	TD-WL
D01901709ABB	536778	3518558	4386.99	13	134	106	0.4	4	3476.17	PerfMid
D01901710BCD	537805	3518131	4380.00	12	136	110	0.4	4	3626.10	PerfMid
D01901712AAB	541958	3518609	4380.00	7	134	127	0.9	2	4375.77	TD-WL
D01901714ADD	540546	3516448	4392.01	7	142	122	0.9	2	4375.77	TD-WL
D01901715BCA	537679	3516683	4429.01	10	142	110	0.4	4	3925.97	TD-WL
D01901716ACA	536890	3516681	4438.00	7	142	107	1	1	4375.77	TD-WL
D01901717BBD	534679	3517012	4567.00	10	140	97	0.4	4	3925.97	PerfMid
D01901718DAB	533840	3516239	4494.99	7	143	94	0.5	9	4375.77	PerfMid
D01901721CCD	536057	3514061	4521.99	6	152	103	0.9	2	4525.70	TD-WL
D01901721DDD	537320	3513942	4479.01	11	153	108	0.4	4	3776.04	PerfMid
D01901727DBA	538612	3513146	4498.01	6	156	114	1	1	4525.70	TD-WL
D01901728ACB	536717	3513447	4508.02	6	155	106	0.2	5	4525.70	WL

Steady-State Calibration Head Targets

Target Name	UTM X Coordinate (NAD83, meters)	UTM Y Coordinate (NAD83, meters)	Target Head (ft msl)	Layer	Row	Column	Weight	Group	Model Layer Midpoint Elevation (ft msl)	Target Approach
D01901731CA1	533357	3511281	4609.00	6	164	92	0.5	9	4525.70	TD-WL
D01901731CAA	533461	3511404	4648.01	7	163	92	0.4	4	4375.77	TD-WL
D01901731CBD1	533041	3511280	4621.99	6	164	91	0.9	2	4525.70	TD-WL
D01901731CBD2	532857	3511248	4640.00	8	164	90	0.9	2	4225.83	PerfMid
D01901732ABD	535275	3512026	4559.00	10	161	100	0.4	4	3925.97	PerfMid
D01901815BAD	547750	3516972	4862.01	4	140	151	0.9	2	4825.56	TD-WL
D01901817BAD	544384	3516926	4623.01	6	141	137	0.9	2	4525.70	TD-WL
D020016004CBD	526519	3509557	4790.85	5	171	64	0.9	2	4675.63	TD-WL
D020016005CBD	524907	3509563	4841.15	5	171	57	0.9	2	4675.63	PerfMid
D020016006DCC	523940	3509159	5098.36	2	172	49	0.9	2	5150.53	PerfMid
D020016008ACD	525716	3508334	4766.08	5	176	61	0.5	9	4675.63	PerfMid
D02001602AAC	530780	3510472	4762.02	4	167	82	0.2	5	4825.56	WL
D02001603BAC	528333	3510373	4748.99	5	167	71	0.2	9	4675.63	TD-WL
D02001603DAA	529308	3509914	4727.01	5	169	75	1	1	4675.63	TD-WL
D02001609DBB1	527102	3508183	4729.99	5	176	66	1	1	4675.63	TD-WL
D02001610DDA	529446	3507790	4707.00	5	178	76	1	1	4675.63	TD-WL
D02001611ADA	530812	3508533	4729.01	5	175	82	0.5	9	4675.63	TD-WL
D02001612BCC	531050	3508349	4682.00	5	176	83	0.2	5	4675.63	WL
D02001612CDD	531657	3507612	4682.00	5	179	85	1	1	4675.63	TD-WL
D02001612DDA	532578	3507953	4660.02	5	177	89	1	1	4675.63	TD-WL
D02001624DAB	532364	3504997	4692.99	5	189	88	0	11	4675.63	TD-WL
D02001624DAD1	532561	3504905	4675.99	5	190	89	0	10	4675.63	TD-WL
D02001624DAD2	532587	3504813	4667.00	6	190	89	0.9	2	4525.70	TD-WL
D02001702CCC	539075	3509146	4582.00	8	172	116	0.4	4	4225.83	PerfMid

Steady-State Calibration Head Targets

Target Name	UTM X Coordinate (NAD83, meters)	UTM Y Coordinate (NAD83, meters)	Target Head (ft msl)	Layer	Row	Column	Weight	Group	Model Layer Midpoint Elevation (ft msl)	Target Approach
D02001704AAC	537148	3510524	4578.00	13	167	108	0.4	4	3476.17	PerfMid
D02001706DCA	533810	3509342	4642.00	5	172	94	0.2	5	4675.63	WL
D02001707ADD	534156	3508297	4652.99	5	176	95	0.2	5	4675.63	WL
D02001707CDD	533395	3507525	4658.01	5	179	92	0.2	5	4675.63	PerfMid
D02001709AAA	537259	3509046	4586.00	6	173	108	1	1	4525.70	TD-WL
D02001710DAB	538841	3508313	4586.00	6	176	115	1	1	4525.70	TD-WL
D02001711BBB	539180	3509084	4575.01	6	173	116	0.2	5	4525.70	WL
D02001714ADB	540451	3507150	4546.99	6	181	121	1	1	4525.70	TD-WL
D02001715CCA	537638	3506246	4596.01	6	184	110	0.5	9	4525.70	TD-WL
D02001715CDC	536348	3505995	4629.01	6	185	104	0.9	2	4525.70	TD-WL
D02001716DCA	536953	3506305	4650.99	6	184	107	0.9	2	4525.70	TD-WL
D02001717ACC	535214	3506730	4640.99	5	182	100	1	1	4675.63	TD-WL
D02001718CCC	532742	3506014	4673.99	5	185	90	1	1	4675.63	TD-WL
D02001719ACC	533455	3505154	4655.00	5	189	92	1	1	4675.63	TD-WL
D02001720CAC	534773	3504851	4663.99	5	190	98	0.9	2	4675.63	TD-WL
D02001720DAC	535641	3504884	4684.00	6	190	101	0.9	2	4525.70	TD-WL
D02001722ABB	538429	3505880	4627.99	12	186	113	0.4	4	3626.10	TD-WL
D02001722CBA	537721	3504923	4673.99	6	190	110	0.9	2	4525.70	TD-WL
D02001729ABD	535486	3504053	4675.01	5	193	101	0.2	5	4675.63	WL
D02001729BDB	534644	3503896	4671.99	5	194	97	0.2	5	4675.63	WL
D02001730CBC	532698	3503181	4852.99	4	197	89	1	1	4825.56	TD-WL
D02001732BAA	534938	3502542	4700.01	5	199	99	0.2	5	4675.63	WL
D02001732BAB	534648	3502634	4673.99	5	199	97	0.2	5	4675.63	WL
D02001733DDB	537076	3501380	4786.00	5	204	107	0.5	9	4675.63	PerfMid

Steady-State Calibration Head Targets

Target Name	UTM X Coordinate (NAD83, meters)	UTM Y Coordinate (NAD83, meters)	Target Head (ft msl)	Layer	Row	Column	Weight	Group	Model Layer Midpoint Elevation (ft msl)	Target Approach
D17017021BDB	536280	3534149	3913.01	10	37	104	0.1	9	3925.97	WL
D17017031BBB	532699	3531300	3875.61	10	49	89	0.1	9	3925.97	WL
D17018017ACB	544764	3535893	3657.50	12	30	139	0.5	9	3626.10	TD-WL
D17018026BBD	548980	3532899	4007.69	10	43	156	0.5	9	3925.97	TD-WL
D17018031DCA	543373	3530230	3893.78	10	53	133	0.1	9	3925.97	WL
D18016013CCB	531197	3525436	4227.02	8	73	83	0.1	9	4225.83	WL
D18017032DBD	535303	3520847	4409.99	7	121	100	0.5	9	4375.77	TD-WL
D18017033ADD	537305	3521231	4317.01	8	115	108	0.5	9	4225.83	TD-WL
D18017035BBB	539095	3521842	4274.00	8	105	116	0.5	9	4225.83	TD-WL
D18017036CCB	540741	3520641	4351.00	7	124	122	0.5	9	4375.77	TD-WL
D18018008BBA	544139	3528237	3981.28	10	62	136	0.1	9	3925.97	WL
D19016010CDB	528320	3517426	4671.50	5	138	71	0.1	9	4675.63	WL
D19016012AAC	532318	3518443	4636.00	7	134	88	0.2	9	4375.77	PerfMid
D19016014AAA	530924	3517043	4598.99	6	140	82	0.5	9	4525.70	TD-WL
D19016024CDC	531532	3514036	4709.00	5	152	85	0.5	9	4675.63	TD-WL
D19016026ABB	530331	3513824	4736.00	5	153	80	0.5	9	4675.63	TD-WL
D19016031DDB	524316	3511011	5060.01	2	165	54	0.1	9	5150.53	WL
D19016034ABC	528721	3511946	4705.00	5	161	73	0.5	9	4675.63	TD-WL
D19017008BCC	534322	3518052	4480.00	10	136	96	0.2	9	3925.97	PerfMid
D19017010BAD	538138	3518445	4371.01	9	134	112	0.2	9	4075.90	PerfMid
D19017010BCA	537736	3518250	4369.99	12	135	110	0.2	9	3626.10	PerfMid
D19017010BDC	537937	3518048	4374.00	8	136	111	0.4	9	4225.83	PerfMid
D19017013BCC	540746	3516407	4405.00	7	143	122	0.1	9	4375.77	WL
D19017015BBD	537732	3516848	4417.99	8	141	110	0.2	9	4225.83	PerfMid

Steady-State Calibration Head Targets

Target Name	UTM X Coordinate (NAD83, meters)	UTM Y Coordinate (NAD83, meters)	Target Head (ft msl)	Layer	Row	Column	Weight	Group	Model Layer Midpoint Elevation (ft msl)	Target Approach
D19017016BDA	536526	3516649	4454.01	7	142	105	0.5	9	4375.77	TD-WL
D19017017BBB	534328	3517050	4584.98	9	140	96	0.2	9	4075.90	TD-WL
D19017019BAC	533126	3515242	4569.01	9	147	91	0.2	9	4075.90	PerfMid
D19017020ACB	535123	3515042	4557.00	10	148	99	0.2	9	3925.97	PerfMid
D19017023AAD	540546	3515219	4465.99	8	148	122	0.2	9	4225.83	PerfMid
D19017024DBC	541543	3514430	4461.99	7	151	126	0.5	9	4375.77	TD-WL
D19017031CBD	532933	3511205	4623.01	7	164	90	0.2	9	4375.77	TD-WL
D19017032ADB	535539	3511826	4586.00	10	161	101	0.2	9	3925.97	PerfMid
D19017036CBB	540716	3511420	4502.01	6	163	122	0.5	9	4525.70	TD-WL
D20016010DDD	529313	3507511	4675.01	5	179	75	0.1	9	4675.63	WL
D20017004ABA	536939	3510627	4592.99	8	166	107	0.2	9	4225.83	PerfMid
D20017004BDD	536541	3510023	4573.99	6	169	105	0.1	9	4525.70	WL
D20017005DCC	535140	3509237	4617.50	6	172	99	0.2	9	4525.70	TD-WL
D20017008CBA	534538	3508182	4638.99	5	176	97	0.1	9	4675.63	WL
D20017015CDC	537958	3506003	4621.99	6	185	111	0.5	9	4525.70	TD-WL
D20017015DCD	538558	3506003	4621.99	6	185	113	0.2	9	4525.70	PerfMid
D20017018AAB	533936	3507333	4650.01	5	180	94	0.1	9	4675.63	WL
D20017022CBD	537766	3504806	4665.00	6	190	110	0.5	9	4525.70	TD-WL
D20017029BCA	534550	3503737	4666.71	5	195	97	0.1	9	4675.63	WL
D20017033BAA	536579	3502598	4692.99	5	199	105	0.1	9	4675.63	WL
D20018024ACD	540146	3506810	4642.00	6	182	120	0.5	9	4525.70	TD-WL
(D-18-15)25bdb2_PZ-7 485ft	522681	3522439	5,144.30	3	95	29	1.0	1	4950.50	PerfMid
(D-18-15)25bdb2_PZ-7 800ft	522681	3522439	5,139.10	5	95	29	1.0	1	4675.63	PerfMid
(D-18-15)25bdb2_PZ-7 1245ft	522681	3522439	5,114.40	8	95	29	1.0	1	4225.83	PerfMid

Steady-State Calibration Head Targets

Target Name	UTM X Coordinate (NAD83, meters)	UTM Y Coordinate (NAD83, meters)	Target Head (ft msl)	Layer	Row	Column	Weight	Group	Model Layer Midpoint Elevation (ft msl)	Target Approach
(D-18-15)25bdb2_PZ-7 1680ft	522681	3522439	5,104.80	11	95	29	1.0	1	3776.04	PerfMid
(D-18-15)25bdb2_PZ-7 1810ft	522681	3522439	5,093.70	12	95	29	1.0	1	3626.10	PerfMid
(D-18-15)36abc2_PZ-8_450ft	522308	3521548	5,186.60	3	110	23	1.0	1	4950.50	PerfMid
(D-18-15)36abc2_PZ-8 1150ft	522308	3521548	5,168.50	8	110	23	1.0	1	4225.83	PerfMid
(D-18-15)36abc2_PZ-8 1650ft	522308	3521548	5,143.60	11	110	23	1.0	1	3776.04	PerfMid
(D-18-15)36abc2_PZ-8 1925ft	522308	3521548	5,107.80	13	110	23	1.0	1	3476.17	PerfMid
(D-18-16)30cad2_PZ-5 700ft	523759	3522438	5,125.90	7	95	47	1.0	1	3675.77	PerfMid
(D-18-16)30cad2_PZ-5 1200ft	523759	3522438	5,133.90	10	95	47	1.0	1	3925.97	PerfMid
(D-18-16)30cad2_PZ-5 1900ft	523759	3522438	5,116.70	14	95	47	1.0	1	2885.69	PerfMid
(D-18-16)31bbc_PC-3	523284	3521556	4,971.80	7	109	39	0.0	10	3675.77	PerfMid
Deering_Spring	522599	3519266	5283.66	2	131	27	0	1	5150.53	Spring - intermittent
Helvetia_Spring	521014	3525815	4565.76	6	72	11	0	1	4525.70	Spring - intermittent
MC-1	524015	3523224	4997.45	3	83	51	0	1	4975.50	Spring - intermittent
Questa_Spring	529479	3522033	4604.90	6	102	76	0.5	1	4525.70	Spring-perennial
Rosemont_Spring	524850	3521374	4917.82	4	112	57	0.5	1	4825.56	Spring-perennial
SP1	550724	3516650	5357.91	1	142	163	0	1	5375.26	Spring - intermittent
SP2	551322	3518282	5409.94	1	135	166	0	1	5375.26	Spring - intermittent
SP3	548169	3522424	4764.54	5	95	153	0	1	4675.63	Spring - intermittent

Steady-State Calibration Head Targets

Target Name	UTM X Coordinate (NAD83, meters)	UTM Y Coordinate (NAD83, meters)	Target Head (ft msl)	Layer	Row	Column	Weight	Group	Model Layer Midpoint Elevation (ft msl)	Target Approach
SP4	550199	3527299	4760.08	4	65	161	0	1	4825.56	Spring - intermittent
SP5	526513	3525192	4747.88	5	74	64	0	1	4675.63	Spring - intermittent
SP6	549466	3527520	4679.83	5	65	158	0	1	4675.63	Spring - intermittent
SP7	550377	3527609	4613.72	5	64	162	0	1	4675.63	Spring - intermittent
SP8	533440	3538631	3538.11	13	19	92	0	1	3476.17	Spring - intermittent